NTNU

Norwegian University of
Science and Technology

Prediction of Emulsion Flow in Pipes by Non-Newtonian Flow Models and Emulsion Parameters

A Study of Water-in-Oil Emulsions

Ann-Othilie Helgesen Væhle

Petroleum Geoscience and Engineering
Submission date: June 2017
Supervisor: Harald Arne Asheim, IGP

Norwegian University of Science and Technology
Department of Geoscience and Petroleum

Abstract

The objective of this master's thesis is to measure emulsion properties, and check if these data combined with flow models enable prediction of emulsion flow in pipes. The two non-Newtonian flow models Power law and Herschel-Bulkley are used to predict flow rates, which will be compared to flow rates measured in a pipe.

Engine oil was used to prepare water-in-oil emulsions with varying water content. Shear stress, viscosity, droplet size distribution, temperature effect, aging and stability were investigated. One water-in-oil emulsion prepared from soybean oil was also used for comparison. Viscosity was increasing with increasing water content, and seemed to be slightly decreasing with aging. There was no clear trend for increased droplet size with aging.

Emulsion flow rates were measured in a specially designed flow facility. By combining emulsion parameters from laboratory measurements and the Power law and Herschel-Bulkley flow models, the flow rates were predicted. The averaged deviation between predicted and measured flow was 13%, and the maximum deviation was 35%. This is much above what would be expected for Newtonian fluid, but may be comparable for two-phase flow.

Samandrag

Målsetjinga med denne masteroppgåva er å måla emulsjonseigenskapar, og sjekke om desse kombinert med strøymingsmodellar tillèt berekning av emulsjonsstrøyming i røyr. Dei ikkje-Newtonske strøymingsmodellane Potenslov og Herschel-Bulkley er brukt for prediksjon av strøymingsrater, som vert samanlikna med strøymingsrater målt i eit røyr.

Motorolje vart brukt til å laga vatn-i-olje emulsjonar med ulikt vassinnhald. Skjær rate, viskositet, dråpestørrelsefordeling, temperatureffekt, aldring og stabilitet vart undersøkt. Ein vatn-i-olje emulsjon laga av soyaolje vart òg brukt for samanlikning. Viskositeten var aukande med aukande vassinnhald, og såg ut til å vera svakt minkande med aldring. Det vart ikkje funne nokon klar trend for auka dråpestørrelse med aldring.

Strøymingsraten til emulsjonane vart målt i ein spesialdesigna strøymingsfasilitet. Ved å kombinera emulsjonsparametrar frå laboratoriemålingar og strøymingsmodellane Potenslov og Herschel-Bulkley, vart strøymingsrater estimert. Det gjennomsnittlege avviket mellom predikert og målt strøyming var 13%, medan det største avviket var på 35%. Dette er langt over kva som ville vore forventa for ei Newtonsk fluid, men kan kanskje vera samanliknbart med to-fase strøyming.

Acknowledgement

This master's thesis is written as the final work to complete my Master of Science degree in Petroleum Engineering at the Department of Geoscience and Petroleum at the Norwegian University of Science and Technology (NTNU) in Trondheim, Norway.

I would like to give a special thanks to fellow student Marthe Bodahl Lunde for excellent teamwork in the laboratory, with interesting discussions and a positive attitude the laboratory work has been more fun than a struggle. My supervisor Harald Arne Asheim also deserves a special thanks for always taking time for my questions and giving great feedback and advises. His guidance and theoretical knowledge has been essential for this thesis. Thanks to Knut Gåseidnes for being available to answer questions via e-mail. When it comes to the laboratory work there are several people that deserves to be thanked: Roger Overå, Georg Voss and Håkon Myhren. They have helped us get the needed materials, taught us to use equipment and even designed setups for our experiments.

Last but not least I would like to give a warm and special thank you to my fellow students for five unforgettable years in Trondheim, and supporting lunches and coffee breaks in between the writing.

Ann-Othilie Helgesen Væhle

Trondheim, June 2017

Table of Contents

List of Figures

List of Tables

Nomenclature

E[X]	Arithmetic mean
Var[X]	Arithmetic variance
D_{avg}	Average droplet size
$h_{\text{avg.fluid}}$	Average fluid height in tank
v_{avg}	Average velocity
C	Consistency parameter
D_p	Diameter of pipe (inner diameter)
a	Dispersion parameter
R_d	Droplet radius
n	Flow behavior index
Q	Flow rate
g	Gravitational constant
L_h	Hydrodynamic entry length
L_p	Length of pipe
$L_{\text{under tank}}$	Length of pipe under tank
m	Mass
D_{95}	Maximum droplet size in pipe flow
R_p	Pipe radius (inner pipe radius)
P	Power
Δp	Pressure difference
r	Radius
r_w	Radius at pipe wall = Inner pipe radius
r_0	Radius where plug flow ends
Re	Reynolds number
t	Time
Δh_{avg}	Total average fluid height
Δh	Total fluid height
V	Volume
ρ	Density
ρ_c	Density of the continuous phase

μ	Dynamic viscosity
ε	Energy dissipation per volume unit
σ	Interfacial tension
μ	Location parameter lognormal distribution
σ	Scale parameter lognormal distribution
γ	Shear rate
τ	Shear stress
τ_w	Wall shear stress
τ_0	Yield point

Abbreviations

CDF	Cumulative distribution function
DMG	Distilled monoglyceride
HB	Herschel-Bulkley
HLB	Hydrophilic-lipophilic balance
IFT	Interfacial tension
MCR	Modular compact rheometer
O/O	Oil-in-oil
O/W	Oil-in-water
O/W/O	Oil-in-water-in-oil
PIT	Phase inversion temperature
PGPR	Polyglycerol polyricinoleate
PL	Power law
PDF	Probability density function
RPM	Revolutions per minute
NaCl	Sodium chloride
W/O	Water-in-oil
W/O/W	Water-in-oil-in-water
wt%	Weight percent

1 Introduction

Oil and water are commonly produced simultaneously, and often mix into an emulsion. Emulsification alter the flow pattern and often causes increased pressure drops due to increased viscosity (Wen et al., 2014, p. 9513). The amount of water often exceed the produced oil, if the reservoir is mature and secondary recovery methods are used (Petrowiki, 2016). The many mature reservoirs in the petroleum industry today make emulsion behavior and flow highly relevant.

In this thesis, the focus has been on water-in-oil emulsions created by mixing engine oil and saltwater. Water contents were varied between 30-60%. Engine oil was chosen since it is reasonable to believe that the emulsion properties will be similar for this type of oil and crude oil. The oil used provided stable emulsions and was easily available. Soybean oil emulsions had already been used in the TPG4560 specialization project.

The objective of this master's thesis is therefore to study emulsions in general, with a special focus on emulsion flow in pipes where emulsion parameters and flow models are combined to predict flow rate. There are many studies about emulsion properties, but few where the emulsion properties are used as a foundation for predicting emulsion flow. The flow models used for predictions are the Power law and Herschel-Bulkley model.

To find rheological emulsion properties a modular compact rheometer is used, and emulsion densities are found by using a mud balance. A flow facility is designed based on one of the emulsions, using the Power law model in MATLAB taking rheological properties as input. The dimensions of the flow capacity setup has to be set such that the flow does not become turbulent, and when the design is in place several emulsions will be run through it. The measured flow rates in the flow capacity setup are compared to flow rates predicted by putting emulsion properties in the appropriate flow model. In addition to this, droplet size distribution and emulsion aging is studied by microscopic image analysis.

2 Emulsions

An emulsion is a mixture of two immiscible phases, where one phase is dispersed in the other as small droplets. To be able to get dispersion and a stable emulsion, emulsifiers has to be agitated together with the immiscible phases. The dispersed liquid is called dispersed or internal phase, while the other liquid is called the continuous or external phase. Emulsions usually consist of two liquids, but can also contain gas and smaller particles.

In everyday life emulsions can be found in different products, like foods, lotions, paints and cosmetics. In the petroleum industry, emulsions can be both desired and undesired. Drilling fluids or emulsions to improve oil recovery are created on purpose, whilst other emulsions may be created by mixing during flow and cause problems in production and transportation.

2.1 Interfacial Area and Tension

When mixing two immiscible liquids of different density, the result is two layers with a clear phase boundary. The natural tendency is to reduce the surface energy, meaning reducing the area of contact between the liquids. Thus, agitation is needed to create an emulsion where smaller droplets replace a straight interface; and stabilizers are needed to prevent coalescence.

Adding emulsifiers lowers the interfacial tension and energy needed to create an emulsion. Interfacial tension is the elastic tendency of a fluid surface, which makes it want to have the least surface area possible. The droplet pressure is a component of this surface force, acting perpendicular and inward tending to decrease the area of the interface. Droplet pressure can be described as follows:

$$\Delta p = \frac{2\sigma}{R_d} \tag{2.1}$$

where Δp is the pressure difference, σ is the interfacial tension and R_d is the droplet radius. The interfacial tension is temperature dependent and tends to decrease with increasing temperature. As can be seen in Figure 2.1, interfacial tension is called surface tension when there is a liquid-gas interface instead of a liquid-liquid interface.

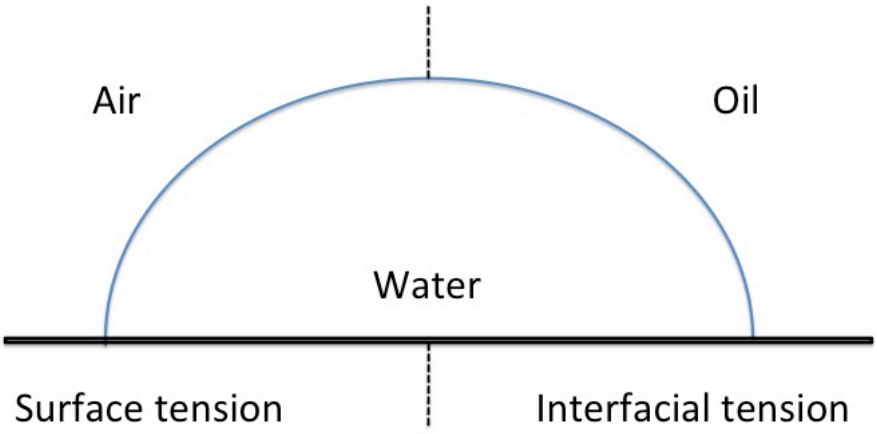

Figure 2.1: Schematic of surface tension and interfacial tension

2.2 Emulsion Classes

Emulsions are divided into classes: water-in-oil emulsions (W/O), oil-in-water emulsions (O/W) and oil-in-oil emulsions (O/O). Intermediate cases and more complex emulsions like W/O/W emulsions can be found, but the focus here will be on W/O emulsions. To validate the emulsion class, a droplet of the emulsion can be put into oil or water. If the droplet does not dissolve in water it is a W/O emulsion, but if it dissolves it is an O/W emulsion. When put in oil, the W/O emulsion should dissolve and the O/W emulsion should not dissolve.

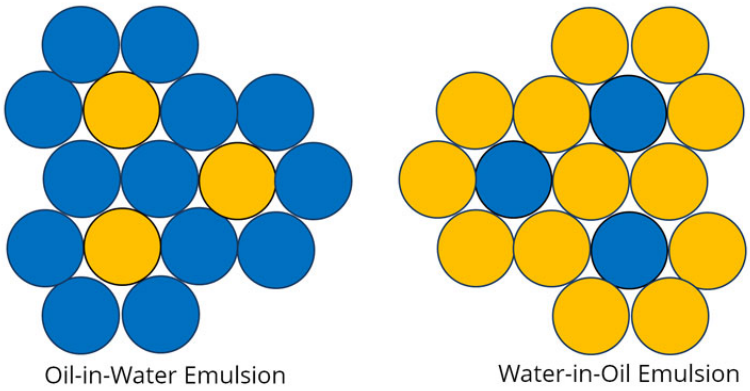

Figure 2.2: O/W emulsion and W/O emulsion illustrated (Molecularrecipes, 2014)

Based on how stable the emulsions are they can be classified as either loose or tight. A loose emulsion is easy to break, while a tight emulsion practically is stable (Schramm, 2000, pp. 592, 607).

2.3 Emulsifiers

By dispersing one liquid in another, the natural equilibrium will be off and the system is unstable due to the wish for recombination. The system is heterogeneous and the stability will be minimal, but emulsifiers can help stabilize the emulsion by adding colloidal repulsive forces (Bibette, 2002, p. 1). An emulsifier reduces the energy needed for emulsification, and can stabilize the emulsion by increasing its kinetic stability meaning that it is stable over a period of time. For emulsions made with mineral engine oil, emulsifiers were already present in the oil. For the emulsions made with soybean oil, margarine emulsifiers were added. The fact that emulsifiers were added manually in one case and were added under manufacture in the other should not have any impact on the results.

An emulsifier has one hydrophilic end that attracts water, and one hydrophobic end that repels water (also called lipophilic). Due to the hydrophilic-lipophilic properties of the emulsifier, the immiscible phases can coexist since the emulsifier positions itself on the fluid interface and balances the phases. Since one end of the surfactant is oil-soluble it will position this part in the oil phase, and the water-soluble part in the water phase as seen in Figure 2.3.

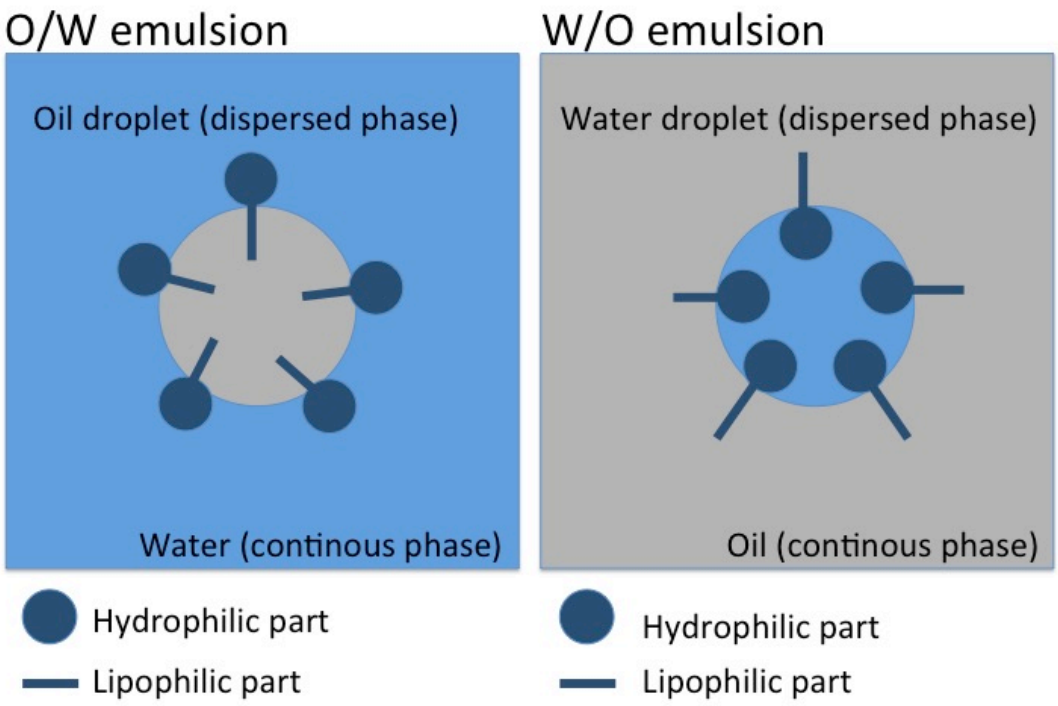

Figure 2.3: Schematic of O/W emulsions and W/O emulsions

When the emulsifier positions itself on the interface it forms an interfacial film. For a W/O emulsion this film will prevent merging of water droplets, since the lipophilic part in the continuous phase will reject colliding water droplets. This can prevent flocculation, coalescence and Ostwald ripening which are emulsion instabilities that will be discussed in Chapter 2.6. If the surfactant is adsorbed or migrates, this can lead to changes in both the droplet's response to deformation, and the viscous behavior of the emulsion (Enjamoori et al., 2011, p. 183).

Emulsifiers will not be able to create one stable phase out of the two immiscible phases unless sufficient mixing energy is present. Several mixers can be used, and for this experiments a high-shear mixer provides mixing energy where rotating blades provides velocity. The working principle is that the fluid experiences shear when there is a rate of change in velocity across the fluid path, like the change in velocity from center of the rotor to the tip of the rotor. To measure the mixing intensity the impeller Reynolds number can be found, but this requires a constant viscosity. For non-Newtonian fluids the viscosity will vary, and therefore energy dissipation is chosen as a measure for mixing intensity instead. Energy dissipation can be defined as "the rate of energy loss due to fluid flow from location (1) to location (2)" (SPE, 2016).

2.4 Agitation and Droplet Dispersion

The applied shear and duration of this exposure can influence the droplet size distribution in the emulsion. It is assumed that an emulsion mixed for a longer time will have finer droplets than an emulsion mixed for a shorter time (Pal, 1996, p. 3184), if the same amount of shear is applied. A general rule is that higher shear gives smaller droplets and also a more stable emulsion (Ross, 2017). Based on this, it is reasonable to believe that higher shear can reduce the mixing time needed to create a stable emulsion. On the other hand, some emulsions might be sensitive to shear, making them unstable if a certain shear is reached (Ross, 2017). Trial and error in the laboratory may be needed to be able to find the appropriate mixing time and shear for each specific emulsion.

When it comes to the droplet size distribution in turbulent pipe flow and rotor mixing, it can be described by the following half-empirical correlation by Hinze (1955):

$$D_{95} = 0.725 \frac{1}{\varepsilon^a} \left[\frac{\sigma}{\rho_c} \right] \tag{2.2}$$

where D_{95} is the droplet size such that 95% of the oil volume is in droplets smaller than this, also called the maximum droplet size. A rule of thumb is that the average droplet size can be approximately 30% of D_{95}. ε is the energy dissipation per volume unit, given in [J/kg s], a is the dispersion parameter and is set to be 0.4. σ is the interfacial tension between water and oil, given in [N/m]. ρ_c is the density of the continuous phase given in [kg/m^3], and ρ_c will be oil for a W/O emulsion (Asheim, 1985, p. 269). Since this correlation is for turbulent pipe flow it will not be applicable for the laminar emulsion pipe flow in this experiment, but it will be used to measure droplet size during mixing. It should also be mentioned that this correlation is based on single droplets in a continuous phase, meaning only a few single droplets in the continuous phase and not many packed droplets.

The droplet size distribution can have a dramatic impact on W/O emulsion rheology (Pal, 1996, p. 3181). A fine emulsion, meaning an emulsion with smaller droplets, will have different properties than a more coarse emulsion with larger droplets. For a W/O emulsion with the same water content, a finer emulsion is expected to show higher viscosity and higher shear thinning effects compared to a coarser emulsion. It is also expected that an emulsion will have higher viscosity with increasing water content (Pal, 1996, p. 3181). Microscopic restructuring may also influence the viscosity, for example increased droplet size and flocculation might increase viscosity (Enjamoori et al., 2011, p. 183).

2.5 Aging

As the emulsion gets older in terms of hours after mixing, it is said that the emulsion is exposed to aging. Aging could lead to emulsion breakdown processes creating instabilities, but it is not defined as a breakdown process itself. After aging the emulsion might have an increased number of larger droplets and an increased mean droplet size, and agglomeration of droplets may occur. Such microscopic restructuring in the emulsion can possible increase viscosity (Enjamoori et al., 2011, p. 183), and viscosity might be more reduced at low to

moderate shear stress (Pal, 1996, p. 3189). Some emulsions might become more stable with aging, due to emulsifiers spreading more evenly between the droplets with time.

The effect of aging can be investigated by studying the emulsion in time intervals with microscopic imaging, giving an estimate of the droplet size distribution and a picture of the microscopic structure. To look for changes in rheology, a modular compact rheometer (MCR) can be used to study the fresh and aged emulsion.

2.6 Emulsion Stability and Breakdown Processes

The stability and lifetime of emulsions depends on the preparation procedure employed. While some emulsions are impossible to prepare by any procedure, others can be stable from seconds to months and even years. A stable emulsion is defined as an emulsion that is able to "resist changes in its physicochemical properties with time" (Alias, 2013), meaning resist both physical and chemical changes.

For a W/O emulsion the stability generally decrease with increased water content, and studies done by Ostwald show that the maximum water fraction should not exceed 74%. Temperature can also influence the emulsion stability, where an increased temperature during mixing and emulsification can create a more stable emulsion, whilst an increased temperature after mixing might decrease the stability (Wen et al., 2014, p. 9513).

Between the dispersed droplets and the continuous phase there is a semipermeable film, where osmosis can happen. By conversation with K Gåseidnes (personal communication, 11.05.2017) it was stated that this relationship could be important for emulsion stability. For example this can be used in drilling fluids where the formation needs to be stabilized. By keeping salt concentration in the emulsion higher than the formation water, the formation water will go through the semipermeable film to lower salt concentration in the internal phase, making the formation more stable.

Even if the emulsion looks stable after preparation, several breakdown processes might occur during storage as the emulsion is aged. These breakdown processes work through several microscopic mechanisms, and can change the physicochemical properties of the emulsion to make it unstable. An overview of these breakdown processes can be seen in Figure 2.4, and these will in order be presented in this section.

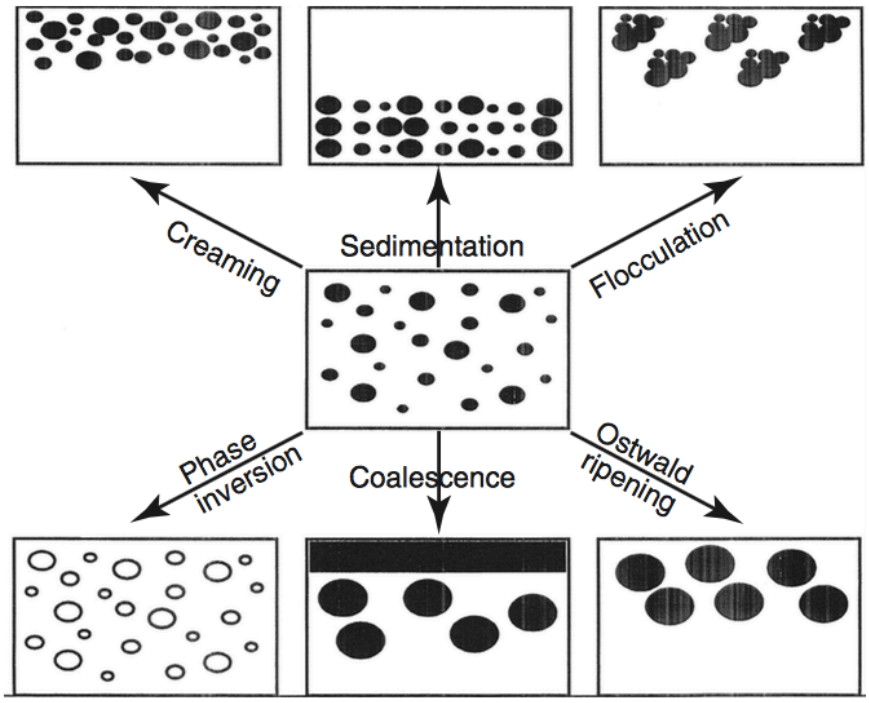

Figure 2.4: Various breakdown processes in emulsions (Tadros, 2013, p. 3)

2.6.1 Creaming and Sedimentation

The reason for creaming and sedimentation is the density difference in the mixed phases and the effect of gravity. When the density of the dispersed phase is lower than the continuous phase, creaming will occur. If the density of the dispersed phase is higher than the continuous phase, sedimentation will occur (Tadros, 2013, p. 36). In a W/O emulsion, the dispersed phase is denser than the continuous phase, and water droplets can gather at the bottom. When these droplets are packed, the oil around the droplets is squeezed out of the grid and floats up to surface while the water droplets remain at the bottom. If stabilizing components are not present, the creamed or sedimented droplets can coalesce to form a continuous phase (Heeres et al., 2014, p. 223), and creaming or sedimentation can lead to demulsification (Becher, 2001, p. 201).

2.6.2 Inversion

Inversion changes the emulsion type, for example from W/O to O/W emulsion. It can be dependent on the emulsifying agent, the HLB-number, volume fraction, temperature and applied shear. HLB stands for hydrophilic-lipophilic balance, and is a number that states how

hydrophilic or lipophilic a surfactant is (Bibette, 2002, p. 97). A temperature increase can lead to a decrease in HLB (Becher, 2001, p. 361), so for example if an O/W emulsion is heated up the decrease in HLB will move the emulsion out of the stable region. The emulsion will at some temperature get a HLB characteristic of a W/O emulsion, and this is known as the phase inversion temperature (PIT).

Volume fraction and mechanical shear can also have an impact on the inversion as illustrated in Figure 2.5 and Figure 2.6. While making emulsions, one have to keep in mind that volume fraction inversion is irreversible whilst shear-induced inversion is reversible. Volume fraction inversion happens when the internal phase exceeds a critical percentage, or the continuous phase is below a critical percentage. The thermodynamics makes it preferable to invert the emulsion, making the continuous phase with smaller volume internal and the internal phase with larger volume continuous (Abbott, 2016). This can be seen in Figure 2.5 where oil started as internal phase but ended up as continuous phase. Shear-induced inversion happens due to dissipated energy, kinetic energy and impulse applied to the emulsion by the impeller (Sjöblom, 2001, p. 403)

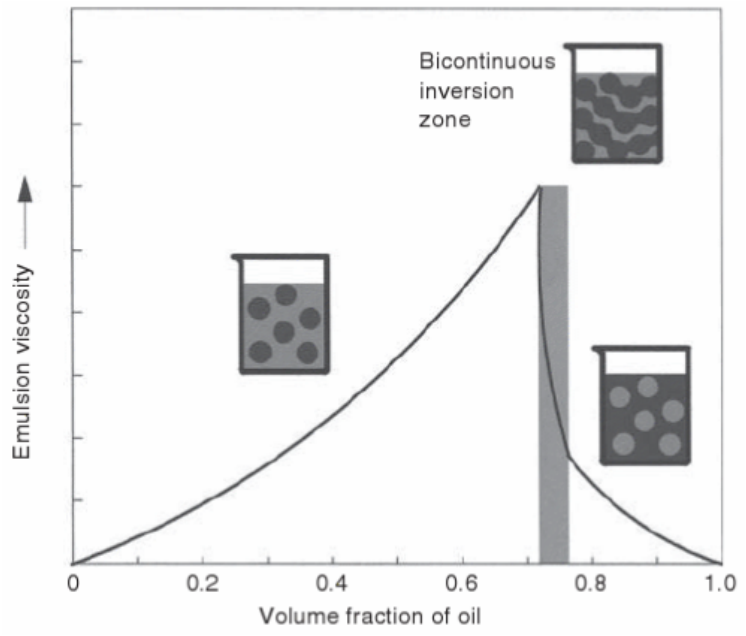

Figure 2.5: Influence of volume fraction on emulsion inversion (Schramm, 2014, p. 262)

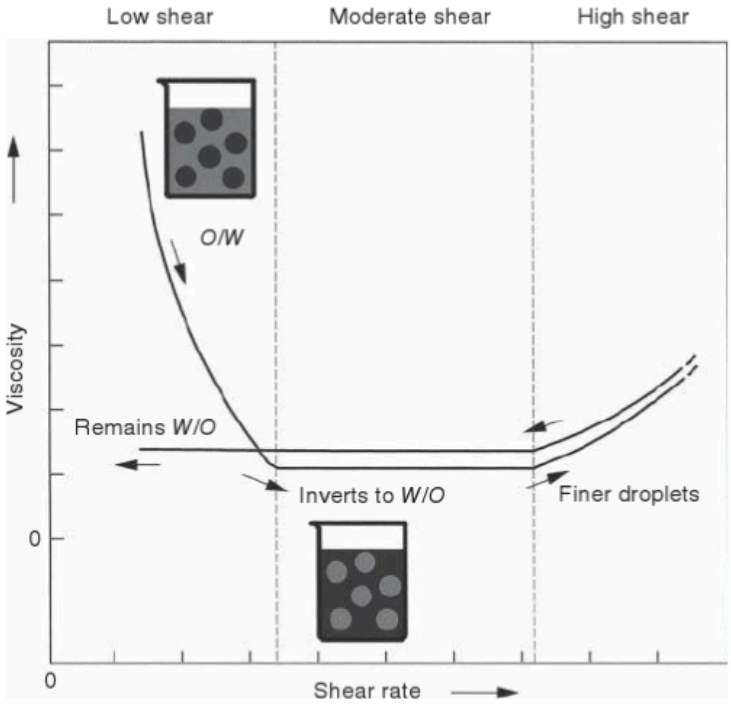

Figure 2.6: Shear-induced inversion of an emulsion (Schramm, 2014, p. 280)

2.6.3 Ostwald Ripening

Ostwald ripening is a thermodynamically driven spontaneous process, causing larger droplets to grow at the expense of smaller droplets. Smaller droplets are less energetically stable compared to larger droplets, leading to smaller droplets going towards larger droplets by molecular diffusion through the continuous phase (Nguyen Hoang et al., 2004, p. 1421). A larger droplet is more stable due to a lower Laplace pressure, which is the pressure difference Δp between the inside and the outside of a curved surface. It is defined in the Young-Laplace equation as

$$\Delta p = \sigma\left(\left(1/r_1\right)+\left(1/r_2\right)\right) \tag{2.3}$$

where σ is the interfacial tension and r_1 and r_2 are the principal radius of curvature. In a sphere, r_1 is equal to r_2 and Equation (2.3) can be simplified to Equation (2.1).

The system tends to decrease its surface energy, and smaller droplets thus become energetically unfavorable. Consequently the number of smaller droplets decrease and larger droplets increase as seen in Figure 2.7.

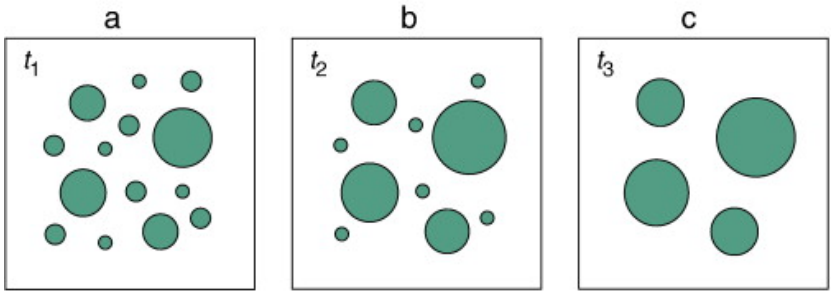

Figure 2.7: Schematic illustration of Ostwald ripening (Werz et al., 2014, p. 186)

In difference to coalescence, Ostwald ripening does not require the droplets to be in close contact (Aulton and Taylor, 2013, p. 461). In conversation with H. Asheim (Personal communication, 02.06.2017) it was stated that the continuous phase would have a certain solubility of water droplets, even if this were small. Thus the droplets diffusing through the continuous phase would be small, and they may be able to get past the emulsion layer and into the larger droplet. It is however hard to tell how fast this process will go.

2.6.4 Flocculation

Flocculation is aggregation of droplets without increasing droplet size, since the droplets are separated by trapped continuous phase (Aulton and Taylor, 2013, p. 460). It happens when the repulsion is not high enough compared to the Van der Waals attraction to keep the droplets apart, and is not dependent on the droplet pressure as in Ostwald ripening. Van der Waals attraction is an intermolecular force, meaning that it holds molecules together by different charges in the two ends of the molecule. This difference in charge arises from electrons orbiting the molecule. The repulsion forces on the other hand, are mainly electrostatic and steric interactions resulting from mixing and overlap of the electrical double layer around the droplet (Nilsen-Nygaard et al., 2014, p. 52221).

The flocculation can be strong or weak, depending on how strong the attractive forces are compared to the repulsive forces. Even if flocculation does not increase the droplet size, the effective particle size is increased as can be seen in Figure 2.10 on page 14. This can also

lead to increased creaming or sedimentation, since larger flocks will rise or settle faster.

2.6.5 Coalescence

When two droplets in an emulsion come in close contact for example due to flocculation, the thin liquid film around the droplet may become thinner and eventually rupture. This is called coalescence and allows two or more droplets to merge together into one larger droplet. Looking at Figure 2.8, the particles are approaching one another in I, the film is drained in II and ruptured in III before the particles merge together in IV becoming one single, larger droplet.

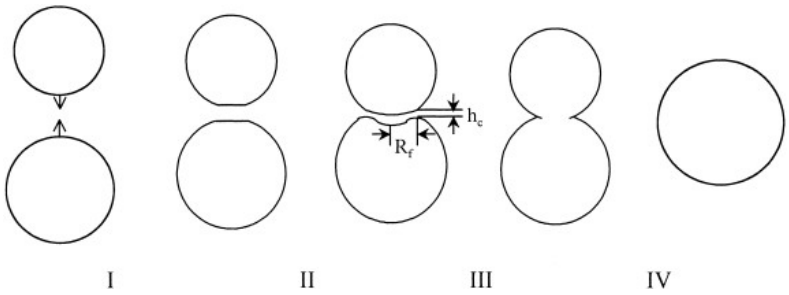

Figure 2.8: Different stages in coalescence (Yu et al., 2000, p. 2380)

Some droplets initially formed may not be completely covered with emulsifier, and these droplets will coalesce such that the surface becomes completely covered with emulsifier (Tcholakova et al., 2008, p. 1610). This is shown in Figure 2.9.

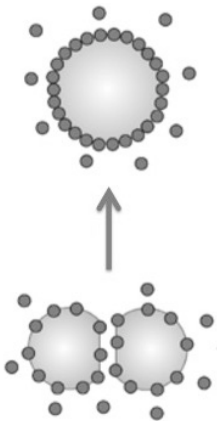

Figure 2.9: Droplets coalescing to make droplet completely covered with emulsifier (Tcholakova et al., 2008, p. 1613)

In Figure 2.10 Ostwald Ripening, flocculation and coalescence can be seen schematically as part of emulsion destabilization. In the first step the droplets are growing, which can happen both due to Ostwald ripening, flocculation and coalescence. As previously mentioned the droplets can coalesce and form a continuous layer of the creamed or sedimented droplets, and the emulsion breaks as shown in the third and fourth step in Figure 2.10.

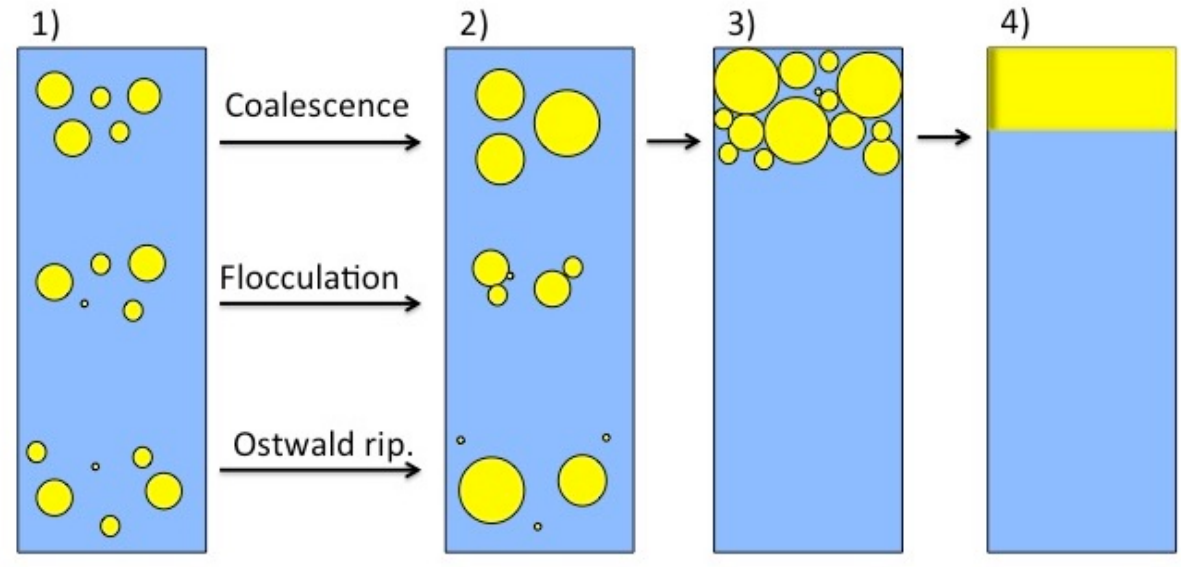

Figure 2.10: Step 1-2: Droplet growth by coalescence, flocculation and Ostwald ripening. Step 2-3: creaming. Step 3-4: Formation of a continuous phase. (Figure is modified from Heeres et al. (2014, p. 223))

3 Fluid Flow

Before starting to describe flow models, some basic fluid terminology has to be defined. One such thing is rheology, which can be defined as the study of deformation and flow of matter (Malkin and Isayev, 2013, pp. 1-3). A fluid will continuously deform when stress is applied, opposite to a solid, which will deform and then stop. Forces applying stress to a fluid can for example be pressure difference in a pipe or rotation of an impeller, and rheology is thus important for both petroleum transportation and emulsion mixing.

Viscosity is also a parameter that has to be defined, and can be explained as the measure of a fluid's internal resistance to flow (Çengel et al., 2010, p. 51). Imagine that the fluid consists of several stacked layers, like in Figure 3.1. Each layer will experience friction, or internal resistance, from the layers around. In everyday terms one could say that viscosity is how "thick" a fluid is, and the viscosity tends to decrease with increasing temperature.

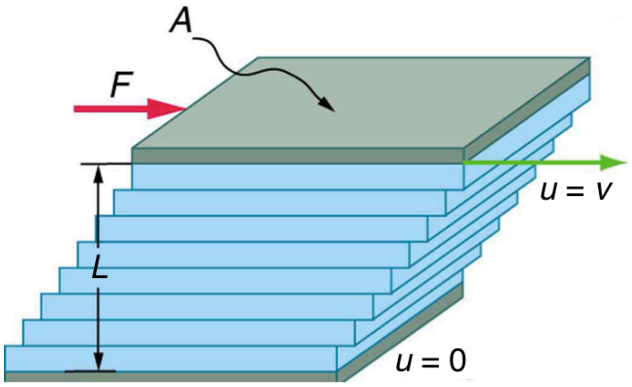

Figure 3.1: Viscosity illustrated as stacked fluid layers experiencing friction (Figure is modified from OpenStax (2016))

When an object is moving with respect to a surrounding fluid, a drag force will be acting opposite to this motion. This is denoted as the shear stress τ . For a Newtonian fluid, shear stress τ can be expressed as

$$\tau = \mu \cdot \gamma \tag{3.1}$$

where γ is the shear rate and μ is the dynamic viscosity. Newtonian fluids are " fluids for which the shear stress is linearly proportional to the shear rate" (Çengel et al., 2010, p. 447).

3.1 Flow in Pipes

Shear stress in a fluid is proportional to the rate of change in velocity across the fluid path, meaning the velocity gradient as seen in Figure 3.2. Thus it will change with changes in the velocity profile and not the absolute velocity. The shear stress will be larger close to the walls compared to in the middle of the flow since the velocity is changing more here than in the center (Southard, 2006, p. 91).

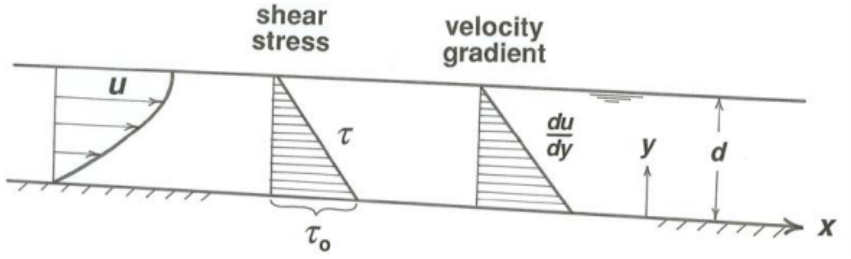

Figure 3.2: Vertical distribution of velocity, shear stress and velocity gradient in a steady, uniform, laminar flow (Southard, 2006, p. 91)

When a flow has smooth streamlines and ordered motion it is said to be laminar, opposite to a turbulent flow with velocity fluctuations and highly disordered motion. These two flow regimes are illustrated in Figure 3.3.

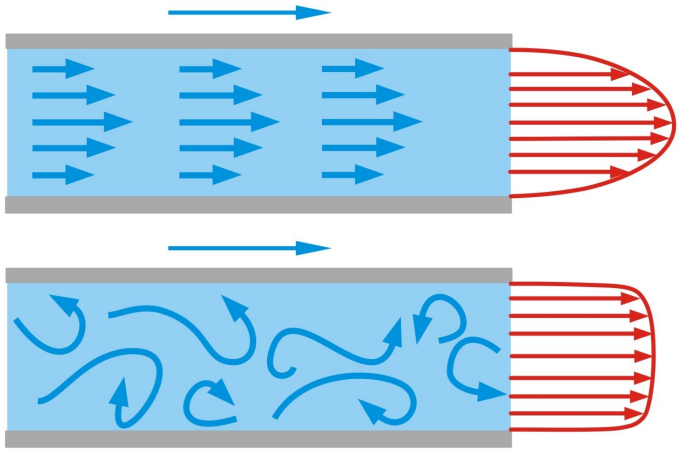

Figure 3.3: Schematic of laminar (upper) and turbulent (lower) flow regime with velocity profile (GUNT, 2016)

The flow regime mainly depends on the ratio of inertial forces to viscous forces in the fluid and this ratio is called the Reynolds number, abbreviated Re (Çengel et al., 2010, pp. 339-

340). For an internal flow in a circular pipe the dimensionless Reynolds number can be expressed in the following way:

$$\mathrm{Re} = \frac{\text{Initial forces}}{\text{Viscous forces}} = \frac{\rho v_{avg} D_p}{\mu} \tag{3.2}$$

where ρ density of the fluid, v_{avg} is the average velocity of the flow, D_p is the diameter of the pipe and μ is the viscosity of the fluid. This dimensionless number can be used to determine the flow regime, based on the boundary conditions shown in Table 3.1.

Table 3.1: When the flow regimes are changing based on the Reynolds number

Reynolds number	**Flow regime**
$\mathrm{Re} \leq 2300$	Laminar flow
$2300 \leq \mathrm{Re} \leq 4000$	Transitional flow
$\mathrm{Re} \geq 4000$	Turbulent flow

As can be seen in Figure 3.1 the velocity at the pipe wall is zero, due to the no-slip condition. The fluid at the wall come to a complete stop, and also slow down the adjacent fluid due to friction between them. This will develop a boundary layer, meaning a region where the viscous effects and velocity changes are significant. It can be seen in Figure 3.4, shown as the solid pink line. The area from the pipe inlet to where the velocity boundary layer merges is called the hydrodynamic entry length L_h, or entrance region (Çengel et al., 2010, p. 341). After this point the velocity profile is fully developed, and the region is called the hydrodynamically fully developed region.

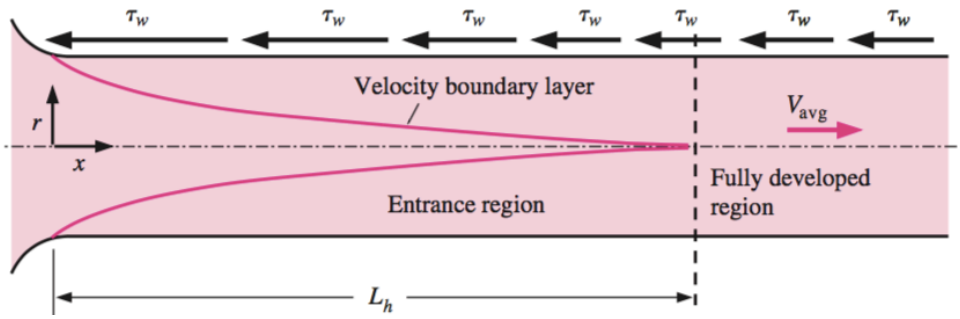

Figure 3.4: Shows boundary layer, entrance and fully developed region, and how wall shear stress is varying in the flow direction (Çengel et al., 2010, p. 342)

By looking at Figure 3.4 it can be seen that the pressured drop will be higher in the entrance region due to a higher wall shear stress, τ_w, and this will increase the average friction factor for the entire pipe. Thus it is important to have this entry length in mind when looking at pipe flow or designing pipe flow setups, in longer pipes it can be negligible but it might be important in short pipes (Çengel et al., 2010, p. 342). The entry lengths can be approximately calculated as

$$L_{h,\text{laminar}} = 0.05\,\text{Re}\cdot D_p \tag{3.3}$$

for laminar flow where L_h is the hydrodynamic entry length, D_p is the diameter of the pipe and Re is the Reynolds number. For turbulent flow the following relation is applicable:

$$L_{h,\text{turbulent}} = 1.259\,\text{Re}^{1/4}\cdot D_p \tag{3.4}$$

For the flow in the flow capacity setup designed for this experiment, the desired flow regime is laminar to avoid lateral mixing of the fluid. In this setup the fluid flow Q can be calculated with the Poiseuille law as long as the flow is laminar:

$$Q = \frac{V}{t} = \frac{\Delta p \pi R_p^{\,4}}{8\mu L_p} \tag{3.5}$$

where t is the measured time required for the given volume V of emulsion with density ρ and

viscosity μ to flow through a capillary pipe of length L_p with radius R_p (Aurand, 2015). Δp is the driving force of the instrument, and is equal to

$$\Delta p = \rho g \Delta h \tag{3.6}$$

where g is the gravitational constant and Δh is the total fluid height.

3.2 Classification of Fluid Behavior

Fluids can generally be divided into four categories: Newtonian fluids, time-independent and time-dependent non-Newtonian fluids, and viscoelastic fluids. Newtonian fluids show linear relationship between shear stress and shear rate, seen in Figure 3.5. If the shear stress is not proportional to the shear rate, the fluid is classified as a non-Newtonian fluid. In this theory section the focus will be on time-independent non-Newtonian fluids, since it is expected that the emulsions will behave in this manner.

Time-independent non-Newtonian fluids show a shear stress behavior dependent on the shear rates only. When the shear rate is low, the viscosity behaves like in a Newtonian fluid. However, when the shear rate is increased, the viscosity will vary with the shear rate. Depending on how the viscosity varies, the time-independent non-Newtonian fluids can be divided into three subgroups:

- Shear thinning or pseudoplastic fluids
- Shear thickening or dilatant fluids
- Viscoplastic fluids

A fluid is shear thinning or pseudoplastic if the viscosity decreases with increasing shear rate (Sochi, 2010, p. 2439). Shear thinning fluids are also called Power law fluids, and an example of such a fluid is paint. Many emulsions are shear thinning fluids, and for such a fluid the behavior will be Newtonian for very high shear rates as seen in Figure 3.5. A fluid is shear thickening or dilatant if the viscosity is increasing with increasing shear rate (Sochi, 2010, p. 2439). An example of shear thickening fluid is wet beach sand. Viscoplastic fluids are able to sustain shear stresses, and a certain amount of shear stress has to be exceeded to initiate the flow (Sochi, 2010, p. 2450). In other words it needs a minimum amount of stress

before deformation, and this stress is knows as yield stress. An example of a viscoplastic fluid is toothpaste.

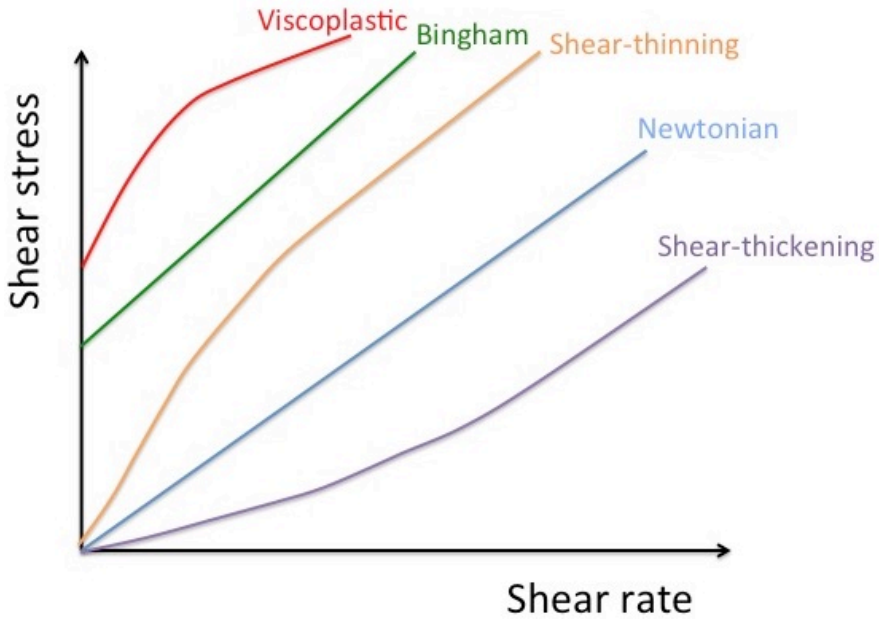

Figure 3.5: Rheology models for non-Newtonian fluids (Figure modified from (Habdas, 2015))

3.3 Non-Newtonian Rheology Models

Since many fluids show complex relationships between shear stress and shear rate, the simple Newtonian relation cannot represent all. This makes it necessary to introduce more complex rheology models, and the most widely used models are:

- Power law model
- Herschel-Bulkley model
- Bingham plastic model
- Maxwell fluid model

When talking about a rheology model, it is thought of a model describing the shear stress and shear stress relation. The corresponding flow model will have the same name (for example Power law), but the flow model is thought of as a model predicting flow rate. Therefore, the rheology model will be determined from the measured plots, stating which flow model should be used to predict flow rate. The two first models will be presented in more detail in this chapter, since these are the models used to calculate emulsion flow in a pipe. After the two models are presented, there will be a section explaining how to determine which model

to use based on the emulsion parameters obtained.

3.3.1 Power Law Model

The Power law model is one of the simplest time-independent rheology models (Sochi, 2010, p. 2439). It states the following relation:

$$\tau = C\gamma^n \tag{3.7}$$

where τ is shear stress, C is the consistency parameter, γ is shear rate, n is the flow behavior index. Both C and n are functions of temperature. When the flow behavior index, n, is equal to one it indicates Newtonian fluid, and when it is less than one it indicates shear thinning fluid type. Usually this model is used for shear thinning fluids, but by n larger than 1 the Power law can be used to model shear thickening fluids as well.

When it comes to expression for Power law pipe flow, this has been derived in Appendix B. It leads to the following expression for the flow rate Q:

$$Q = \frac{\pi R_p{}^3}{3+1/n} \cdot \left(\frac{\Delta p R_p}{2CL_p} \right)^{1/n} \tag{3.8}$$

where Δp is the hydraulic potential:

$$\Delta p = \rho g \Delta h \tag{3.9}$$

and R_p is the pipe radius, n is the flow behavior index, μ_0 is the consistency parameter, L_p is the length of the pipe, ρ is the fluid density, g is the gravitational constant and Δh is the total fluid height. Equation (3.8) is considered the appropriate flow model when a fluid is behaving in a shear thinning manner.

3.3.2 Herschel-Bulkley Model

Herschel-Bulkley can be used to describe both Newtonian fluids and the main classes of time-independent non-Newtonian fluids (Sochi, 2010, p. 2440). Since it takes yield into account, it can also be used to describe viscoplastic fluids. The following relation applies:

$$\tau = \tau_0 + C\gamma^n \tag{3.10}$$

where τ is shear stress, τ_0 is yield point, C is the consistency parameter, γ is shear rate and n is the flow behavior index. As can be seen, Herschel-Bulkley model will reduce to the Power Law model when $\tau_0 = 0$. When $n = 0$ Herschel-Bulkley will reduce to Bingham plastic model, and when both $\tau_0 = 0$ and $n = 1$ Herschel-Bulkley will be reduced to Newton's law for viscous fluids.

The expression for Hershel-Bulkley pipe flow has been derived in Appendix B, and is found to be:

$$Q = \pi v_0 \cdot \left[r_0^{\,2} + \left(\frac{2n+2}{2n+1} \right) \cdot \left(r_w - r_0 \right) r_0 - \left(\frac{n+1}{3n+1} \right) \cdot \left(r_w - r_0 \right)^2 \right] \tag{3.11}$$

where

$$r_0 = \tau_0 \frac{2L_p}{\Delta p} \tag{3.12}$$

and

$$v_0 = -\left(\frac{\Delta p}{2CL_p} \right)^{1/n} \cdot \frac{n}{n+1} \cdot \left(r_w - r_0 \right)^{(n+1)/n} \tag{3.13}$$

where r_0 is the radius where the plug flow ends, n is the flow behavior index, r_w is the radius at the pipe wall meaning the inner pipe radius R_p, τ_0 is the yield point, L_p is the length of

pipe, Δp is the hydraulic potential as shown in (3.9) and C is the consistency parameter. Equation (3.11) is considered the appropriate flow model when a fluid is behaving in a viscoplastic manner.

3.3.3 Model Determination

To determine the most accurate rheology model to use, the shear stress versus shear rate and viscosity versus shear stress plots have to be analyzed. For the shear stress versus shear rate plot, the shape of the measured curve has to be compared to the red and blue curve in Figure 3.6, noticing that the Power law starts in zero unlike the Herschel-Bulkley model. This is better illustrated in Figure 3.7, where the yield point is marked.

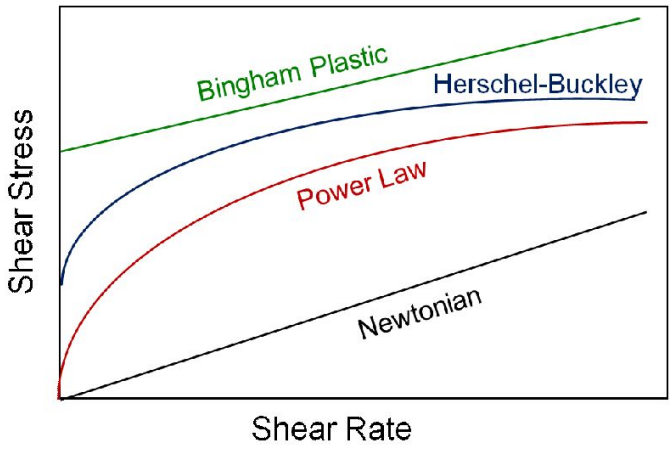

Figure 3.6: Graphical representation of different rheology models (Montgomery, 2013, p. 17)

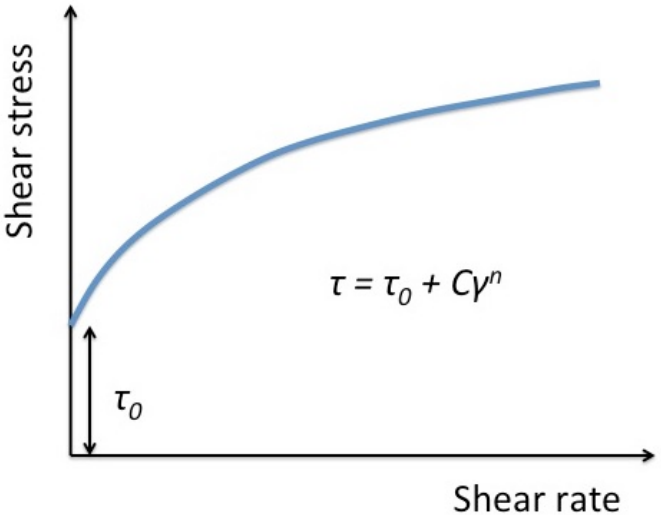

Figure 3.7: Graphical representation of Herschel-Bulkley model with yield point τ_0 (Figure is modified from AZoM (2013))

The viscosity versus shear rate plot can help determine the rheology model by looking at the trend of the viscosity. For the Power law model to be the more correct it is assumed that the viscosity should be decreasing with increasing shear stress, meaning that the fluid is shear thinning and are behaving like the dotted line in Figure 3.8. For the Herschel-Bulkley model to be the more correct model to use, a yield viscosity should to be observed before the viscosity starts to decrease, like it is shown for the solid line in Figure 3.8.

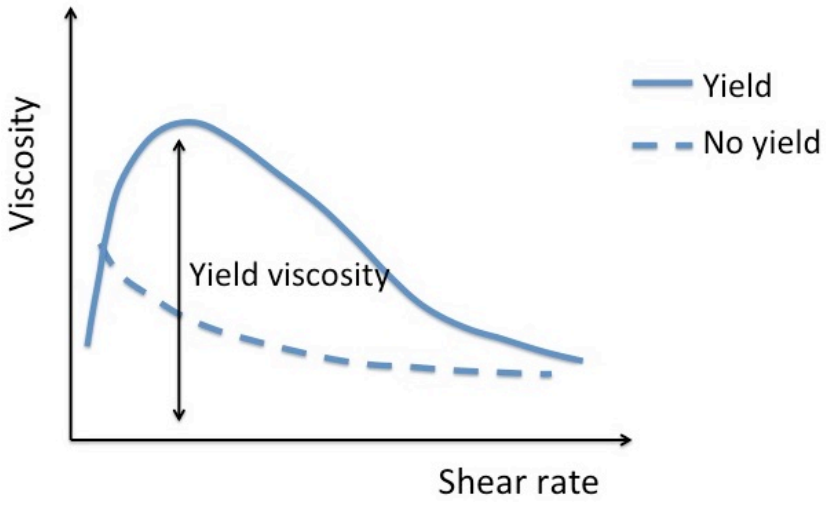

Figure 3.8: Showing yield viscosity (Figure is modified from AZoM (2013))

4 Experiments

The purpose of these experiments is to investigate W/O emulsion behavior in general; meaning in terms of rheology and aging, with special focus on emulsion flow in pipes. The objective of the pipe flow experiments is to check if emulsion flow can be predicted based on emulsion properties and two flow models. To study the rheological properties an Anton Paar modular compact rheometer (MCR) is used, providing shear rates, shear stress and viscosity. Aging effects are investigated by looking at droplet size distribution by using microscopic image analysis, together with visual inspection. After aging the emulsions are run through the MCR again. How temperature is affecting rheology and aging is also studied.

Emulsion parameters estimated from the MCR measurements, combined with the Power law flow model, are used to design the flow facility. After building and testing this flow capacity setup, the different emulsions are run through it. These measured flow rates are compared to the flow rates predicted from the two flow models and emulsion parameters.

In this chapter the procedures will be presented together with apparatus and software used. Some results will also be presented in the form of plots and tables, but the majority of results will be presented in Chapter 5.

4.1 Emulsion Preparation

To create the W/O emulsions, engine oil was chosen after discussion with K. Gåseidnes. This oil contains a W/O-emulsifier, is easy accessible and does not draw away attention from the results by chemical discussion. It is reasonable to believe that emulsions made out of this oil would show similar rheological properties as a crude oil emulsion, however this oil will not be able to represent dispersion and natural creation of emulsions in the sea. Even so, this oil is convenient for studying emulsion properties, since the oil does not have to be evaporated in order to be emulsifiable. One soybean oil emulsion was also created, chosen based on its promising tendency for behaving viscoplastically during experiments for the specialization project. It was not clear if the engine oil emulsions would behave in a viscoplastic manner, so in case they would only behave like a shear thinning fluid it was necessary to have another emulsion as well.

Instead of using tap water or distilled water, saltwater with 3 wt% NaCl was used. To be able to look at the emulsion in a microscope it had to be dissolved in clear oil, and Exxsol D60 was chosen for this purpose.

To distinguish between emulsions made with engine oil and soybean oil, the emulsions will be marked with a capital E (engine oil) or S (soybean oil) before the numbers indicating water and oil fraction. For example E30-70 is an emulsion created with engine oil containing 30% water and 70% oil, and S60-40 is created with soybean oil containing 60% water and 40% oil. All emulsions will be W/O emulsions, so this will not be specified. More detailed descriptions emulsion mixing, design of the flow facility and execution of the experiments will now be explained in the upcoming sections.

4.1.1 Fluids Used

The two oils used to create emulsions and the oil used to dissolve the emulsion will be shortly presented here. In addition, saltwater and soybean oil emulsifiers will be presented.

The engine oil is of the type 15W-40 and is designed for petrol and diesel engines, containing long chain calcium alkaryl sulfonate and succinimide polyamine polyolefin. The naming indicates a multi-grade oil, meaning that it has a wide temperature range and has been tested for colder temperatures than 100°C. The color of the oil can be seen in Figure 4.1.

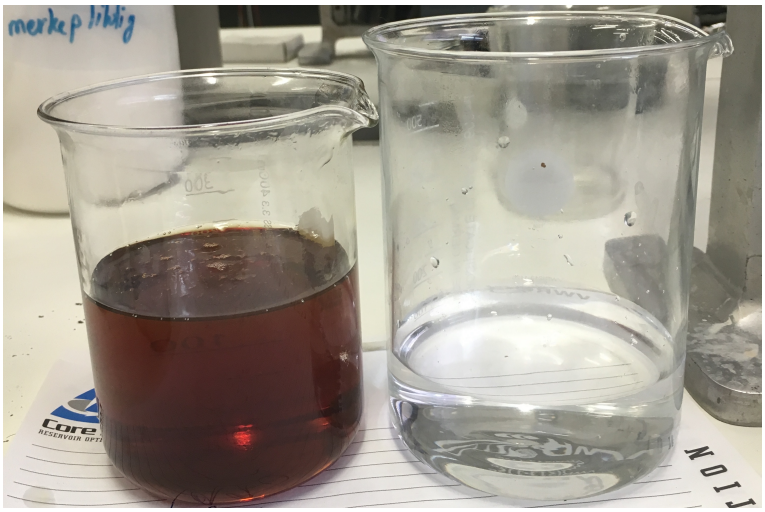

Figure 4.1: 15W-40 engine oil to the left, saltwater to the right

The soybean oil was mixed with two margarine emulsifiers: Palsgaard® PGPR 4175 and Palsgaard® DMG 0298. Palsgaard® PGPR 4175 is a polyglycerol polyricinoleate (PGPR), which is a synthetic molecule often used in W/O and W/O/W emulsions. Palsgaard® DMG 0298 is a distilled monoglyceride of vegetable fatty acids used to emulsify low fat and very low fat margarine. PGPR 4175 increases the viscosity of the emulsion and both emulsifiers reduces interfacial tension between water and oil, making it possible to create a stable and homogeneous W/O emulsion. The emulsifiers can be seen in Figure 4.2, and the soybean oil mixed with emulsifiers in Figure 4.3.

Figure 4.2: PGPR 4175 to the left and DMG 0298 to the right

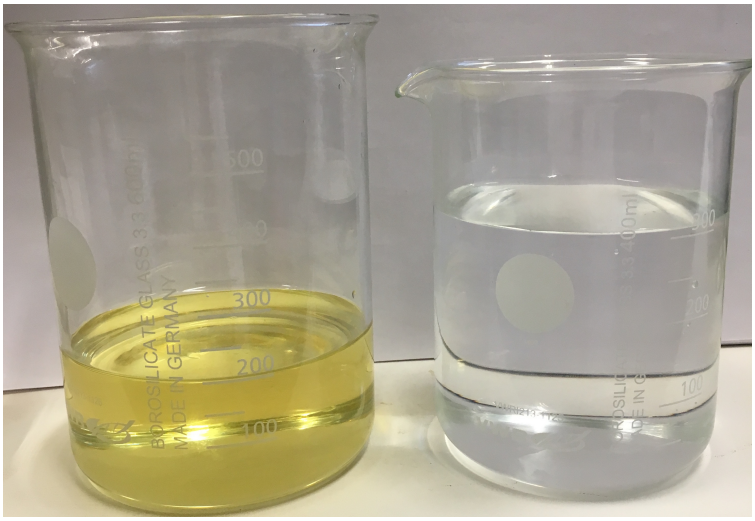

Figure 4.3: Soybean oil to the left, saltwater to the right

To mix the emulsifiers into the soybean oil, they were heated with a portion of oil on IKAMAG RCT as seen in Figure 4.4. IKAMAG RCT is a magnetic stirrer with a variety of mixing speeds and also additional temperature control for heating up the medium (IKA, 2016).

Figure 4.4: IKAMAG RCT

Saltwater was created by mixing distilled water with 3 wt% NaCl. The saltwater was prepared in a 2000 ml volumetric flask. 60 g NaCl was weighed up in the volumetric flask, before distilled water was added until the scale showed 2000 g. Then IKAMAG RCT was used to mix the solution for 15-20 minutes.

The major components in Exxsol™ D60 include normal paraffins, isoparaffins and cycloparaffins. It is produced to be a low odor and low aromatic hydrocarbon solvent, by treating it with hydrogen in the presence of a catalyst (ExxonMobil, 2016, p. 1). This oil was chosen since it is light and transparent.

The oil properties for both engine oil and soybean oil had to be specified at laboratory temperature, 20 °C. Density was found by using a pycnometer, and the results are presented in Table 4.1.

Table 4.1: Densities for the fluids used to create emulsions

Fluid	**Density**
15W-40 engine oil	0.880 g/cm^3
Soybean oil	0.9180 g/cm^3
Palsgaard® DGPR 4175	0.9829 g/cm^3
Palsgaard® DGM 0298 (melted)	0.9575 g/cm^3
Saltwater 3 wt% NaCl	1.0200 g/cm^3

Interfacial tension between the engine oil and the saltwater was measured by using a drop shape analyzer. The Drop Shape Analyzer DSA100S (seen in Figure 4.5) is an instrument for measuring surface tension and interfacial tension by using the pendant drop method (Kruss-GmbH, 2017). The Young-Laplace equation, already presented in Equation (2.3), is used to calculate the interfacial tension between the inner and outer phase:

$$\Delta p = \sigma\left(\left(1/r_1\right)+\left(1/r_2\right)\right) \tag{2.3}$$

Figure 4.5: Drop Shape Analyzer DSA100S (Kruss-GmbH, 2017)

The pendant drop method was performed with the engine oil as drop phase and saltwater as the surrounding phase, reporting mean interfacial tension presented in Chapter 4.2.1. Measurements were conducted at three temperatures: 4, 20 and 60 °C.

4.1.2 Mixing

All emulsions were mixed by using a Waring 8010ES Two Speed Blender as seen in Figure 4.6. All emulsions were mixed at the lowest mixing speed corresponding to 18 000 RPM.

Figure 4.6: Waring 8010ES blender (Clarkson-Laboratory, 2017)

The engine oil emulsions created are summarized in Table 4.2, together with the corresponding amounts of oil and water used. 400 ml was mixed at a time since it gave a properly mixed and stable emulsion. The maximum water content was determined by trial and error, and when the water content reached 70%, the emulsion showed instability immediately after mixing. Therefore maximum water content was set to 60%. Since the emulsifier was already in the oil, the emulsions consisted of engine oil and saltwater only.

Table 4.2: Water and oil amounts for the different engine oil emulsions

Name of Emulsion	Water Content	Water Amount [g]	Oil Amount [g]
E60-40	60%	244.800	140.080
E50-50	50%	204.000	175.100
E40-60	40%	163.200	210.120
E30-70	30%	122.400	245.140

The quantities of water and engine oil were prepared, adjusted to the desired water content for each emulsion. Since the engine oil was quite viscous it was more accurate to weigh the oil than use a graded cylinder. To convert volume to mass the following relation were used:

$$m = \rho \cdot V \tag{4.1}$$

To create the emulsion, the whole amount of oil and water was poured into the blender before it was mixed for 90 seconds. Figure 4.7 shows the emulsion right after mixing.

Figure 4.7: Engine oil emulsion right after mixing

The soybean oil emulsion created is presented in Table 4.3, with the desired amounts of oil, emulsifiers and saltwater. The amounts are adjusted to a total volume of 500 ml, since this was a volume giving stable soybean oil emulsions in the project thesis.

Table 4.3: Water, oil and emulsifier amounts for the S60-40 emulsion

Ingredient	**Volume percent**	**Amount [ml]**	**Amount [g]**
Soybean oil	39.60	198.0	181.764
Saltwater 3 wt%	60.00	300.0	306.000
DGPR 4175	0.200	1.000	0.983
DMG 0298	0.200	1.000	0.958
Total	100.0	500.0	489.705

Since one emulsifier was solid and the other was very viscous, the emulsifiers had to be heated and melted together with the soybean oil. A small beaker with both emulsifiers and a portion of oil was placed on IKAMAG RCT to be heated to 40 °C, as seen in Figure 4.8. It was not necessary to use the magnet stirring in this case.

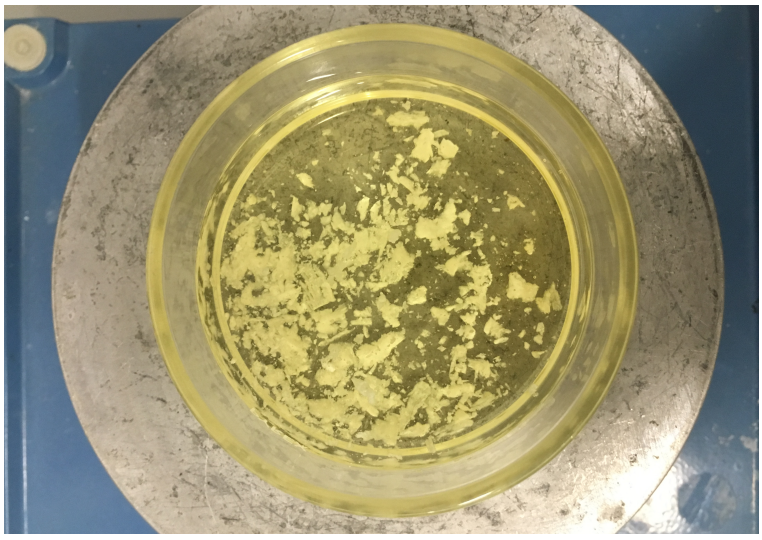

Figure 4.8: Emulsifiers in oil during heating

The melted emulsifiers and the whole amount of oil and water were poured into the blender. Several mixing durations were tested, and 15 seconds were chosen. If mixed for a longer time

the emulsion quickly became too viscous to flow, and if mixed for a shorter time the emulsion did not become stable. The fresh emulsion can be seen in Figure 4.9.

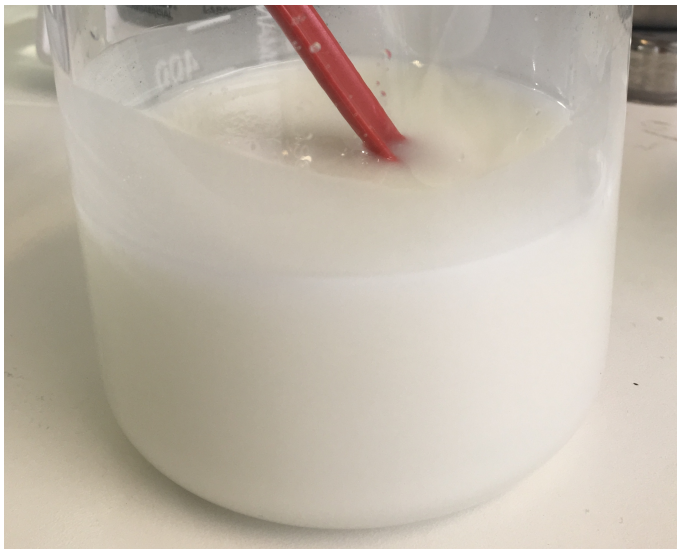

Figure 4.9: The soybean oil emulsion right after mixing

Immediately after mixing some air bubbles were present on the emulsion surface, especially for the engine oil emulsion. Before doing rheological measurements a needle was used to slightly stir the emulsion surface and remove most of the air bubbles.

4.1.3 Water-in-Oil Emulsion Test

After the emulsions were mixed, the emulsion class had to be checked. To do so, water was poured into the mixer after pouring out the emulsion. There would still be some emulsion left in the mixer due to its viscous behavior. Emulsion droplets would form and if these droplets did not dissolve, the emulsion should be W/O. The same could be done with oil instead of water, where the emulsion droplets should dissolve in the oil to prove that the emulsion was W/O.

As the pictures in Figure 4.10 and Figure 4.11 shows, both the engine oil and soybean oil emulsions were indeed W/O, since the emulsion droplets did not dissolve in water. The engine oil emulsion was sticking more to the wall than the soybean oil emulsion, so there are more droplets floating around for the latter. Even if the droplets did flocculate for both emulsions, stirring by hand could break them up again.

Figure 4.10: Engine oil emulsion in water

Figure 4.11: Soybean oil emulsion in water

In Figure 4.12 engine oil is poured into the engine oil emulsion. One can see that the emulsion is behaving completely different than in Figure 4.10. Instead of forming droplets the emulsion looks dragged out, indicating that it is soluble in the oil. When stirring gently by hand, the emulsion easily dissolved, confirming that it is is indeed a W/O emulsion.

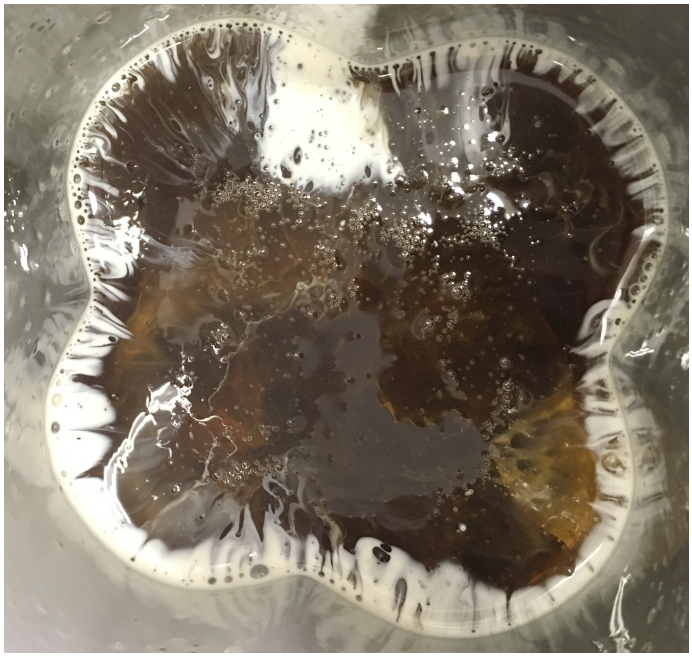

Figure 4.12: Engine oil emulsion in engine oil

4.2 Properties Investigated

4.2.1 Interfacial Tension

When doing measurements at 4 °C, the first 12 measurements (also called steps) did not have the correct temperature, and were not included in the calculation for mean interfacial tension. For the measurements at 20 °C the five first steps were removed since these were deviating a lot from the others, and were thought of as outliers. For the 60 °C case all measured steps were included to find mean interfacial tension. The mean interfacial tensions calculated are summed up in Table 4.4, and the measurements taken at the different steps can be seen in Figure 4.13.

Table 4.4: Interfacial tension for engine oil in saltwater for different temperatures

Temperature	Interfacial tension [mN/m]
4 °C	17.255 ± 0.567
20 °C	10.103 ± 0.497
60 °C	8.454 ± 0.618

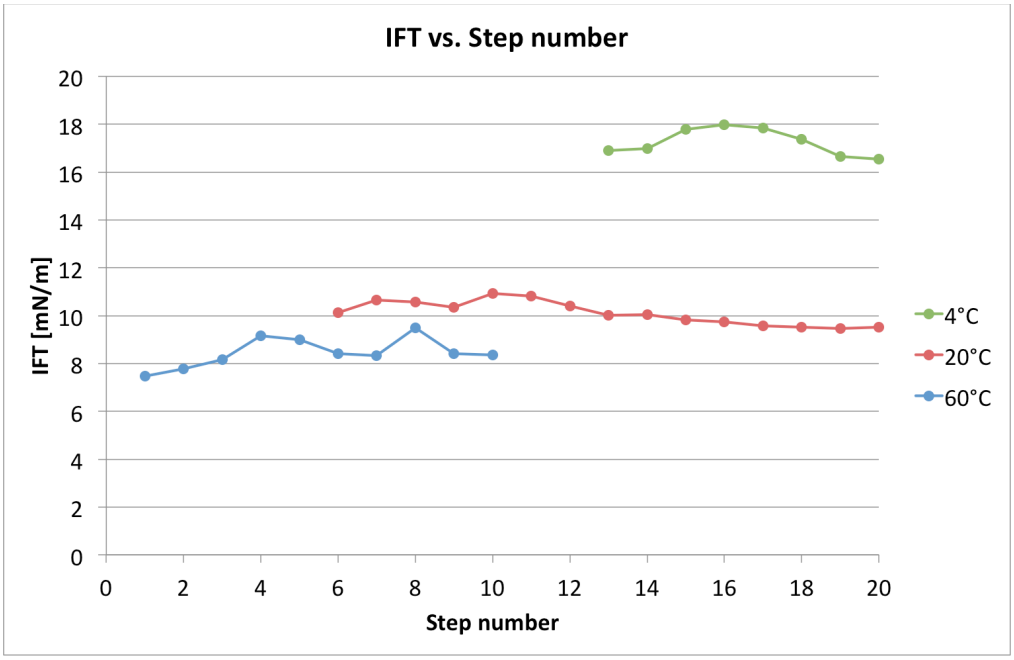

Figure 4.13: Interfacial tension measured during different steps at three temperatures

The interfacial tension is decreasing with increasing temperature, which is in line with the presented theory. Based on Equation (2.1), the interfacial tension will decrease with decreasing droplet radius. Figure 4.14 is confirming this, where the droplet size is decreasing with increasing temperature, consequently decreasing with decreasing interfacial tension.

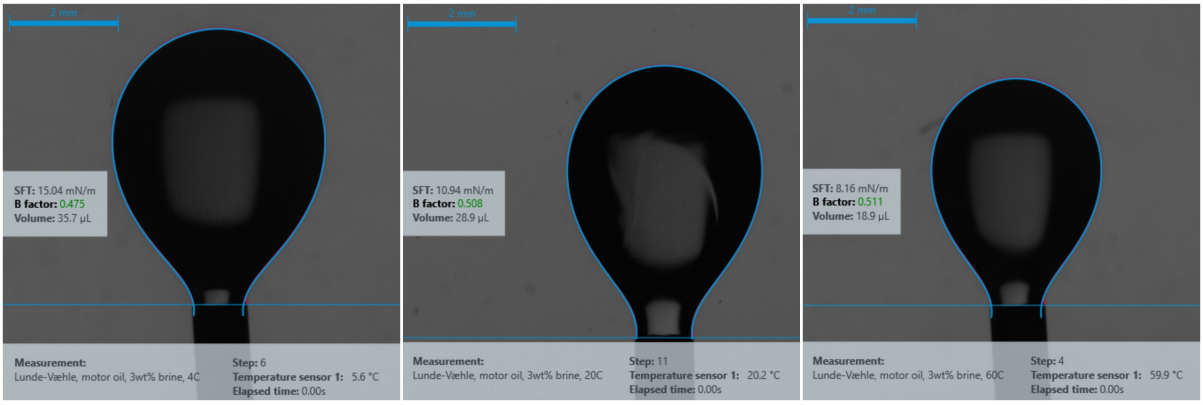

Figure 4.14: Left to right: Droplets at 4, 20 and 60 °C during measurements taken by the Drop Shape Analyzer.

4.2.2 Emulsion Density

At first the densities of the emulsions were measured by using a pycnometer, but since the emulsions were quite viscous it was more convenient to use a mud balance. This was done by filling up the volume cup on the mud balance, putting on the lid to remove air bubbles, before wiping off excessive emulsion. The slider-weight was adjusted so the balance was level, and the density could be read off by the position of this slider weight. The emulsion densities are presented in Table 4.5, but will be further discussed in Chapter 5.1.

Table 4.5: The densities for the different emulsions

Name of Emulsion	Density [kg/m^3]
E30-70	815
E40-60	870
E50-50	910
E60-40	940
S60-40	950

4.2.3 Rheology

All the rheological measurements were taken by a modular compact rheometer, Anton Paar MCR 302 (can be seen in Figure 4.16). This MCR has a variety of measurement opportunities both in rotational and oscillatory mode, and provides accurate temperature control (Anton-Paar-GmbH, 2016, p. 8). Cylinder measuring system CC27 was used for these experiments, and a schematic of the cylinder during measurements is shown in Figure 4.15.

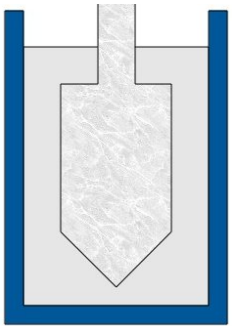

Figure 4.15: Schematic of the measuring cylinder in the sample cup (CyberColloids, 2017)

Figure 4.16: Picture of the Anton Paar MCR 302 (UW, 2017)

Before starting the apparatus, a connected water flow and airflow had to be switched on. While the apparatus was initializing, the sample was poured into the sample cup such that the fluid level matched the fill line. The desired measuring temperature was set when the measuring cylinder was lowered into the emulsion. Shear stress and shear rate were examined over a shear rate ranging from 0 to 1200 s^{-1}, but in cases where the emulsion broke the measurements were stopped before reaching1200 s^{-1}. Viscosity was examined over the same shear rate range.

The fluids used to create the emulsions, meaning soybean oil, engine oil and 3 wt% saltwater, was first measured in the MCR to see their rheological relationship. Measurements were taken at 20 °C, and can be seen in Figure 4.17 and Figure 4.18. It can be seen that engine oil has higher shear stress with shear rate and also higher viscosity than soybean oil and saltwater.

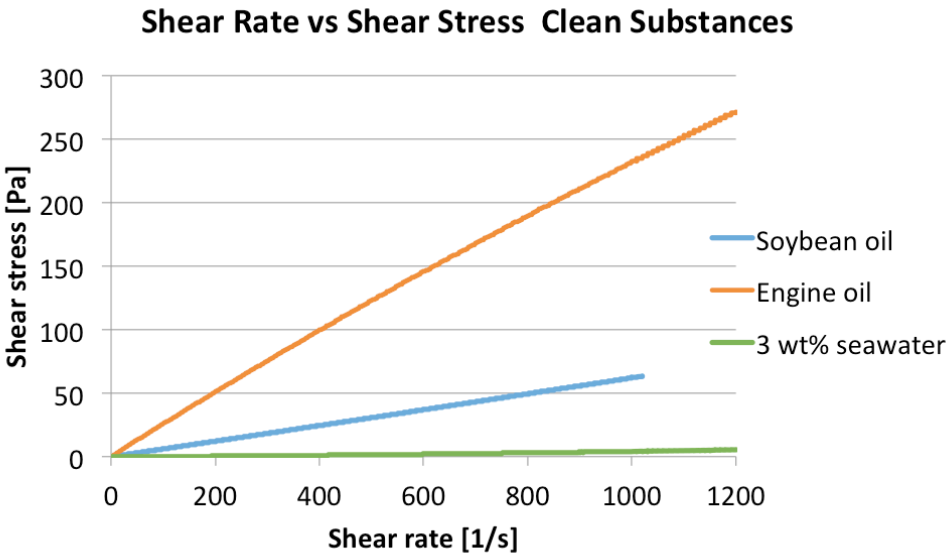

Figure 4.17: Shear stress vs. shear rate for soybean oil, engine oil and 3 wt% saltwater

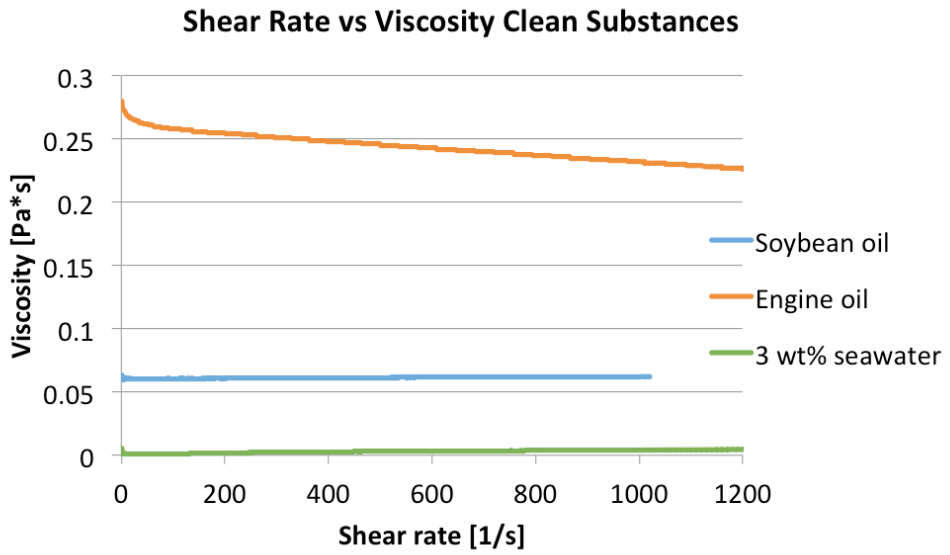

Figure 4.18: Viscosity vs. shear rate for soybean oil, engine oil and 3 wt% saltwater

After this, the different emulsions could be evaluated in the MCR to find rheological properties at 20 °C, before they were run in the flow capacity setup. The data found by the MCR are presented in plots such as in Figure 4.19. Based on these plots found by the MCR, the appropriate rheology model could be found, and the corresponding flow model were used to predict the flow rate based on the estimated emulsion parameters.

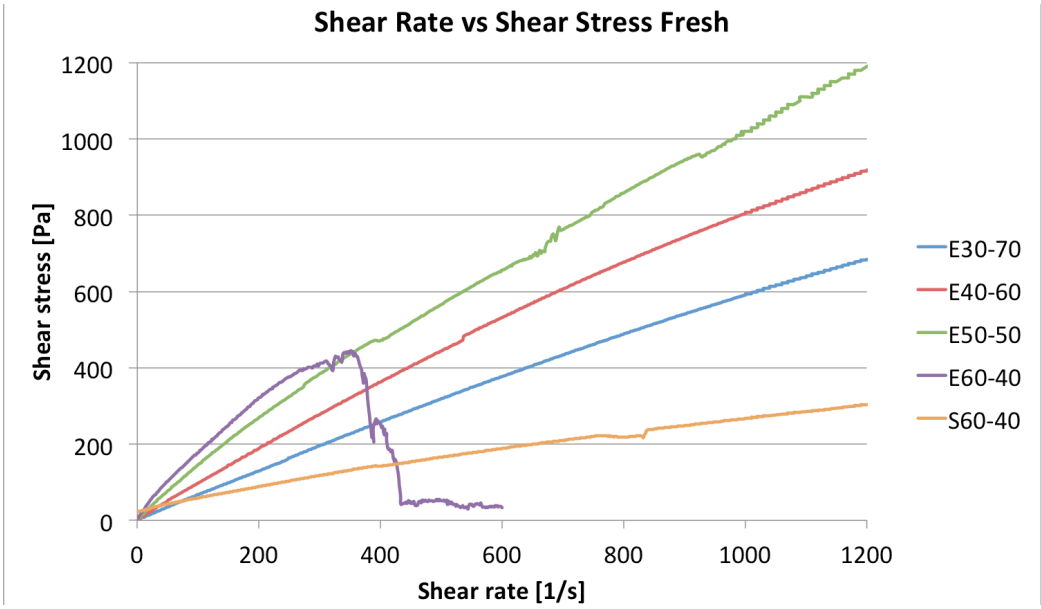

Figure 4.19: Example of plot found from MCR

4.2.4 Temperature Effect on Rheology

The engine oil emulsions with the lowest and highest water content, E30-70 and E60-40, were run in the MCR on lower and higher temperatures, namely 4 °C and 60 °C. The procedure was the same as stated in the previous section, and one of the plots found can be seen in Figure 4.20

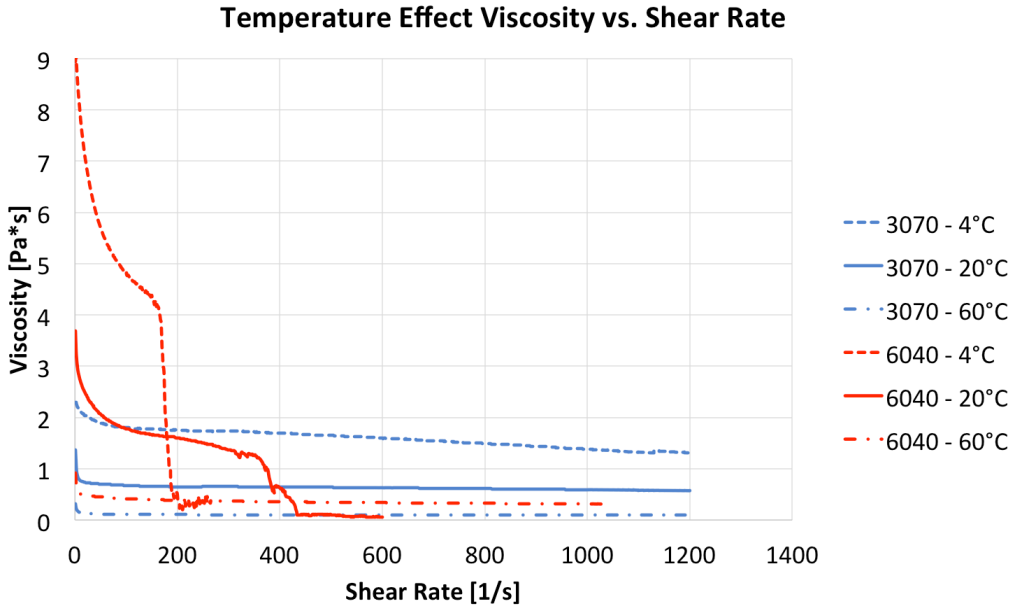

Figure 4.20: Viscosity vs. shear rate plot showing the effect of varying temperature

4.2.5 Aging Effect on Rheology

All the emulsions were run in the MCR after aging, as fresh, 4 hours, 24 hours, 5 days and 12 days old to see if the aging had any impact on the emulsion rheology. One plot and a zoomed section of this can be seen in Figure 4.21 and Figure 4.22, but most results will be discussed in Chapter 5.5.2.

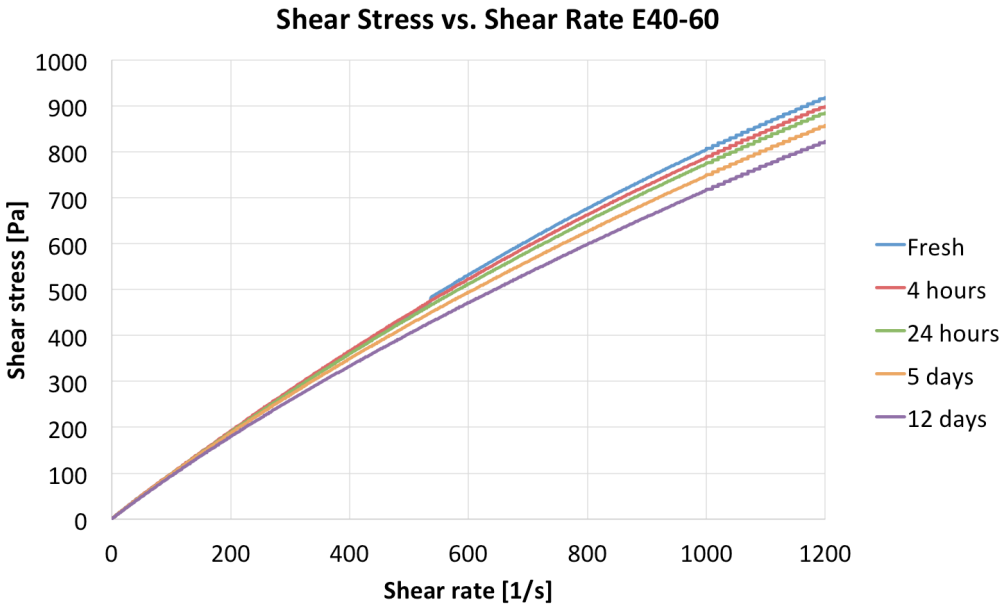

Figure 4.21: Shear stress vs. shear rate with aging for E40-60

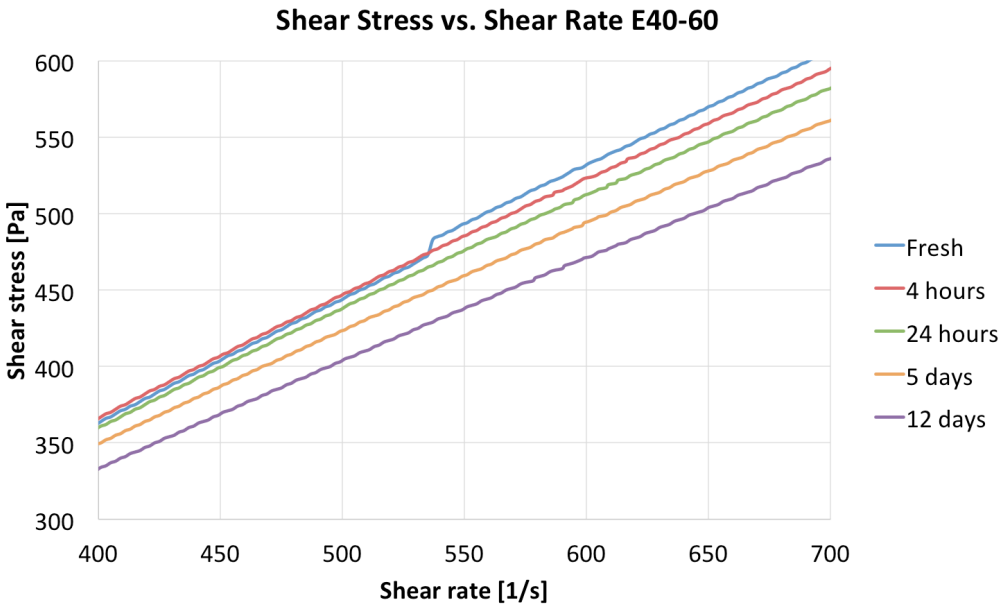

Figure 4.22: Zoomed section of Figure 4.21

4.3 Flow Experiments

4.3.1 Equipment Design

To design the flow capacity setup, the E60-40 emulsion was tested in the MCR, to find emulsion parameters for prediction of flow rate. This flow facility was inspired by a capillary viscometer, which measures time taken for a defined quantity of fluid to flow through a capillary with known diameter and length (SI-Analytics, 2017). By visually inspecting the shear stress versus shear rate plot and viscosity versus shear stress plot for the E60-40 emulsion, the rheology model was found to be Power law. Thus, the Power law flow model would be used to predict flow rate. Even if the flow capacity setup was designed based on calculations with Power law model, it was reasonable to believe that the same flow capacity setup could be used for the Herschel-Bulkley model as well.

After determining the rheology and flow model, the corresponding script had to be run in MATLAB, which is a software used to solve engineering problems built on a matrix-based language. All the MATLAB scripts can be found in Appendix C, and will also be further described in the next section. First the "Parameters_PL" script had to be run, estimating the Power law parameters C (consistency parameter) and n (flow behavior index) from the MCR data. After estimating these parameters, the next script, "Flowrate_PL", predicted the flow rate based on these same MCR data and the parameters found, using the relation showed in Equation (3.8). Since the dimensions of the flow facility (such as pipe diameter and length) were to be determined, these had to be put into the script as guesses. If the script gave turbulent flow or a severe entry length, a new guess had to be set as input. After several guesses the dimensions showed in Table 4.6 was chosen, and the flow capacity setup was created with great help from H. Myhren. The setup can be seen in Figure 4.23 and Figure 4.24.

Figure 4.23: Picture of the designed flow facility

Table 4.6: Dimensions for the flow capacity setup and relevant parameters

Description	**Symbol**	**Dimension**
Total length of pipe	L_p	1.8000 m
Average fluid height in tank	$h_{avg\ fluid}$	0.0736 m
Length of pipe under tank	$L_{under\ tank}$	1.7900 m
Total average fluid height	Δh_{avg}	1.8636 m
Inner diameter of pipe	D_p	0.0250 m
Inner radius of pipe	R_p	0.0125 m

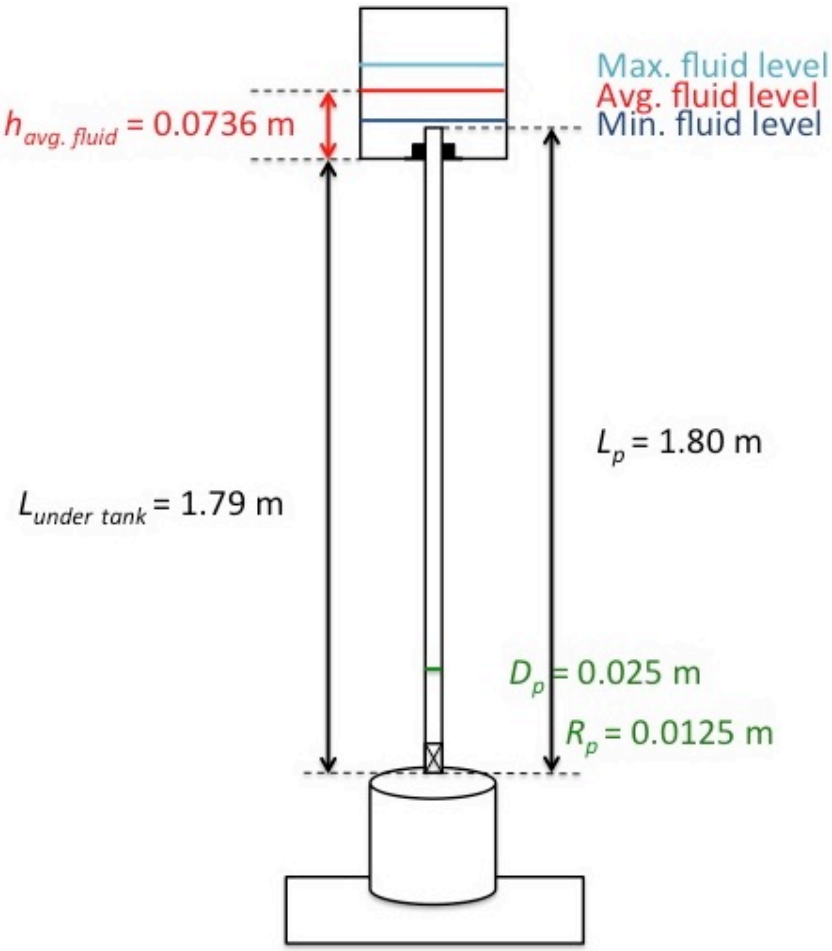

Figure 4.24: Drawing of the flow capacity setup, showing the most relevant dimensions

As can be seen in Figure 4.24 there are three fluid levels in the tank: maximum, minimum and average fluid height. Maximum is when the full emulsion volume is poured into the setup and minimum is when the valve is closed after a run. As indicated on the minimum fluid level line, the experiment was stopped before the liquid level reached the pipe inlet. The average fluid height was used since the bottom of the tank was not completely even, and thus the measurements of the maximum and minimum fluid level was not constant.

The flow facility was installed over a scale, such that the weight could be continuously recorded as the emulsion was flowing through the pipe. This provides higher accuracy than if the emulsion level was recorded with the bare eye.

4.3.2 Model Parameter Estimation

As done in the design process, the shear stress versus shear rate and viscosity versus shear stress plot were investigated for each emulsion, to determine the appropriate rheology and flow model. When the rheology model was determined, the scripts calculating flow rate with the corresponding flow model had to be run in MATLAB for each emulsion.

For Power law the following parameters had to be estimated: consistency parameter C and flow behavior index n. The script "Parameters_PL" was run in order to find these, reading the file with emulsion parameters obtained by the MCR, plotting the data and fitting a power series model to the plot. For the Power law model the fitted line was created by using the built-in MATLAB function "`fit`" and model type '`power`', (MathWorks, 2016). After this, the script "Flowrate_PL" predicted the flow rate based on the same emulsion parameters, density and the Power law parameters found. The flow rate was predicted by using the relation showed in Equation (3.8).

For Herschel-Bulkley the following parameters had to be estimated: consistency parameter C, flow behavior index n and yield point τ_0. The script "Parameters_HB" was run in order to find these, reading the file with emulsion parameters obtained by the MCR, plotting the data and fitting a power series model to the plot. For the Herschel-Bulkley model the fitted line was created by using the "`fit`" function and model type '`power2`'(MathWorks, 2016). After this the script "Flowrate_HB" predicted the flow rate based on the same emulsion parameters, density and the Herschel-Bulkley parameters found. The flow rate was predicted by using the relation showed in Equation (3.11).

Both the "Flowrate_PL" and the "Flowrate_HB" scripts calculate the Reynolds number and prints out the associated flow regime, to make sure the flow is not intermediate or turbulent. No built-in functions were used for this, only for-loops and execute statements. The entry length was also calculated in the scripts, to check that the flow became fully developed within a smaller part of the pipe length.

After the appropriate flow models were used to predict the flow rates, the inappropriate model was used to see if this had an impact on the results. The procedure was the same as explained over here, except that the inappropriate model was chosen on purpose. This means

that the Herschel-Bulkley model was used for shear thinning fluids, and Power law model was used for viscoplastic fluids.

4.3.3 Flow Measurements vs. Model Prediction

After the flow capacity setup was designed, all emulsions shown in Table 4.2 and Table 4.3 were mixed using the procedure already explained in Chapter 4.1.2. The volume chosen for flowing through the flow facility was 3 liters so eight 400 ml beakers with engine oil emulsion were mixed, and seven 500 ml beakers with soybean oil emulsion. The beakers were added together in 1 liter bottles, and parts of the excessive volume was used to measure density of the emulsion.

The whole emulsion volume was poured into the tank on the flow facility, with the valve closed such that the pipe became completely filled. Measurements started by opening the valve and simultaneously starting the timer, and the valve was closed before the emulsion level reached the pipe inlet. This was done since the flow would slow down significantly if the fluid level reached the pipe inlet. All emulsions were run through the flow capacity setup twice in a row before the data was analyzed and flow rates were found by Equation (3.5). Then these measured flow rates could be compared to the flow rate predicted from emulsion parameters and flow models.

Measured flow rates for shear-thinning emulsions were compared to flow rates predicted by Power law model, while measured flow rates for viscoplastic emulsions were compared to flow rates predicted by Herschel-Bulkley model. To look at the effect of using the inappropriate model, predictions were also done with the opposite model. Percentage deviations were used to easier compare the measured and predicted results:

$$\text{Percent deviation} = \frac{\left(\text{observed value} - \text{expected value}\right)}{\text{expected value}} \tag{4.2}$$

where observed value was the flow rate measured in the flow capacity setup, and expected value was the flow rate predicted by flow models based on emulsion parameters. These results will be presented in Chapter 5.2 through Chapter 5.4.

4.4 Droplet Size Estimation and Aging

The aging and droplet size estimation was only investigated for the engine oil emulsions, since the soybean oil emulsion was made for flow rate comparison.

4.4.1 Maximum and Average Droplet Size

Before the droplet size was studied by microscopic image analysis, Equation (2.2) was used to predict the possible maximum and average droplet size during mixing. First the energy dissipation had to be found:

$$\varepsilon = \frac{P_{mixer}}{m_{emulsion}} = \frac{P_{mixer}}{\rho_{emulsion} \cdot V_{emulsion}} \tag{4.3}$$

where P is power in [W], m is mass in [kg], ρ is density in [kg/m^3] and V is volume in [m^3]. When the energy dissipation was calculated, the maximum droplet size, D_{95}, could be predicted by using Equation (2.2). Then the average droplet size, D_{avg}, could be predicted by

$$D_{avg} = 0.3 \cdot D_{95} \tag{4.4}$$

4.4.2 Droplet Size Distribution

The droplet size distribution was looked at in different aging stages, by studying the emulsions in an Optika microscope connected to a microscope digital camera of the type OLYMPUS UC90 (as seen in Figure 4.25). This camera is able to deliver images up to 4K ultra-high-definition, with maximum image information and noise reduction technology (Olympus-Lifescience, 2016).

Figure 4.25: Optika microscope connected to Olympus UC90 microscope digital camera

To get a better image in the microscope, the emulsion droplet was mixed with Exxsol D60 before placing the droplet between two microscopic slides. 0.5 ml Exxsol D60 was stirred in a small container together with a small emulsion droplet from the outside of a plastic pipette. If this had not been done, the emulsion would look like the image to the left in Figure 4.26. The image to the right would clearly be easier to process than the image to the left, where the number of droplets is larger and the droplets are lying very close.

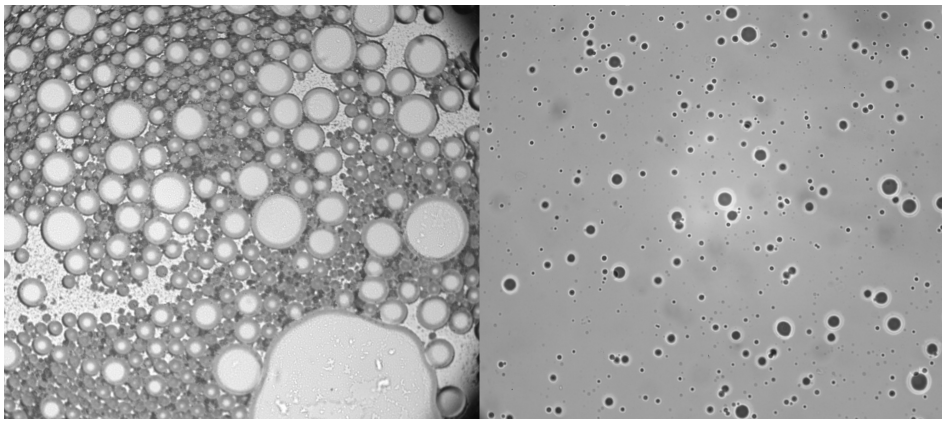

Figure 4.26: Left: W/O emulsion not mixed with Exxsol D60. Right: W/O emulsion after being mixed with Exxsol D60

The emulsions were studied right after mixing, 4 hours, 24 hours, 5 days and 12 days after mixing. If some oil had been separated out on top with aging, the surface of the emulsion was slightly stirred by hand before taking measurements.

Images taken with the OLYMPUS camera were processed in the ImageJ software, which is a Java-based image-processing program. The software feature possibilities to calculate area and other pixel-value statistics, such as droplet diameter (Ferreira and Rasband, 2012). To be able to predict the droplet diameter, the droplet area, Feret diameter and minimum Feret diameter were found. Feret diameter is defined as: "The longest distance between any two points along the selection boundary, also known as maximum caliper" (Ferreira and Rasband, 2012). An overview of the operation order for the image processing in ImageJ can be seen in Table 4.7

Table 4.7: Overview of the operation order used when processing images in ImageJ

Operation order	**Operation**
1.	Set the scale
2.	Crop the picture
3.	Subtract background
4.	Change image to black and white
5.	Adjust brightness
6.	Adjust threshold
7.	Make image binary
8.	Remove noise
9.	Fill in holes (droplets)
10.	Convert to mask
11.	Watershed the droplets
12.	Check consistency with original image
13.	Define measurands
14.	Export results and save image

First, the scale had to be set to give the image the right dimensions. The scale provided on the original image was used, since this had a known length. Then a section of the image was cropped, before the background was subtracted to get a cleaner image of the droplets. The image was then changed to black and white, before the brightness and threshold could be adjusted. For threshold it was important to choose a threshold where the droplets were as

visible as possible without too much noise. To add several features the image was made binary.

Noise had to be removed manually, by comparison with the original image. If some of the droplets did not appear complete, the line around them had to be drawn manually. Now the command “fill in holes” were used, filling all complete droplets. After this, the picture was converted to mask, to allow the command “watershed”. This drew a thin line between droplets that were lying together. It was important to always check the consistency with the original image, to see the droplet pattern and check that noise was removed. Finally, the measurands could be defined and all droplets on the edges were excluded. The image was saved and the results exported to Excel, before the data was further evaluated in MATLAB.

To be able to predict the droplet size distribution based on the data obtained from ImageJ, the MATLAB script “volumedistribution” was used, which can be found in Appendix C. This script is calculating volume distribution for the droplets based on a lognormal distribution function. Lognormal distribution is a continuous probability distribution in which the logarithm of a variable has a normal distribution (Weisstein, 2016). An example of the shape of a lognormal probability density function (PDF) and a cumulative distribution function (CDF) is shown in Figure 4.27.

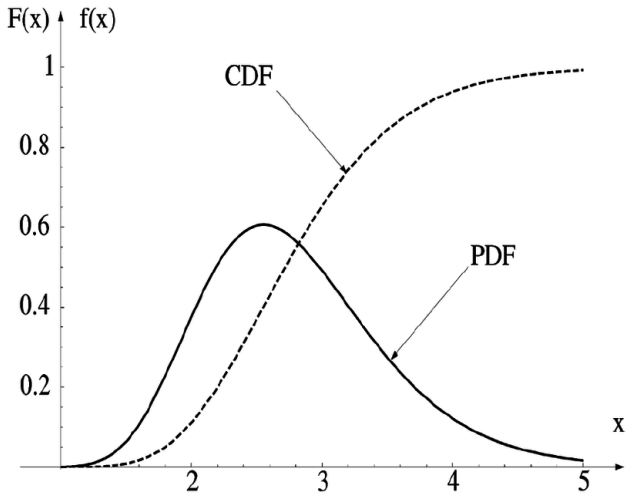

Figure 4.27: Lognormal PDF and CDF (Albadran, 2013)

The lognormal distribution is very convenient to use for finding the droplet size distribution, since it is dependent only on two variables: the location parameter μ and the scale parameter

σ. This simplifies the process, since the whole distribution can be described by these two parameters instead of thousands of measured points. What MATLAB does is to take the measured data, and find a lognormal distribution based on arithmetic variance Var[X], arithmetic mean E[X], the location parameter μ and the scale parameter σ. The following equations are used:

$$\mu = \log\left(\mathrm{E}[X]\right) - 0.5\log\left(1 + \frac{\mathrm{Var}[X]}{\mathrm{E}[X]^2}\right) \tag{4.5}$$

$$\sigma^2 = \log\left(1 + \frac{\mathrm{Var}[X]}{\mathrm{E}[X]^2}\right) \tag{4.6}$$

MATLAB also finds an optimized curve, which minimizes the distance between measured values and the lognormal prediction. This is done by the function ”optfun” which uses least squares method to optimize the distribution, and is also provided in Appendix C. The output from MATLAB will be a curve showing the CDF and the PDF, including the optimized distribution and the mean droplet volume as seen in Figure 4.28 and Figure 4.29.

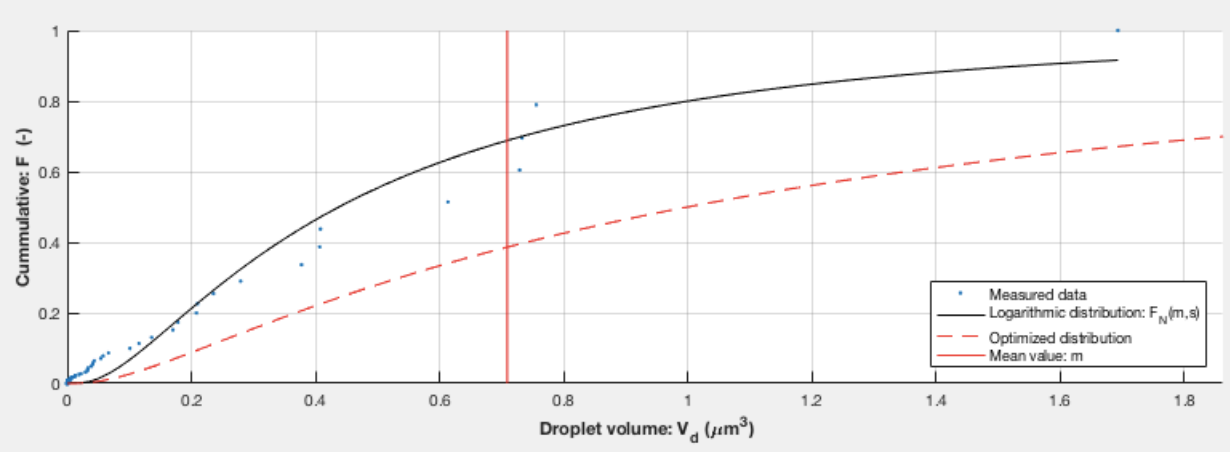

Figure 4.28: Cumulative distribution function (CDF) of the droplet volumes

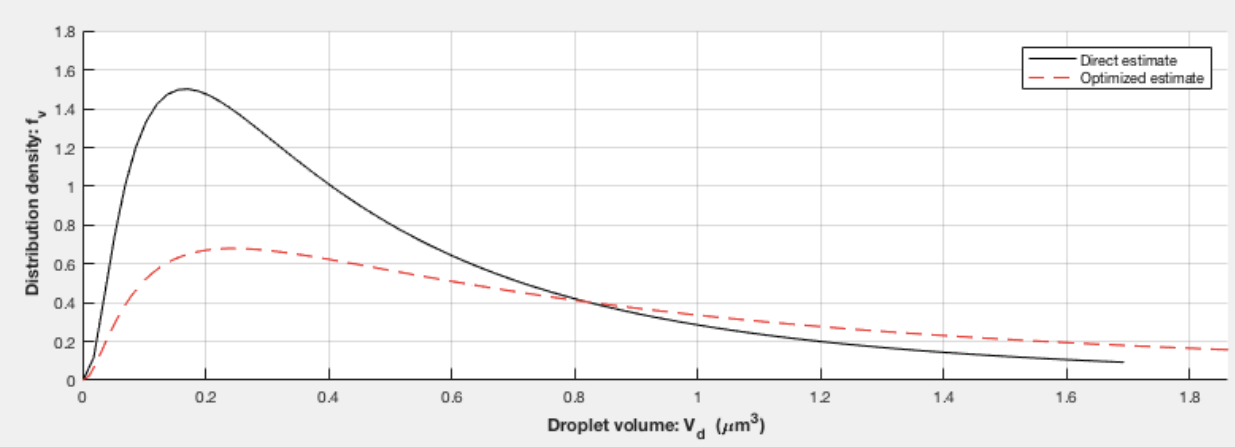

Figure 4.29: Probability density function (PDF) of the droplet volumes

However, not all the data provided by the scripts will be studied in the results. The focus will be on the measured droplet volumes (called measured data in Figure 4.28), the mean droplet size (red vertical line in Figure 4.28) and also the logarithmic distribution if it fits the measured points is well (black solid line in Figure 4.28). The measured droplet volumes will be displayed in separate plots, and the logarithmic distributions will be displayed together with the measured droplet volumes to check the fit, such as in Figure 4.30.

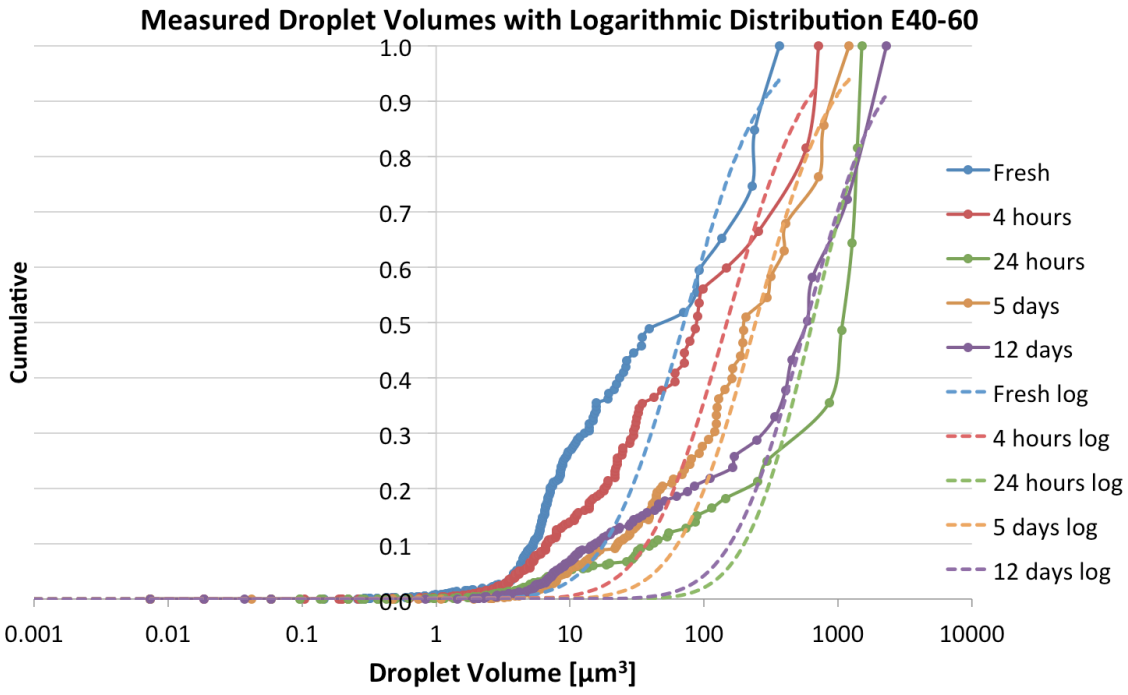

Figure 4.30: E40-60 emulsion with logarithmic volume distribution estimated from the measured droplet volumes found by microscopic image analysis, logarithmic x-axis

4.4.3 Visual Inspection in Varying Temperature

To study if higher or lower temperature would influence the aging process, two engine oil emulsions were put in a fridge with 4 °C and an oven with 60 °C. The emulsions chosen for this were E60-40 and E30-70, since these were the emulsions with highest and lowest water content. Right after the emulsions were mixed they were put in three 25 ml graduated cylinders, and one was put in the fridge, one in the oven and one was kept in the laboratory. Each emulsion was checked and taken pictures of with a regular camera in the following time intervals: 1, 2, 3, 4, 7, 10 and 22 days. When checking the emulsions it was looked for any visual signs of aging or breakdown.

5 Results and Discussion

The results obtained from the experiments will be presented and discussed in this section. Due to a large amount of results in the form of plots, most of these are moved to the appendices, respectively Appendix D through Appendix H. To make the results more readable, the presented results will be followed up by an analyzing discussion right after.

5.1 Emulsion Density

The soybean oil emulsion showed the highest density. This makes sense, since the soybean oil has higher density than engine oil, respectively 918 kg/m^3 compared to 880 kg/m^3. The soybean oil emulsifiers also have higher densities, 982.9 kg/m^3 and 957.5 kg/m^3. Even if the added amounts are small compared to the total volume, the emulsifiers might contribute to density increase to some extent. If the E60-40 emulsion is compared to the S60-40 emulsion, it has quite high density considering the difference in oil density.

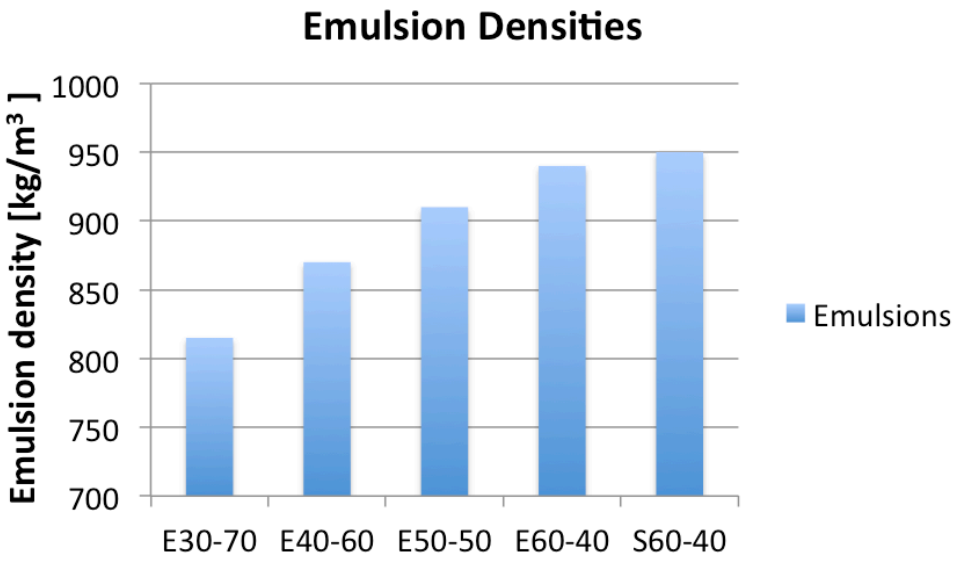

Figure 5.1: Graphic representation of the increase in density

All engine oil emulsions have increasing density with increasing water content as can be seen in Figure 5.1. The saltwater had a density of 1020 kg/m^3, which is higher than the engine oil, and the increase with water content is obvious.

5.2 Rheological Measurements by Modular Compact Rheometer

The MCR were used to take measurements of shear rate, shear stress and viscosity, where shear rate was examined up to 1200 s^{-1} and the temperature was kept at 20 °C. The engine oil emulsions with the highest and lowest water contents were studied in terms of temperature impact on rheology, where measurements were taken at 4 °C and 60 °C as well. Emulsion parameters found from the rheological measurements were used to predict the emulsion flow by Power law and Herschel-Bulkley flow models.

5.2.1 Shear Stress and Shear Rate

All the fresh emulsions are presented together in Figure 5.3. When looking at the plotted lines for the engine oil emulsions, they are starting approximately in zero. The shape of the plotted curves looks downwards concave, even if the curves are not completely smooth. Based on these two observations, the engine oil emulsions will be considered shear thinning and Power law model will be considered appropriate rheology and flow model.

For all engine oil emulsions the shear stress is decreasing with decreasing water content up to a shear rate of about 300 s^{-1}. At this point the E60-40-curve goes abruptly down, and a possible explanation for this is that the emulsion breaks. If this happens the water will no longer be dispersed in the oil, and the water could lubricate the surface of the measuring cylinder in the MCR. This would cause the dramatic decrease in shear stress. The emulsions with 30-50% water content did not break in the shear rate interval studied, and they all show higher shear stress when water content is increased.

The plotted line for the soybean oil emulsion, S60-40, starts in a value higher than zero and does not show as much downwards-concave shape as the engine oil emulsions. The fact that the curve is not starting at zero indicates a yield stress is needed to initiate the flow, and is more in compliance with a viscoplastic fluid. Therefore, Herschel-Bulkley model will be considered the appropriate rheology and flow model for the soybean oil emulsion. The S60-40 emulsion did not break in the shear rate interval, and it showed the lowest shear rate of all the fresh emulsions.

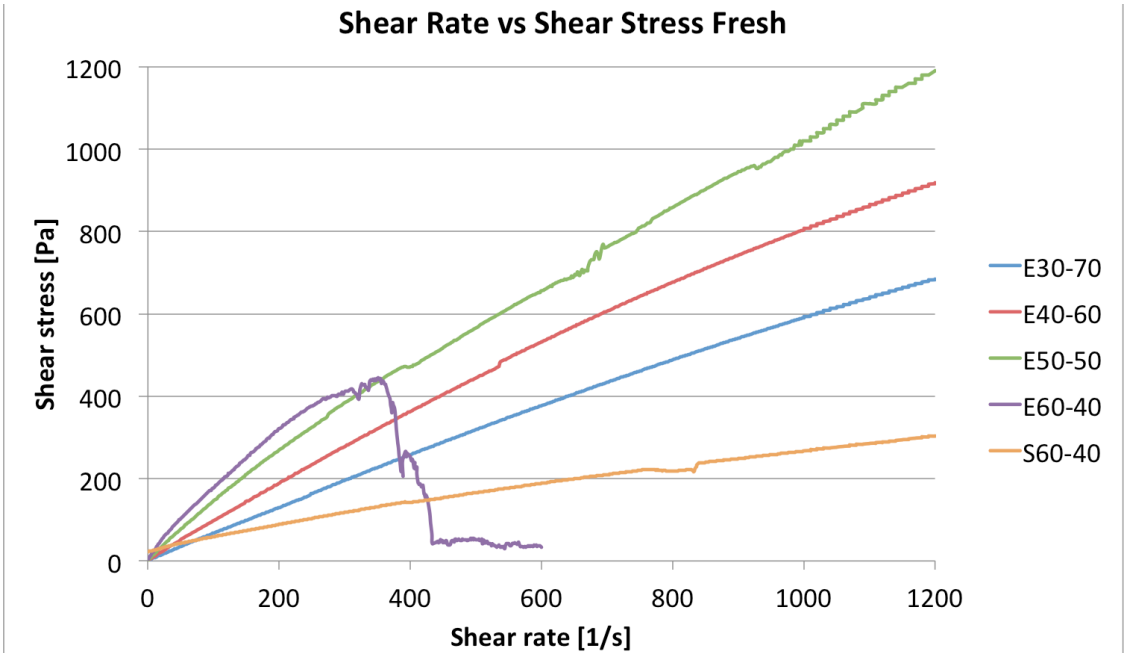

Figure 5.2: Shear stress vs. shear rate plot for all emulsions while fresh

5.2.2 Viscosity

To be able to plot all the emulsions in the viscosity versus shear rate plot, a secondary axis had to be set for the S60-40 emulsion. This emulsion starts out at a much higher viscosity than the other emulsions, and then quickly drops and ends up showing the lowest viscosity in Figure 5.4. Even if there is not shown a clear yield viscosity the behavior is still considered to be viscoplastic. This is based on the deviation from the other viscosity curves, and the fact that the shear stress versus shear rate curve indicated a viscoplastic fluid. Therefore the Herschel-Bulkley model is still assumed to be the appropriate rheology and flow model.

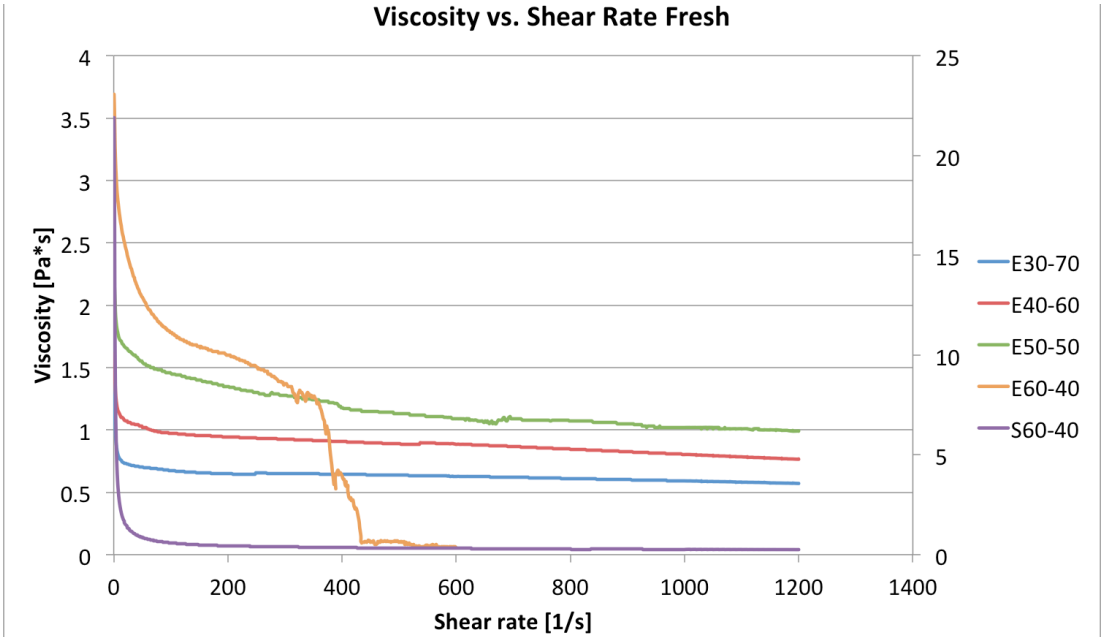

Figure 5.3: Viscosity vs. shear rate plot for all emulsions while fresh, with the S60-40 emulsion having a secondary axis on the right hand side

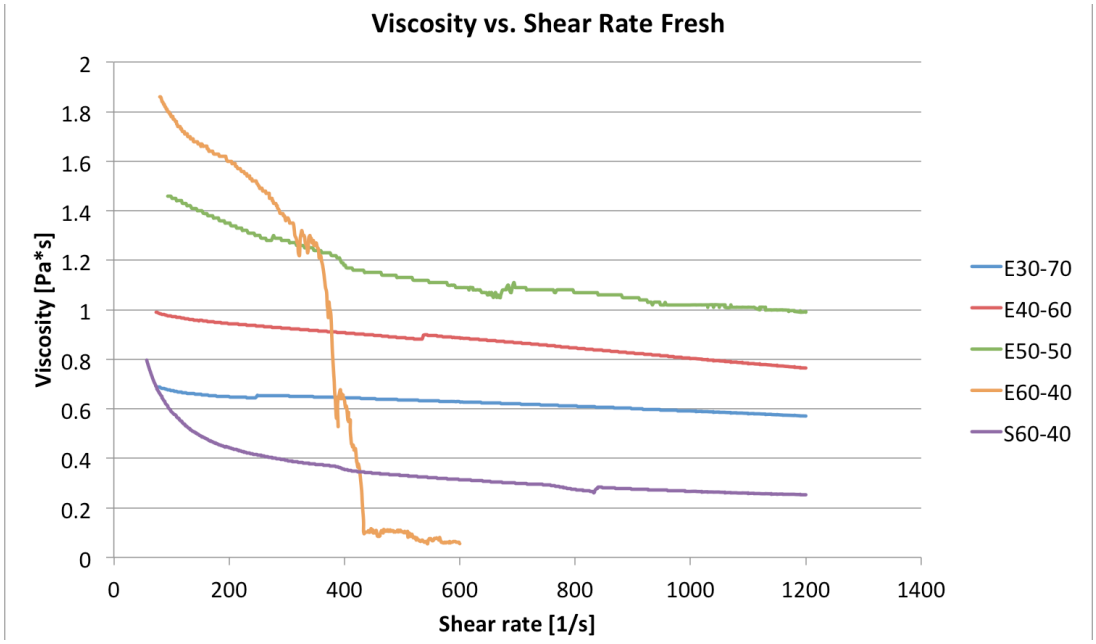

Figure 5.4: Zooming in on Figure 5.3 to see S60-40 on the same axis as the other emulsions

Before the E60-40 emulsion breaks the engine oil emulsions have increasing viscosity with increasing water content. This is in compliance with what was expected based on studies done by Pal (1996, p. 3181). After the E60-40 emulsion breaks, the other engine oil

emulsions stays in the same pattern and seems to be flattening out with increasing shear rate. The S60-40 emulsion starts with a viscosity over 20 Pa·s, before the curve quickly goes down and approaches a value of 0.2 Pa·s. Since there are no other soybean oil emulsions with different water content, this viscosity cannot be compared in terms of that.

The emulsion droplet size will be discussed in more detail in Chapter 5.5, but some results relevant for the viscosity is presented in Figure 5.5. This figure shows that the droplet size is smallest for the emulsion with the lowest water content. Based on studies by Pal (1996, p. 3181) it is assumed that the viscosity would be higher for W/O emulsions with smaller droplet size. Combining the results in Figure 5.5 and this theory, the emulsion with the lowest water content should be having higher viscosity. However, in Figure 5.4 it was seen that the viscosity was increasing with increasing water content, opposite to what is expected based on Figure 5.5 and theory by Pal. It has to be noted that Pal's study was based on the droplet size in one W/O emulsion, and not between W/O emulsions with different water contents. Therefore it may not be as relevant here since the droplet size is compared between different water contents. Based on uncertainties with the microscopic image analysis as well, the MCR measurements will be considered more representable in this case.

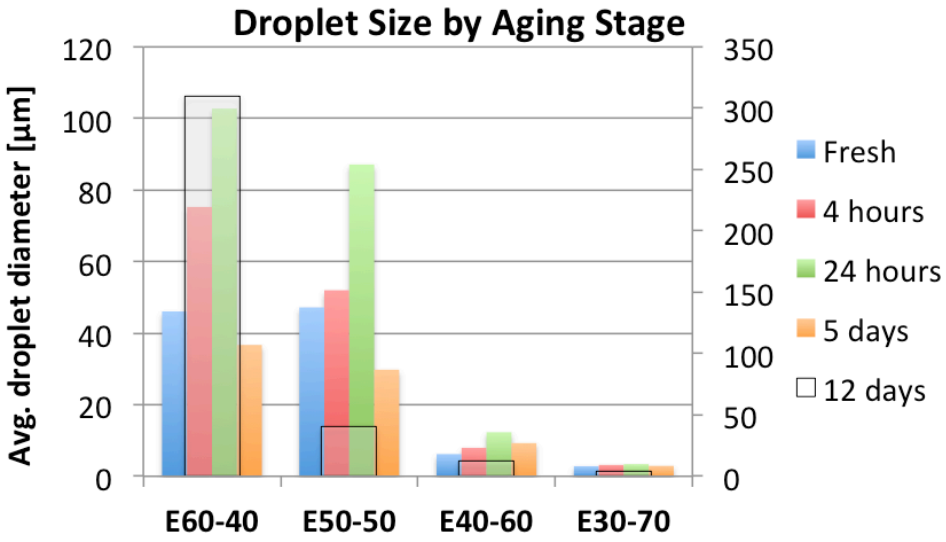

Figure 5.5: Average droplet size found by microscopic image analysis, sorted by aging stage. The 12 day case has it's own axis on the right hand side

For the soybean oil emulsion, the short mixing might give quite large droplet size. As mentioned, a W/O emulsion with smaller droplets is expected to show higher viscosity. Thus,

short mixing time might explain the low viscosity, but since the droplet size has not been studied it is hard to tell if this is the reason.

5.2.3 Temperature Effect

It can be seen in Figure 5.6 that both the E60-40 and the E30-70 emulsion gets a steeper gradient, meaning a higher shear stress with shear rate, for decreasing temperature. All the emulsions still shows a shear thinning behavior with an overall downwards concave shape. When the same temperatures but different emulsions are compared it can be seen that the E30-70 curves always lies under the E60-40 curves, as expected compared to the results in Chapter 5.2.1.

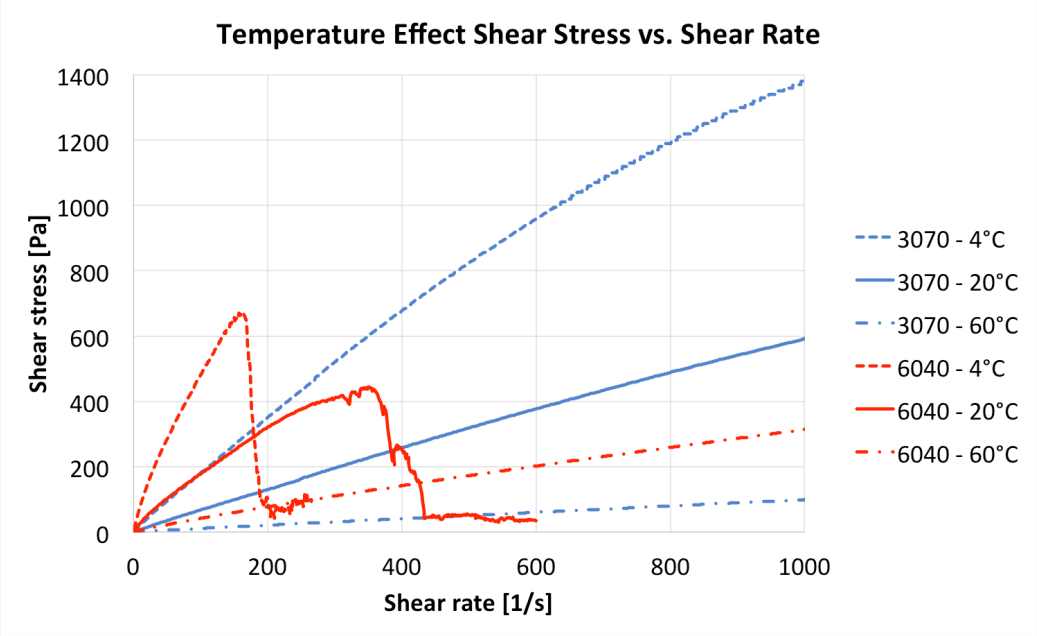

Figure 5.6: Shear stress vs. shear rate plot showing the effect of varying temperature

None of the E30-70 temperature cases indicates a breaking of the emulsion, since none of the curves are abruptly decreasing. The E60-40 emulsion breaks before the measurement ends for both 4 °C and 20 °C and, but not for 60 °C. This is interesting and unexpected, since heating and not cooling of the emulsion is used when trying to break it. Even so, the coldest emulsion is the first to break, and what is causing this is hard to tell. However, in the publication by Wen et al. (2014, p. 9513) it is said that increased temperature during mixing might increase emulsion stability. The measurements are taken with increased temperature right after mixing, and it is possible that the applied shear from the MCR can be counted as additional

mixing. In that case, this can explain why the 60 °C case does not break. However, it does not look like the temperature increase has any impact on the E30-70 emulsion. This emulsion might not be affected since it has lower water content and should be more stable in the first place. Despite the theories discussed here, no conclusions can be drawn without further investigation.

For the viscosity it can be seen in Figure 4.20 on page 40 that it is decreasing with increasing temperature for both emulsions, as expected from the viscosity-temperature relation. The most dramatic changes are happening for the E60-40 emulsion at 4 °C and 20 °C. When it comes to water content compared between the emulsions at the same temperature, it can be seen that the E60-40 emulsion lies above the E30-70 emulsion here as well, like in Chapter 5.2.2. This is in accordance with the theory of viscosity increasing with increasing water content, and increased or decreased temperature does not affect this pattern.

5.2.4 Predicted Flow by Power Law Model

The plots showing the curve fit done in MATLAB to find the Power law constants can be seen in Appendix D, both when the appropriate and inappropriate model is used. The Reynolds number is calculated for the minimum and maximum viscosity measured in the MCR, and is therefore presented as a range. The same applies for the entry length, since it is dependent on the Reynolds number.

Table 5.1: Results for using the appropriate model: Power law model for shear thinning emulsion flow

Emulsion	Q [l/s]	v [m/s]	Re	L_h [m]
E30-70	0.1153	0.2349	3.5189 – 7.6206	0.0044 – 0.0095
E40-60	0.0818	0.1667	2.2522 – 4.0880	0.0028 – 0.0051
E50-50	0.0438	0.0892	0.9103 – 1.9150	0.0011 – 0.0024
E60-40	0.0345	0.0703	0.4480 – 1.2066	$5.56 \cdot 10^{-4}$ – 0.0015

In Table 5.1 it can be seen that the flow rate is decreasing with increasing water content for all the engine oil emulsions, which sounds reasonable since the emulsions are getting more viscous with increasing water content. As seen in Poiseuille law in Equation (3.5) the flow

rate is inversely proportional to the viscosity, and this coincides with the data presented in Table 5.1. There is not shown any clear pattern regarding how much the flow rate is decreasing with a 10% increase in water content, since this varies from 21% to 46%.

The Reynolds number reaches the highest value for the E30-70 emulsion, and is also decreasing with increasing water content. The Reynolds number is dependent on the density, velocity, pipe diameter and the viscosity. The pipe diameter is constant, but the other parameters are varying with increasing water content. The density and viscosity is increasing with increasing water content, while the velocity is decreasing with increasing water content. Based on this is seems like the velocity is the dominant parameter.

Since the entry length is dependent on Reynolds number and the constant pipe diameter, the entry length will be dependent on the same parameters as the Reynolds number. However, it is worth mentioning that the entry lengths do not dominate the pipe flow. The total length of the pipe is 1.8 m, and thus the longest entry length, 0.0095m, corresponds to 0.5% of the total pipe length, which can be considered negligible.

In Table 5.2 the inappropriate flow model is used, and it does not make much sense to discuss these results alone. This will be discussed further in Chapter 5.4 where the results will be compared to the flow in the flow capacity setup.

Table 5.2: Results for using the inappropriate model: Power law model for viscoplastic emulsion flow

Emulsion	**Q [l/s]**	**v [m/s]**	**Re**	**L_h [m]**
S60-40	0.1447	0.2948	0.3197 – 23.7301	$4.0 \cdot 10^{-4}$ – 0.0297

5.2.5 Predicted Flow by Herschel-Bulkley Model

The plots showing the curve fit done in in MATLAB to find the Herschel-Bulkley constants can be found in Appendix D, both when the appropriate and inappropriate model is used. Also here the Reynolds number is calculated for the minimum and maximum viscosity measured in the MCR, and is therefore presented as a range. The same applies for the entry length, since it is dependent on the Reynolds number.

Table 5.3: Results for using the appropriate model: Herschel-Bulkley model for viscoplastic emulsion flow

Emulsion	Q [l/s]	v [m/s]	Re	L_h [m]
S60-40	0.1226	0.2498	0.2709 – 20.1143	$3.38 \cdot 10^{-4}$ – 0.0251

If the results in Table 5.3 are compared to he results in Table 5.1, it can be seen that the S60-40 emulsion shows a slightly higher flow rate than the highest flow rate for the engine oil emulsions. The S60-40 Reynolds number is also the highest reported for all the emulsions. Since the Reynolds number is the highest in this case, the entry length also reaches its highest value here. Still, the entry length cannot be said to dominate the pipe, since the longest entry length, 0.0251m, will be approximately 1.4% of the total pipe length.

In Table 5.4 the inappropriate flow model is used, and it does not make much sense to discuss these results alone. This will be discussed further in Chapter 5.4 where the results will be compared to the flow measured in the flow capacity setup.

Table 5.4: Results for using the inappropriate model: Herschel-Bulkley model for shear thinning emulsion flow

Emulsion	Q [l/s]	v [m/s]	Re	L_h [m]
E30-70	0.1157	0.2356	3.5304 – 7.6454	0.0044 – 0.0096
E40-60	0.0823	0.1667	2.2655 – 4.1121	0.0028 – 0.0051
E50-50	0.0567	0.1156	1.1788 – 2.4800	0.0015 – 0.0031
E60-40	0.0384	0.0782	0.4981 – 1.3426	$6.23 \cdot 10^{-4}$ – 0.0017

5.3 Measured Flow in Flow Facility

The four engine oil emulsions and the one soybean oil emulsion were all run through the flow capacity setup twice in a row.

5.3.1 Measured Flow for Shear Thinning Fluids

All the engine oil emulsions show a decrease in flow rate with increasing water content, both for run 1 and 2 as seen in Table 5.5 and Table 5.6. The decrease in flow rate is between

41-46% for run 1 and 40-47% for run 2, so the flow rate decrease with increased water content is more stable here than it was for the predicted flow rates.

Table 5.5: Results for running the shear thinning emulsions through the flow facility, run 1

Emulsion	Volume [l]	Time [s]	Flow rate Q [l/s]
E30-70	2.3018	18.10	0.1271
E40-60	2.0989	29.85	0.0703
E50-50	2.0396	49.46	0.0412
E60-40	1.7723	79.52	0.0223

Table 5.6: Results for running the shear thinning emulsions through the flow facility, run 2

Emulsion	Volume [l]	Time [s]	Flow rate Q [l/s]
E30-70	2.3387	17.28	0.1353
E40-60	2.0782	29.02	0.0716
E50-50	2.1451	50.09	0.0428
E60-40	2.0128	84.99	0.0237

Looking at Figure 5.7 it can be seen that the engine oil emulsions with lower viscosity, meaning less water content, are running faster through the flow facility.

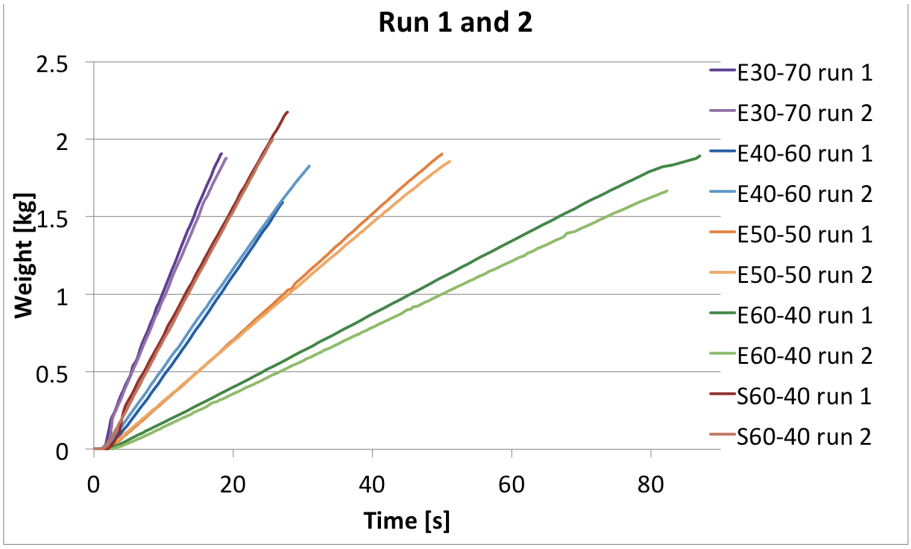

Figure 5.7: Weight vs. time for all the emulsions flowed in the flow capacity setup

5.3.2 Measured Flow for Viscoplastic Fluids

Looking at the time versus weight plot in Figure 5.6, the soybean oil emulsion curve falls in between the E30-70 and the E40-60 emulsion curves. Since only one soybean oil emulsion has been run, it does not have any similar emulsion to be compared to. It can however be seen that the flow rate is lying in between the maximum and minimum flow rate for the engine oil emulsions.

Table 5.7: Results for running the viscoplastic emulsion through the flow facility, run 1

Emulsion	Volume [l]	Time [s]	Flow rate Q [l/s]
S60-40	2.0989	24.47	0.0858

Table 5.8: Results for running the viscoplastic emulsion through the flow facility, run 2

Emulsion	Volume [l]	Time [s]	Flow rate Q [l/s]
S60-40	2.2884	26.00	0.0880

5.4 Comparison Flow Measurements and Model Prediction

To compare the flow rates predicted by flow models and emulsion parameters to the flow rates measured in the flow capacity setup, the percent deviation was found for both runs as seen in Table 5.9 and Table 5.10. When the appropriate model is used, the percent deviation is varying from 2-31% in run 1 and from 6-35% in run 2, with an average deviation of 13%. The deviations are quite large considering that the appropriate model is used, but it should be mentioned that both the models used for prediction and the method used to measure the flow rate probably has some uncertainties that will be discussed in further detail in Chapter 5.7.

In Table 5.9 and Table 5.10 it can be seen that all the deviations are smaller when using the appropriate model. The exception is the E30-70 emulsion, where the percentage deviations are equal independent on both flow model used and run. The highest percent deviations are found when the inappropriate model is used, respectively 39% for the S60-40 emulsion in run 1 and 42% for the E60-40 emulsion in run 2. The average deviation between the predicted and measured flow rate is 21% when the inappropriate model is used, 8% higher than the average deviation when the appropriate flow model is used. There is no shown coherence

between the water content and viscosity with the percent deviation.

Table 5.9: Percentage deviation flow rates, appropriate and inappropriate models run 1

Emulsion	Percent Deviation appropriate model	Percent Deviation inappropriate
E30-70	17%	17%
E40-60	-12%	-13%
E50-50	-2%	-24%
E60-40	-31%	-38%
S60-40	-28%	-39%

Table 5.10: Percentage deviation flow rates, appropriate and inappropriate models run 2

Emulsion	Percent Deviation appropriate model	Percent Deviation inappropriate
E30-70	10%	10%
E40-60	-14%	-15%
E50-50	-6%	-27%
E60-40	-35%	-42%
S60-40	-30%	-41%

Table 5.11: Sum up of values

	Percent Deviation appropriate model	Percent Deviation inappropriate model
Average	13%	21%
Maximum	35%	42%

5.5 Droplet Size Estimation and Aging

Before starting microscopic image analysis, the maximum and average droplet sizes are predicted based on a correlation by Hinze (1955). Next, rheological measurements taken by

the MCR in aging intervals will be presented, as well as images studied in the same time intervals by microscopic image analysis. Droplet size distributions are found by microscopic image analysis, and visual signs of instabilities are looked for. Emulsion samples exposed to aging and varying temperature will also be visually inspected.

5.5.1 Prediction for Maximum and Average Droplet Size

In Table 5.12 the predictions for maximum and average droplet size are presented.

Table 5.12: Maximum and average droplet size predicted from Hinze's correlation

Name of Emulsion	Max Droplet Size [µm]	Average Droplet Size [µm]
E30-70	0.484	0.145
E40-60	0.497	0.149
E50-50	0.506	0.152
E60-40	0.512	0.154

It has to be emphasized that Hinze's correlation is based on single droplets in a continuous phase, and in an emulsion the droplets will be packed and maybe also in clusters. Consequently, this correlation will have substantial uncertainties when used for emulsions, but it is still interesting to see if the results can be compared to droplet sizes found by other methods. In addition to this, the energy dissipation is calculated based on the power given in [W] on the mixer. Since this power is not checked in any other way, it might be varying a bit during mixing and this can also lead to uncertainties.

5.5.2 Rheological Measurements with Aging

In this section the shear stress versus shear rate plots and viscosity versus shear rate plots will be presented for different aging stages: fresh, 4 hours, 24 hours, 5 days and 12 days. In addition to this, a zoomed section of the plot will be showed, since some of the curves are lying very close and it can be hard to distinguish between them. The plots not presented here can be found in Appendix E.

All the shear stress versus shear rate curves still shows shear thinning behavior after aging. The E60-40 emulsion starts to break around 400 s^{-1} for the fresh emulsion, while the 12 day case is the last to break as seen in Figure 5.8. This can indicate that the E60-40 emulsion did

become more stable with aging, possibly due to emulsifiers spreading more evenly out. However, the other emulsions did not break and it is unclear if the increase in stability happens in those. The behavior before the E60-40 emulsion breaks is still shear thinning for all the aging stages.

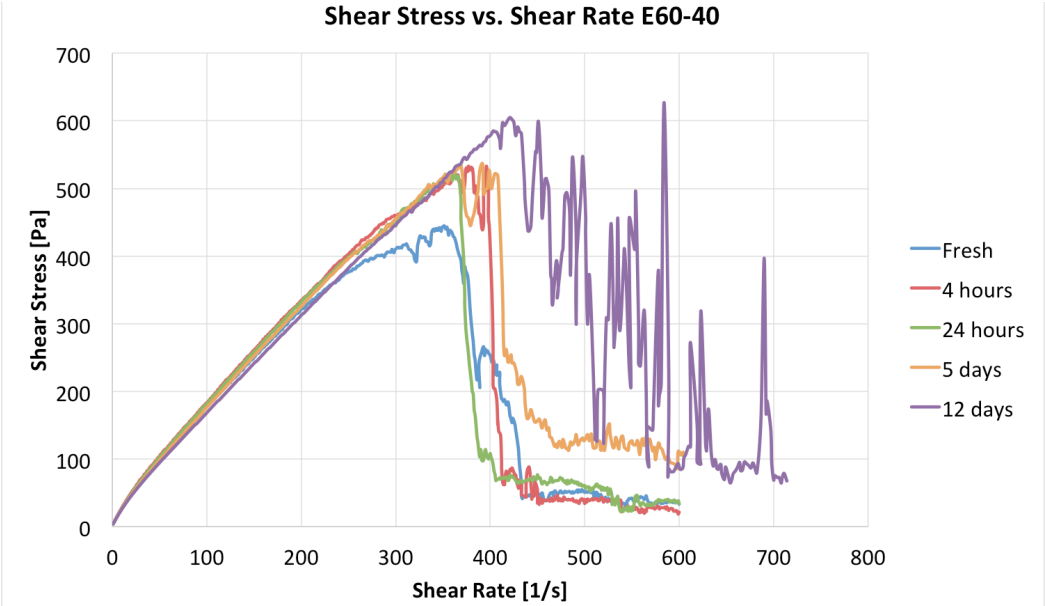

Figure 5.8: Shear stress vs. shear rate with aging for E60-40 emulsion

When it comes to water content, the E30-70 emulsion seems to be least influenced by aging in the shear stress versus shear rate plot, but on the contrary the E40-60 and E50-50 emulsions seems to be more influenceed than the E60-40 emulsion.

For the emulsions with the three lower water contents the viscosities are decreasing with aging. The 4 hour case is sometimes showing a slightly higher viscosity than the fresh case, but since this difference in terms of viscosity and time step is small this will not be assumed to alter the decreasing viscosity pattern. However, the emulsion with the highest water content does not agree with the assumption about viscosity decreasing with aging, where the 4 hour case has the highest viscosity and the fresh case has the lowest viscosity. Even so, it seems like the emulsion viscosity is decreasing with aging since this happens in three out of four emulsion cases.

Figure 5.9: Viscosity vs. shear rate with aging for E40-60

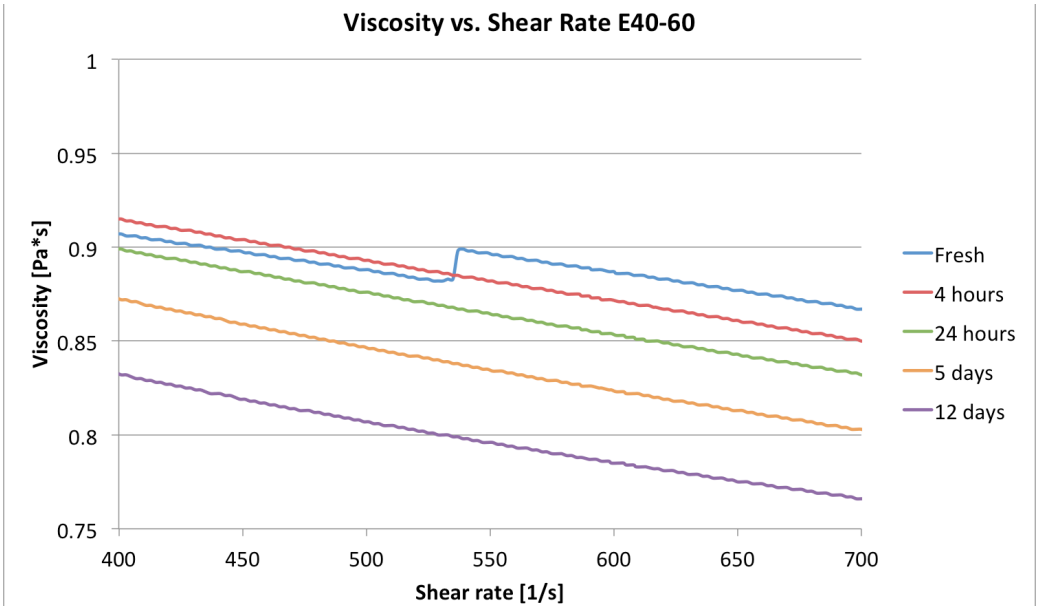

Figure 5.10: Zoomed section of Figure 5.9

Even if the viscosity tends to decrease with aging, the change is not that large. Another interesting thing is that microscopic restructuring in the emulsion, for example by flocculation, is said to possibly increase the viscosity. Even if this kind of microscopic restructuring might be present here, it does not seem to increase viscosity with aging. A possible reason for this is that emulsion exposed to shear, for example by the MCR, may

separate flocculated droplets. If the droplets are separated they go back to behaving like small droplets again, decreasing viscosity.

5.5.3 Microscopic Image Analysis with Aging

Many images were processed in order to study the droplet size distribution, but to present all here would take up way too much space. Therefore an example of the image before and after processing will be showed, together with a selection of images showing tendencies for emulsion breakdown processes.

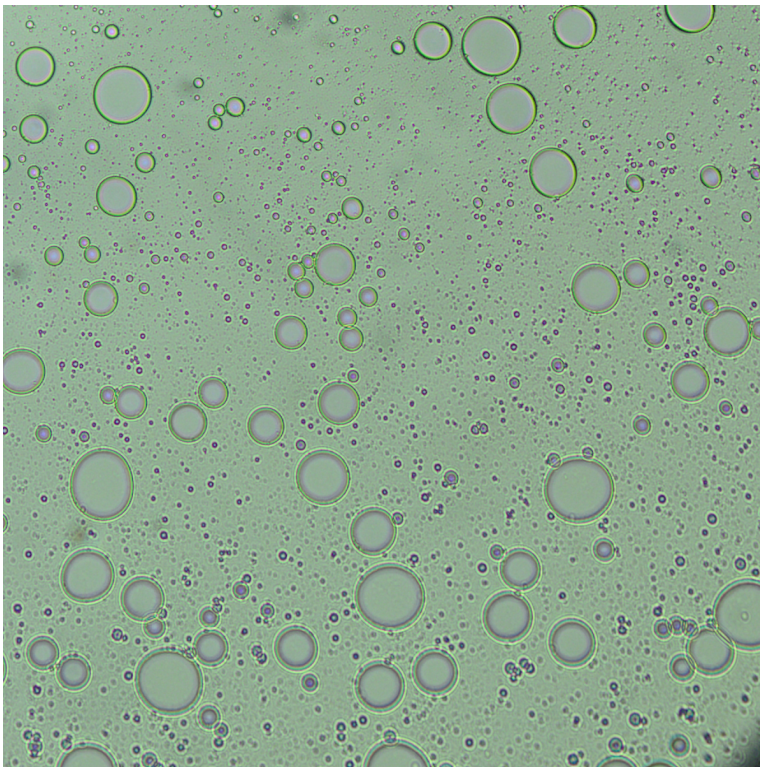

Figure 5.11: Raw image from the Optika microscope, E50-50 emulsion after 24 hours aging

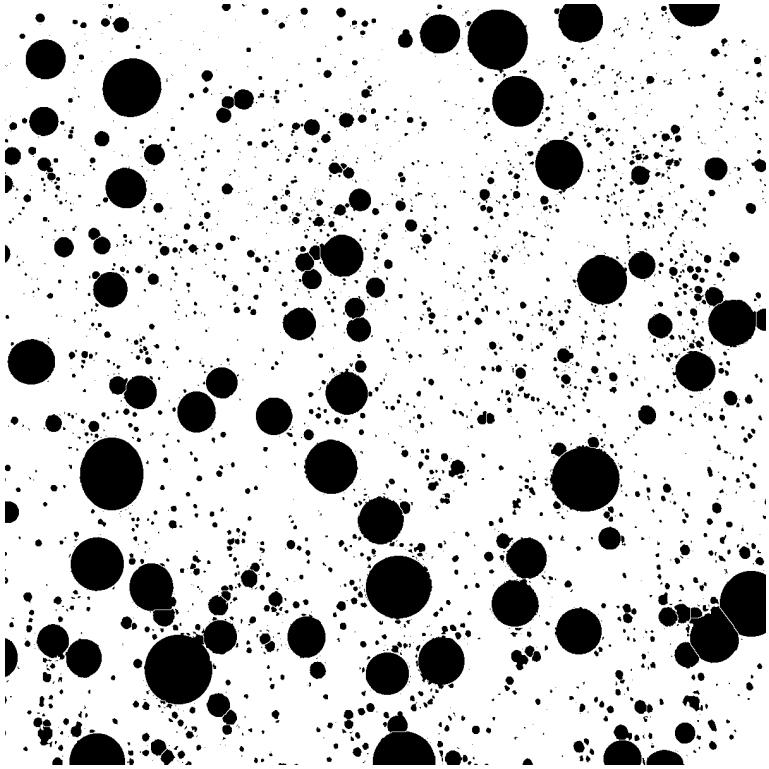

Figure 5.12: Final processed image in Figure 5.11 . This is an E50-50 emulsion, after 24 hours aging

The microscopic image analysis was mainly conducted in order to provide an estimate for the droplet size distribution, but can also indicate if any breakdown processes have occurred. Three pictures of the E60-40 emulsion are presented here. In Figure 5.15 flocculation can clearly be seen. Ostwald Ripening may be happening between the fresh and the 24 hour case in Figure 5.13 and Figure 5.14, since the droplet size is increasing and it is not clearly shown that many droplets are flocked together. However, since the time scale for the Ostwald ripening is not known, 24 hours might not be enough time for this to happen. Between the 24 hour case and the 12 day case it can look like coalescence is happening, since some droplets are lying very close in Figure 5.14 and then the droplet size is increased in Figure 5.15. Still, not all droplets have gone through coalescence, since there still are many droplets lying close in flocks without being merged together in Figure 5.15.

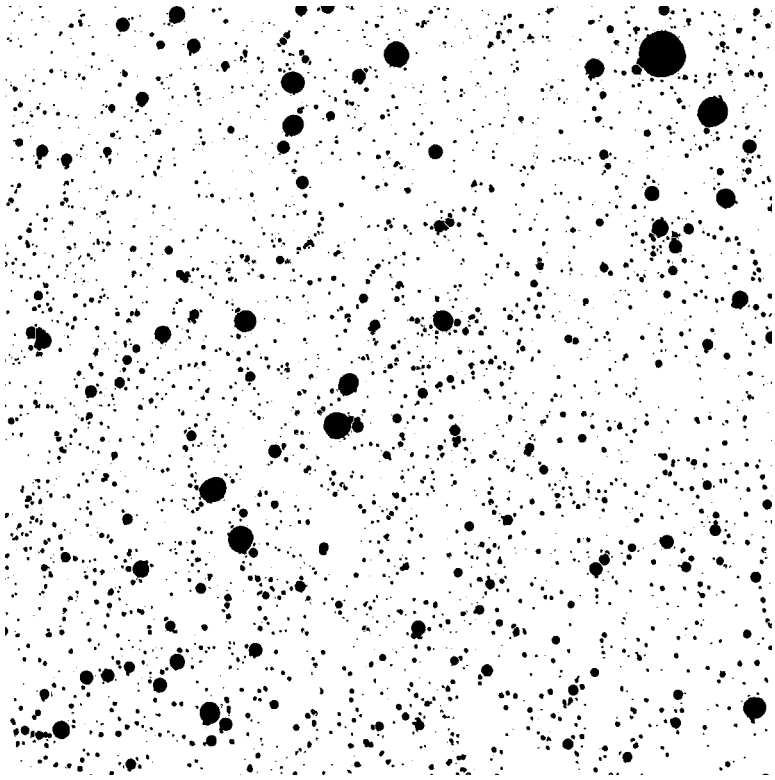

Figure 5.13: E60-40 emulsion as fresh

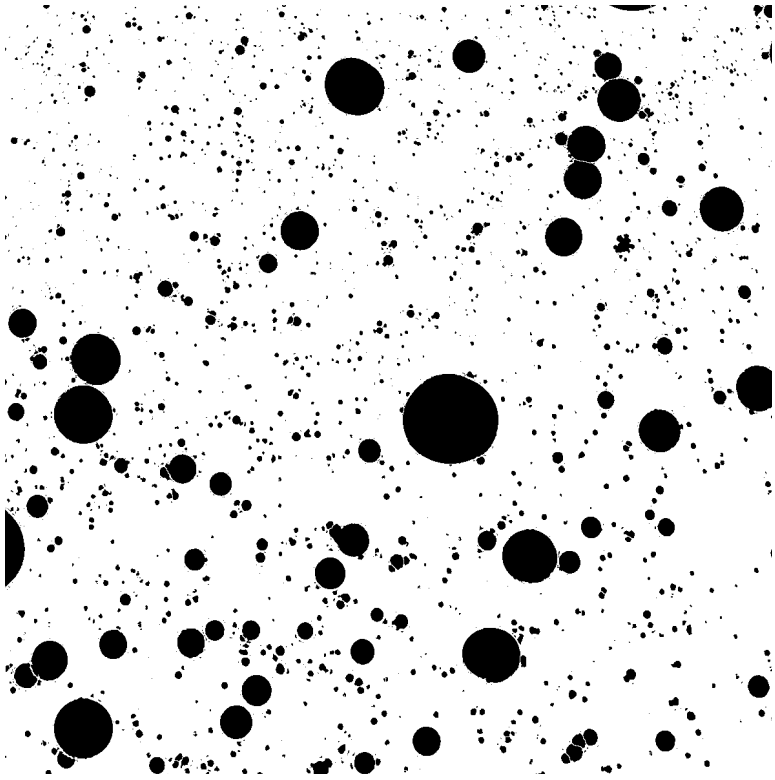

Figure 5.14: E60-40 emulsion after 24 hours

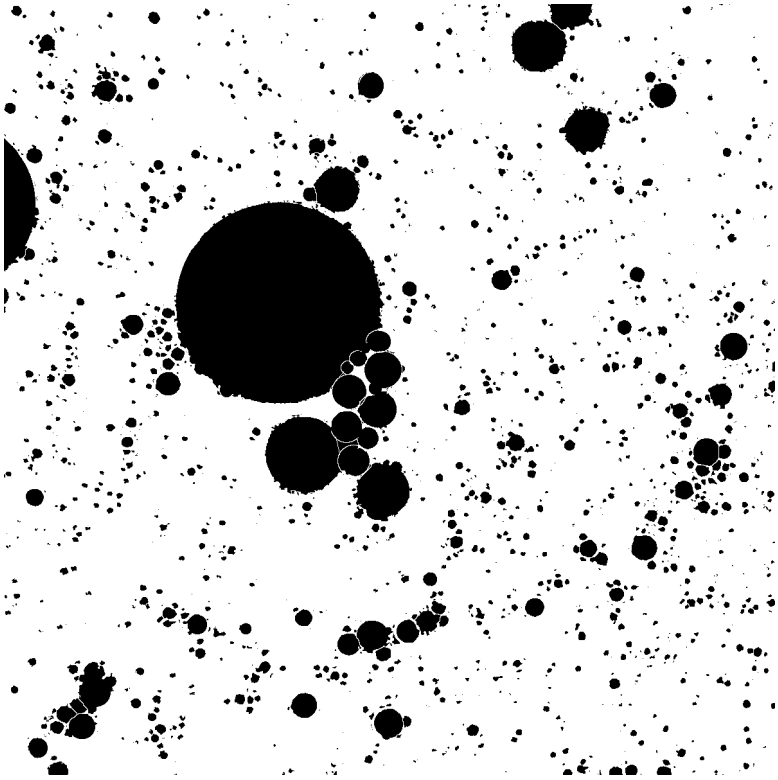

Figure 5.15: E60-40 emulsion after 12 days

5.5.4 Droplet Size Distribution with Aging

In this section both the droplet volume and the droplet diameter are representing droplet size. The droplet volumes are found by microscopic image analysis in ImageJ and will be presented in plots. The MATLAB script also provided a logarithmic distribution for the measured droplet volumes, and these plots will be shown together with the measured droplet volumes. The plots not presented here can be found Appendix F. For the droplet diameter, this will be presented in plots where it is compared to the average and maximum droplet size found by Hinze's correlation. Not all plots will be shown here, but the rest can be found in Appendix G.

For the E30-70 emulsion the measured droplet volumes in increasing order are fresh, 4 hours, 5 days, 24 hours and 12 days as seen in Figure 5.16. Even if the cases in between fresh and 12 hours are not increasing, the fresh emulsion has the smallest droplet volumes and 12 days the largest. This is almost in line with the theory about aged emulsions getting a larger amount of larger droplets. For the E40-60 emulsion it has smallest droplets for the fresh case, but the largest droplets seems to be found in the 24 hour case. The emulsions with the two highest water contents does not have a clear pattern at all when it comes to measured droplet

volumes, where both emulsions shows the smallest droplets for the 5 day or 12 day case.

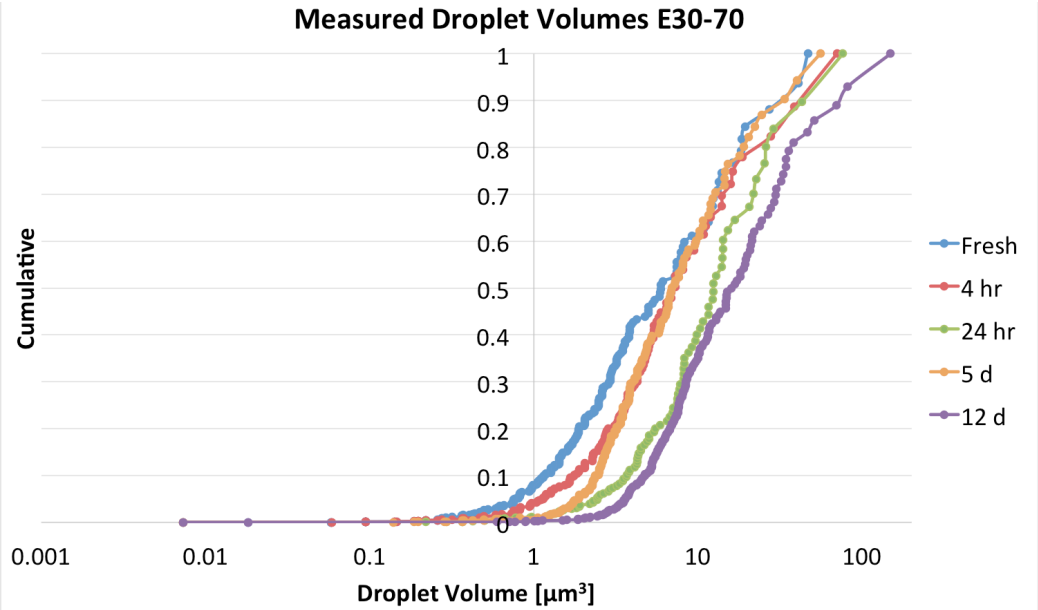

Figure 5.16: Droplet volumes found for the E30-70 emulsion, with logarithmic x-axis

Based on the plots for measured droplet volumes in ImageJ, it is hard to draw a conclusion about the droplet size with aging. For the emulsions with 30-40% water content, the pattern was closer to but did not completely comply with increasing droplet size with aging. In the emulsions with 50-60% water content, the pattern was not close to having an increasing trend. Most of the logarithmic distributions does not fit the measured points very well, as shown for example in Figure 4.30. For the other emulsions, the best fit is found for the emulsion with the lowest water content, E30-70, and it seems like the fit gets worse with increasing water content.

The average droplet size for the different emulsions and aging stages will now be presented. This droplet size is also compared to the maximum and average droplet size predicted by the correlation shown in Equation (2.2). As can be seen in Figure 5.17 and the other plots in Appendix G, this calculation for the droplet size is way lower than what is found by microscopic image analysis. It has to be kept in mind that this correlation would most likely be inaccurate to use in this setting, as mentioned in Chapter 5.5.1.

There is no clear trend in the average droplet size for either of the emulsions, if compared to the expected trend that the average droplet size could increase with aging. However, up to 24 hours this trend is followed. The 5 day case shows a decrease in average droplet size for all emulsions, and then the 12 day case shows increased values compared to the 24 hour case for three out of four emulsions. It is hard to tell why the 5 day case is decreasing for all the emulsions, but it has to be noted that the microscopic image analysis most likely has its flaws as will be discussed further in Chapter 5.7.

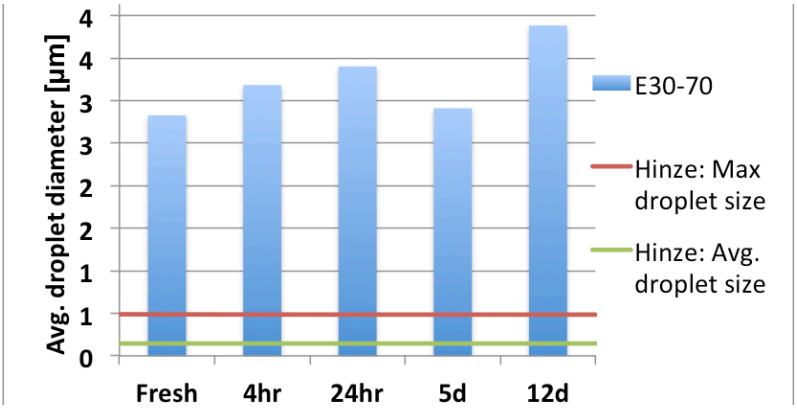

Figure 5.17: Average droplet size with aging 30-70

5.5.5 Varying Temperature During Aging

The E30-70 and the E60-40 emulsion studied by visual inspection reacted differently when exposed to varying temperatures during aging. For both emulsions, no change could be seen with aging when put in a fridge with 4 °C. Some bubbles were present at the bottom of the graduated cylinder, possible water droplets, but these were constant through the aging. While kept in laboratory temperature at 20 °C, the E60-40 emulsion did not show any changes with time until 10 days were reached. In the E30-70 emulsion some oil separated out, and tendencies for this was showed after 3 days. The pictures of these two cases are shown in Appendix H. Both emulsions responded more when the temperature was turned up to 60 °C, and oil gathered on top for both emulsions already after 24 hours. This can be seen in Figure 5.18 and Figure 5.19, and it shows that the E30-70 emulsion separated out about 8 ml oil while the E60-40 emulsion separated out about 1 ml oil.

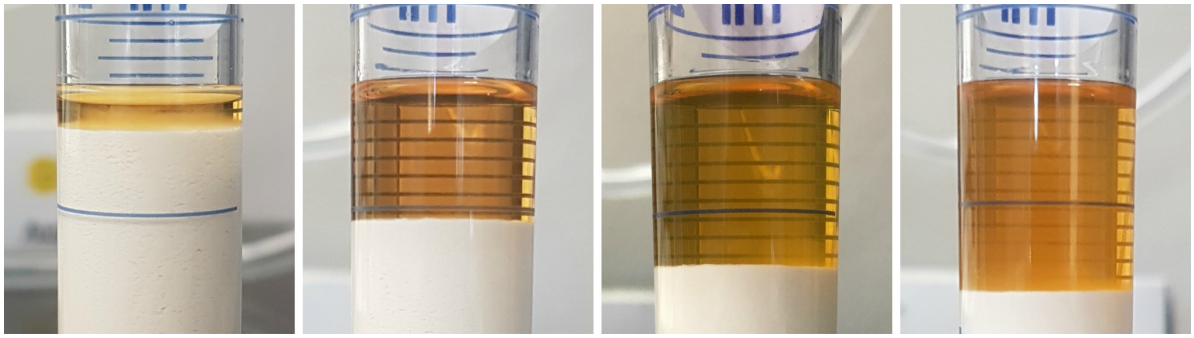

Figure 5.18: Visual separation of a E30-70 emulsion in temperature 60 °C, time from left to right is 1, 4, 10 and 22 days

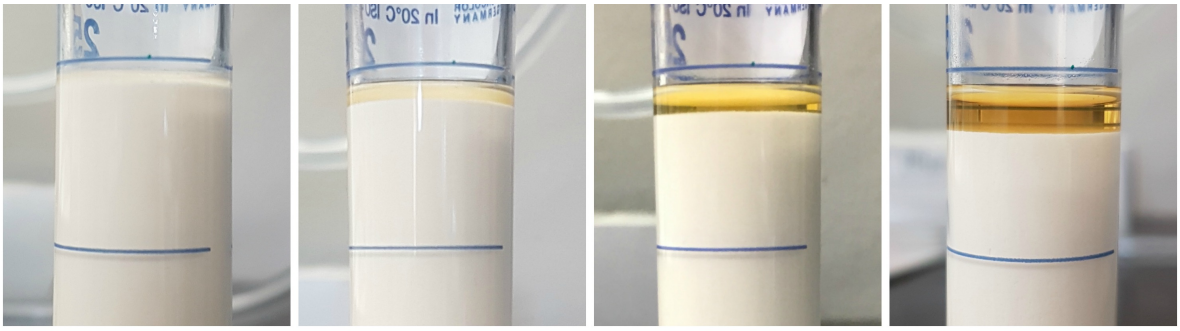

Figure 5.19: Visual separation of a E60-40 emulsion in temperature 60 °C, time from left to right is 1, 4, 10 and 22 days

Based on the pictures presented here, it can look like the emulsions are creaming with aging, since a continuous phase of oil is formed on top of the emulsion. This continuous phase on top could be due to water droplets growing by coalescence or gathering in flocks at the bottom, squeezing out oil that would flow up to the emulsion surface. However, there are no visible water droplets at the bottom of the emulsion, but still there is a continuous phase of oil at the top. Thus, there might be another reason for the oil phase separated out.

It is not reasonable to believe that the emulsion has inverted to an O/W emulsion. Even if it is exposed to a higher temperature than laboratory temperature, there are no indications of inversion. It is not likely that the emulsion has broken, since the emulsion under the oil looks intact, and the amount of oil separated out does not correspond to the total oil content in the emulsion.

Since there is no visible water phase, the water droplets are most likely still covered with emulsifiers preventing merging of droplets. However, it is possible that there is some excess

oil, meaning that some oil is not in contact with the dispersed droplets. This oil may be drained out and are gathering on top. Since the emulsion with lowest water content is separating out less oil than the emulsion with higher oil content, excess oil might be a possible explanation.

5.6 Problems

Before starting to use the Waring blender, an overhead stirrer from IKA was used. This mixer was shaped as a propeller, and provided RPM control. By using this, a mixing time of about 20 minutes was necessary to create the engine oil emulsions at 300 RPM. This would have been very time consuming, since only 400 ml emulsion was mixed at a time and 3 liters was needed to flow in the flow facility. Therefore it was experimented with the Waring blender, and it turned out that the way higher RPM reduced the mixng time significantly.

For the soybean oil emulsion different mixing times had to be experimented with, to get a stable emulsion that was also able to flow in the flow facility. As seen in Figure 5.20 the emulsion became very viscous when mixed for too long, and looked more like yoghurt than a fluid that would flow easily through the flow capacity setup.

Figure 5.20: Soybean oil emulsion mixed too long, becoming very viscous

5.7 Sources of Error

There are several possible sources of error in the laboratory work conducted. For the emulsion properties the emulsion density is measured with a mud scale instead of a pycnometer, even if a pycnometer is assumed to be more accurate. When it comes to the flow predicted by flow models and emulsion parameters, it has to be taken into account that some parameters put into MATLAB was put in manually and there is a possibility that inappropriate parameters could have been set as input. The possibility of errors in the script also has to be taken into account, along with the risk for having errors in the derivations of the two expressions for flow rate. More importantly, the scripts does not take all emulsion properties into account, such as the droplet size, emulsion change with aging (for example microstructural changes) and uncertainties in the apparatus used to measure emulsion properties. If these parameters were taken into account, there is a possibility that the measured and predicted results would deviate less.

In the flow capacity setup there are several possible sources of error. First and most important is the use of an average fluid height, since the bottom of the upper tank was uneven and an average height was calculated. Another thing is that the measurements were stopped when a change in the flow was observed, and it is hard to tell if the runs were stopped at the exact same point. The data recorded was done by video taping the scale and a timer, before the video was gone through in slow motion afterwards, writing down the weight versus time in proper intervals. If an electronic scale was used instead, and the fluid height could be determined more accurately than by average, this might also help reduce the deviations between measured and estimated flow rates. Also, the flow facility was not cleaned in between the runs of engine oil emulsions, and residue of the previous emulsion may affect the next run slightly.

For the droplet size predicted by Hinze's correlation, there is a large uncertainty, since the correlation is based on single droplets in a continuous phase. When it comes to the microscopic image analysis there are several uncertainties, since only one small droplet is studied and this may not represent the whole emulsion. From this small droplet several images were taken, but only one of these images were processed. Also, a smaller part of the image was processed and analyzed. In addition to this, the analysis done in ImageJ depends a lot on the user and how the user interprets the results. Especially since noise removal is done

by hand, it is possible that some droplets are removed and that some noise is not removed. Some images also had poorer quality than other images, and this can also affect the results.

5.8 Further Work

First of all the experiments could have been conducted more repeatedly. For example the emulsions could have been mixed several times before running the same tests again. This may help reduce the percentage deviation between the runs in the flow capacity setup and the predicted results. A flow capacity setup where the total fluid height could have been measured more accurately than by average could also have been built.
More importantly, if the scripts predicting the flow rates could be able to take changes in the emulsion into account, such as microstructural and droplet size changes, the results would most likely become more accurate. Exactly how this script should have been made has not been looked into, but maybe such a model could be found by conducting more experiments. The script predicting flow rates should also take the equipment uncertainty into account.

Several images could also have been processed in ImageJ, but this was a very time consuming task since the emulsions had way more droplets than what was experienced during the TPG4560 specialization project. Maybe it would be possible to find a trend for the droplet size with aging if several images were processed, and this might also be necessary in order to improve the scripts predicting flow rates.

In addition to this, several emulsions could have been studied, for example by changing the water content with 5% in each step instead of 10%. If longer mixing time was used, emulsions with higher water content might also be possible to study. Another oil could also have been used for comparison, and several emulsions with Herschel-Bulkley behavior could have been studied. It would also be possible to run the emulsion in flow capacity setups with other dimensions for comparison. An interesting but time-consuming extension of this thesis could be to do the same tests for O/W emulsions as well.

6 Conclusion

Water-in-oil emulsions were prepared in the laboratory based on engine oil, soybean oil and saltwater. The rheological properties of these were studied by a series of experiments. Emulsion flow rates were measured by a special designed flow facility and predicted by two non-Newtonian flow models and measured emulsion parameters. Based on the experiments discussed above, the following conclusions can be drawn:

- Emulsion viscosity was increasing with increasing water content, and showed a slightly decreasing tendency with aging
- The emulsion droplet size did not show a clear increasing trend with aging, even if the average droplet size was increasing from fresh to the 24 hour aged emulsion
- All engine oil emulsions were behaving in a shear thinning manner, even after aging. The soybean oil emulsion behaved in a viscoplastic manner
- The deviations between measured and predicted emulsion flow rates were on average 13%, and maximum 35% when the appropriate models were used. These deviations are much larger than what would be expected for Newtonian fluid, but may be comparable for two-phase flow
- When the inappropriate flow models were used the deviation between measured and predicted flow rates were higher, on average 21% and maximum 42%
- The deviation between predicted and measured flow rates might be decreased if emulsion droplet size and microstructural changes were taken into account in the flow prediction script

Based on the results achieved in terms of flow rate, non-Newtonian flow models and emulsion parameters can give a prediction for the emulsion flow in pipes. However, it is hard to tell how accurate these predictions are since the deviations are quite large. It would be interesting to develop this further by making an extended flow rate script taking emulsion changes into account, to see if the deviations could be reduced. More experiments and further investigations have to be conducted in order to make such a model.

Bibliography

Abbott, S. (2016) *Surfactant Science: Principles and Practice*: Creative Commons BY-ND. Available at: https://www.stevenabbott.co.uk/practical-surfactants/the-book.php (Accessed: 02.05.2017).

Albadran, M. (2013) *Structural Reliability Analysis of Corroded Steel Girder Bridge*. Available at: https://www.researchgate.net/publication/271516661_Structural_Reliability_Analysis_of_Corroded_Steel_Girder_Bridge (Accessed: 03.06 2017).

Alias, A. K. (2013) *Emulsion stability*. Available at: https://www.slideshare.net/akarim717/emulsion-stability (Accessed: 19.04 2017).

Anton-Paar-GmbH (2016) *The Modular Compact Rheometer Series*. Available at: http://www.anton-paar.com/?eID=documentsDownload&document=18378&L=6 (Accessed: 26.01 2017).

Asheim, H. (1985) *Petroleumsproduksjon og prosessering på plattformen.* Oslo: TANO, p. 269.

Aulton, M. E. and Taylor, K. M. G. (2013) *Aulton's Pharmaceutics: The Design and Manufacture of Medicines.* Elsevier, p. 460-461.

Aurand, K. (2015) *Density and viscosity [Class handout].* Trondheim, Norway: Department of Geoscience and Petroleum, Norwegian University of Science and Technology.

AZoM (2013) *Yield Stress Calculation Methods*. Available at: http://www.azom.com/article.aspx?ArticleID=9929 (Accessed: 01.03 2017).

Becher, P. (2001) *Emulsions : theory and practice.* 3rd ed. edn. Washington: American Chemical Society, p. 201, 361.

Bibette, J. (2002) *Emulsion science : basic principles : an overview. Springer tracts in modern physics* Berlin: Springer, p. 1, 97.

Çengel, Y. A., Cimbala, J. M. and Kanoğlu, M. (2010) *Fluid mechanics : fundamentals and applications.* 2nd ed. in SI units. edn. Boston: McGraw-Hill, p. 51, 339-342, 447.

Clarkson-Laboratory (2017) *Blender 1-Liter 2-Speed Stainless Steel Container with Timer 230V*. Available at: http://store.clarksonlab.com/8010ES.aspx (Accessed: 22.02 2017).

CyberColloids (2017) *Rheology - Geometries*. Available at: http://www.cybercolloids.net/information/technical-articles/rheology-geometries (Accessed: 03.06 2017).

Enjamoori, S., Azaiez, J. and Maini, B. (2011) 'Effects of aging of oil-in-water emulsions on flow instabilities in a Hele-Shaw cell', *International Journal of Emerging Multidisciplinary Fluid Sciences,* 3(4), pp. 183.

ExxonMobil (2016) *Product Safety Summary EXXSOL D60 FLUID*. Available at: https://www.exxonmobilchemical.com/Chem-English/Files/Resources/exxsol-d60-fluid-product-safety-summary-en.pdf (Accessed: 22.02 2017).

Ferreira, T. and Rasband, W. (2012) *ImageJ User Guide*. Available at: https://imagej.nih.gov/ij/docs/guide/user-guide.pdf (Accessed: 02.12 2016).

GUNT, G. G. (2016) *Pipe Friction for Laminar / Turbulent Flow*. Available at: http://happevanrijn.com/media/1009/hm-15001-1.pdf (Accessed: 03.02 2017).

Habdas, P. (2015) *non-Newtonian fluids - time independent*. Philadelphia, US: Department of Physics, Saint Joseph's University. Available at: http://people.sju.edu/~phabdas/physics/rheo.html (Accessed: 02.05 2017).

Heeres, A. S., Picone, C. S. F., van Der Wielen, L. A. M., Cunha, R. L. and Cuellar, M. C. (2014) 'Microbial advanced biofuels production: overcoming emulsification challenges for large-scale operation', *Trends in Biotechnology,* 32(4), pp. 223.

Hinze, J. O. (1955) 'Fundamentals of the hydrodynamic mechanism of splitting in dispersion processes', *AIChE Journal,* 1(3), pp. 289-295.

IKA (2016) *RCT Basic*. Available at: http://www.ika.com/owa/ika/catalog.product_detail?iProduct=3810000&iProductgroup=&iSubgroup=&iCS=1&iAcc=&iCon= (Accessed: 05.12 2016).

Kruss-GmbH (2017) *Drop Shape Analyzer – DSA100S*. Available at: https://www.kruss.de/products/contact-angle/dsa100/drop-shape-analyzer-dsa100s/ (Accessed: 05.03 2017).

Malkin, A. I. A. k. and Isayev, A. I. (2013) 'Rheology - Concepts, Methods, and Applications (2nd Edition)', in *Rheology*. pp. 1-3 [Online]. Version.

MathWorks (2016) *Power Series*. Available at: https://se.mathworks.com/help/curvefit/power.html (Accessed: 13.02 2017).

Molecularrecipes (2014) *Emulsion Types*. Available at: http://www.molecularrecipes.com/emulsions/emulsion-types/ (Accessed: 02.06 2017).

Montgomery, C. (2013) 'Fracturing Fluids', *International Society for Rock Mechanics*, pp. 17.

Nguyen Hoang, T. K., Binh La, V., Deriemaeker, L. and Finsy, R. (2004) 'Ostwald ripening and solubilization in alkane in water emulsions stabilized by different surfactants', *Physical Chemistry Chemical Physics,* 6(7), pp. 1421.

Nilsen-Nygaard, J., Sletmoen, M. and Draget, K. I. (2014) 'Stability and interaction forces of oil-in-water emulsions as observed by optical tweezers – a proof-of-concept study', *The Royal Society of Chemistry* pp. 52221.

Olympus-Lifescience (2016) *One Camera for Brightfield and 4K UHD Imaging*. Available at: http://www.olympus-lifescience.com/en/camera/color/uc90/ -!cms[tab]=%2Fcamera%2Fcolor%2Fuc90%2Fresources (Accessed: 09.12 2016).

OpenStax (2016) *College Physics*: OpenStax, OpenStax College Physics. Available at: http://cnx.org/contents/031da8d3-b525-429c-80cf-6c8ed997733a@9.38 (Accessed: 12.10 2016).

Pal, R. (1996) 'Effect of droplet size on the rheology of emulsions', *AIChE Journal,* 42(11), pp. 3181, 3184, 3189.

Petrowiki (2016) *Produced oilfield water*. Available at: http://petrowiki.org/Produced_oilfield_water (Accessed: 08.03 2017).

Ross, C. (2017) *Improve emulsion stability through ultra-high shear mixing*. Available at: http://www.mixers.com/insights/mti_17.pdf (Accessed: 17.02 2017).

Schramm, L. L. (2000) *Surfactants : Fundamentals and Applications in the Petroleum Industry.* Cambridge: Cambridge University Press, p. 592, 607.

Schramm, L. L. (2014) *Microscience and Applications of Emulsions, Foams, Suspensions, and Aerosols. Emulsions; Foams; Suspensions; and Aerosols* Hoboken: Wiley, p. 262, 280.

SI-Analytics (2017) *Capillary Viscometry*. Available at: http://www.si-analytics.com/en/products/capillary-viscometry.html (Accessed: 27.01 2017).

Sjöblom, J. (2001) *Encyclopedic handbook of emulsion technology.* New York: Marcel Dekker, p. 403.

Sochi, T. (2010) 'Flow of non-newtonian fluids in porous media', *Journal of Polymer Science Part B: Polymer Physics,* 48(23), pp. 2439-2440, 2450.

Southard, J. (2006) *Introduction to Fluid Motions, Sediment Transport, and Current-Generated Sedimentary Structures*: Massachusetts Institute of Technology: MIT OpenCourseWare. Available at: https://ocw.mit.edu/courses/earth-atmospheric-and-

planetary-sciences/12-090-introduction-to-fluid-motions-sediment-transport-and-current-generated-sedimentary-structures-fall-2006/course-textbook/ch4.pdf (Accessed: 29.01.2017).

SPE (2016) *Energy dissipation rate*. Available at: http://petrowiki.org/Energy_dissipation_rate - Energy_dissipation_rate_in_the_duct_flow (Accessed: 13.05 2017).

Tadros, T. F. (2013) *Emulsion Formation and Stability. Topics in Colloid and Interface Science* Hoboken: Wiley, p. 3, 36.

Tcholakova, S., Denkov, N. D. and Lips, A. (2008) 'Comparison of solid particles, globular proteins and surfactants as emulsifiers', *Physical Chemistry Chemical Physics,* 10(12), pp. 1610, 1613.

UW (2017) *Facilities at Center for Cryo-Biomedical Engineering and Artificial Organs, UW*. Available at: https://depts.washington.edu/cryolabs/home/?page_id=12 (Accessed: 08.02 2017).

Weisstein, E. W. (2016) *Log Normal Distribution*. Available at: http://mathworld.wolfram.com/LogNormalDistribution.html (Accessed: 28.11 2016).

Wen, J., Zhang, J., Wang, Z., Zhang, Z., Zheng, F., Zhu, Y. and Han, S. (2014) 'Full and partial emulsification of crude oil-water systems as a function of shear intensity, water fraction, and temperature', *Industrial and Engineering Chemistry Research,* 53(22), pp. 9513.

Werz, T., Baumann, M., Wolfram, U. and Krill, C. E. (2014) 'Particle tracking during Ostwald ripening using time-resolved laboratory X-ray microtomography', *Materials Characterization,* 90, pp. 186.

Yu, W., Zhou, C. and Inoue, T. (2000) 'A coalescence mechanism for the coarsening behavior of polymer blends during a quiescent annealing process. I. Monodispersed particle system', *Journal of Polymer Science Part B: Polymer Physics,* 38(18), pp. 2380.

Appendices

Appendix A Risk Assessment

Detailed Risk Report

ID	20268	**Status**	**Date**
Risk Area	Risikovurdering: Helse, miljø og sikkerhet (HMS)	Created	01.06.2017
Created by	Marthe Bodahl Lunde	Assessment started	01.06.2017
Responsible	Harald Arne Asheim	Actions decided	01.06.2017
		Closed	01.06.2017

Risk Assessment:

Risk Assessment - Master Thesis Spring 2017

Valid from-to date:
1/11/2017 - 6/11/2020

Location:
Petroleumsteknisk Senter

Goal / purpose
We want to conduct a risk assessment in order to be aware of the possible nonconformities that might occur, and how to handle it in the right way.

Background
By doing this risk assessment we want to address the possible risks of doing laboratory work related to the master thesis.

Description and limitations
Units that might be affected by the subject of this risk assessment are ourselves and co-workers in the lab. There are no previous risk assessments used as reference. This risk assessment is only applicable for work in the mud lab at PTS, and for the spring semester 2016.

Prerequesites, assumptions and simplifications
Similar measurements were done in the laboratory last semester.

Attachments
[Ingen registreringer]

References
[Ingen registreringer]

Summary, result and final evaluation

The summary presents an overview of hazards and incidents, in addtition to risk result for each consequence area.

Hazard: **Contact with skin over time**

Incident:

Not to be analyzes.

Hazard: **Inhalation**

Incident:

Not to be analyzes.

Hazard: **Swollowing**

Incident:

Not to be analyzes.

Hazard: **Waste**

Incident: **Waste Handling**

Consequence area: Materielle verdier Risk before actions: Risiko after actions:

Planned action	Responsible	Registered	Deadline	Status
Waste Handling	Marthe Bodahl Lunde	01.06.2017	01.06.2017	Evaluated

Hazard: **Spilling**

Incident:

Not to be analyzes.

Final evaluation

It is important to inform new lab - visitors about the waste bucket measure. If they are working with very viscous fluids, they should use the black waste bucket with the big inlet, instead of the waste bucket in the fume hood with the pipe inlet.

Organizational units and people involved

A risk assessment may apply to one or more organizational units, and involve several people. These are lsited below.

Organizational units which this risk assessment applies to

- Institutt for geovitenskap og petroleum

Participants

Ann-Othilie H. Væhle
Marthe Bodahl Lunde

Readers

[Ingen registreringer]

Others involved/stakeholders

[Ingen registreringer]

The following accept criteria have been decided for the risk area Risikovurdering: Helse, miljø og sikkerhet (HMS):

Helse	Materielle verdier	Omdømme	Ytre miljø

Overview of existing relevant measures which have been taken into account

The table below presents existing measures which have been take into account when assessing the likelihood and consequence of relevant incidents.

Hazard	Incident	Measures taken into account
Waste	Waste Handling	Fume hood and waste bucket

Existing relevant measures with descriptions:

Personal protective equipment

Safety boots, goggles, labcoat and gloves for different tasks

Fume hood and waste bucket

When pouring the oil into beakers, the fume hood will be used to prevent inhaling the oil mist.
A waste bucket will be used when throwing the oil away.

Lab tour

Introductory tour to get to know the lab and get some guidance.

HSE Introductory Course

Online Course

Risk analysis with evaluation of likelihood and consequence

This part of the report presents detailed documentation of hazards, incidents and causes which have been evaluated. A summary of hazards and associated incidents is listed at the beginning.

The following hazards and incidents has been evaluated in this risk assessment:

- **Waste**
  - Waste Handling

Detailed view of hazards and incidents:

Hazard: Waste

Incident: Waste Handling

The viscous emulsion clogged the waste bucket inlet.

Cause: Cause of incident

Description:

Too much emulsion were poured in the waste bucket inlet, so it was difficult to notice the clogged pipe.

Likelihood of the incident (common to all consequence areas): **Likely (3)**

Kommentar:

[Ingen registreringer]

Consequence area: Materielle verdier ***Risk:***

Assessed consequence: **Small (1)**

Comment: The pipe is only temporarily clogged, and the only concequence is that people have to wait in line to use the waste bucket. There are other available waste buckets in the laboratory.

Overview of risk mitiating actions which have been decided:

Below is an overview of risk mitigating actions, which are intended to contribute towards minimizing the likelihood and/or consequence of incidents:

- Waste Handling

Overview of risk mitigating actions which have been decided, with description:

Waste Handling

Empty the emulsion in mud waste bucket instead of in the waste collectors in fume hoods.

Action decided by:	Marthe Bodahl Lunde
Responsible for execution:	Marthe Bodahl Lunde
Deadline for execution:	6/1/2017

Detailed view of assessed risk for each hazard/incident before and after mitigating actions

Hazard: Waste

Incident: Waste Handling

Likelihood assessment (common to all consequence areas)

Initial likelihood: Likely (3)

Reason:

Likelihood after actions: Unlikely (1)

Reason:

Consequence assessments:

Consequence area: Materielle verdier ***Risk:***

Initial consequence: Small (1)

Reason: The pipe is only temporarily clogged, and the only concequence is that people have to wait in line to use the waste bucket. There are other available waste buckets in the laboratory.

Consequence after actions: Small (1)

Reason: When the waste bucket inlet pipe gets clogged, it needs time to drain into the bucket. Maybe other people have to wait in line to use the waste bucket, but there are other buckets available in the laboratory.

Appendix B Derivation of Pipe Flow for non-Newtonian Fluids

Power Law

Area $A = \pi r^2$

Circumference $S = 2\pi r$

Pressure $p = \frac{F}{A}$

Force $F = p \cdot A$

Setting up force balance:

$\Delta p \cdot A = \tau \cdot S \cdot L$

$\Rightarrow \Delta p \cdot \pi r^2 = \tau \cdot 2\pi r \cdot L$

$\Rightarrow \tau = \frac{\Delta p \cdot \pi r^2}{2\pi r \cdot L} \Rightarrow \underline{\tau = \frac{\Delta p r}{2L}}$

Using boundary condition at wall: $r = R, \tau = \tau_w$

$\Rightarrow \tau_w = \frac{\Delta p R}{2L}$

Rewriting $\tau = \frac{\Delta p r}{2L}$:

$\frac{\Delta p}{L} = \frac{2\tau}{r}$

See that $\frac{\Delta p}{L}$ is independent of r $\Rightarrow \frac{2\tau}{r}$ also has to be independent of R

This gives $\tau = K \cdot r$ where K is a constant

Using boundary conditions:

$$\begin{cases} r = 0 \Rightarrow \tau = 0 \\ r = \frac{D}{2} \Rightarrow \tau = \tau_w \end{cases}$$

The second boundary condition gives

$\tau_w = K \frac{D}{2} \Rightarrow K = \frac{2\tau_w}{D}$

$\Rightarrow \tau = K \cdot r = \frac{2\tau_w r}{D}$

Know that

$D = 2R \Rightarrow \tau = \frac{2\tau_w r}{2R} = \underline{\tau_w \frac{r}{R}}$

$$\int du = -\left(\frac{\Delta p}{2CL}\right)^{1/n} \cdot \int r^{1/n}\, dr$$

$$\Rightarrow u(r) = -\left(\frac{\Delta p}{2CL}\right)^{1/n} \cdot \frac{n \cdot r^{1/n+1}}{n+1} + C_1$$

Using boundary condition:

$u = 0$ at the wall $\Rightarrow r = \frac{D}{2} = R$

$$\Rightarrow u(R) = -\left(\frac{\Delta p}{2CL}\right)^{1/n} \cdot \frac{n \cdot R^{1/n+1}}{n+1} + C_1 = 0$$

$$\Rightarrow C_1 = \left(\frac{\Delta p}{2CL}\right)^{1/n} \cdot \frac{n \cdot R^{1/n+1}}{n+1}$$

$$\Rightarrow u(r) = -\left(\frac{\Delta p}{2CL}\right)^{1/n} \cdot \frac{n \cdot r^{1/n+1}}{n+1} + \left(\frac{\Delta p}{2CL}\right)^{1/n} \cdot \frac{n \cdot R^{1/n+1}}{n+1}$$

Simplifying:

$$u(r) = \left(\frac{\Delta p}{2CL}\right)^{1/n} \cdot \left[\frac{n \cdot R^{1/n+1}}{n+1} - \frac{n \cdot r^{1/n+1}}{n+1}\right]$$

$$\underline{u(r) = \left(\frac{\Delta p}{2CL}\right)^{1/n} \cdot \left[\frac{R^{1/n+1} - r^{1/n+1}}{1+1/n}\right]}$$

$$Q = \int u \cdot dA = \int u(r) \cdot 2\pi r \cdot dr = 2\pi \int u(r) \cdot r \cdot dr$$

Have that $u(r) = \left(\frac{\Delta p}{2CL}\right)^{1/n} \cdot \left[\frac{n \cdot R^{1/n+1}}{n+1} - \frac{n \cdot r^{1/n+1}}{n+1}\right]$

$$\Rightarrow Q = \frac{2\pi n}{n+1} \cdot \left(\frac{\Delta p}{2CL}\right)^{1/n} \cdot \int_0^R \left(R^{1/n+1} - r^{1/n+1}\right) \cdot r \cdot dr$$

$$\Rightarrow Q = \frac{2\pi n}{n+1} \cdot \left(\frac{\Delta p}{2CL}\right)^{1/n} \cdot \int_0^R \left(r \cdot R^{1/n+1} - r^{1/n+2}\right) \cdot dr$$

$$\Rightarrow Q = \frac{2\pi n}{n+1} \cdot \left(\frac{\Delta p}{2CL}\right)^{1/n} \cdot \left[\frac{r^2}{2} R^{1/n+1} - \frac{n \cdot r^{1/n+3}}{3n+1}\right]_0^R$$

$$\Rightarrow Q = \frac{2\pi n}{n+1} \cdot \left(\frac{\Delta p}{2CL}\right)^{1/n} \cdot \left[\frac{R^2}{2} R^{1/n+1} - \frac{n \cdot R^{1/n+3}}{3n+1}\right]$$

$$\Rightarrow Q=\frac{2\pi n}{n+1}\cdot\left(\frac{\Delta p}{2CL}\right)^{1/n}\cdot\left[\frac{R^{1/n+3}\left(3n+1\right)-2n\cdot R^{1/n+3}}{2\cdot\left(3n+1\right)}\right]$$

$$\Rightarrow Q=\frac{2\pi n}{n+1}\cdot\left(\frac{\Delta p}{2CL}\right)^{1/n}\cdot\left[\frac{3nR^{1/n+3}+R^{1/n+3}-2n\cdot R^{1/n+3}}{2\cdot\left(3n+1\right)}\right]$$

$$\Rightarrow Q=\frac{2\pi n}{n+1}\cdot\left(\frac{\Delta p}{2CL}\right)^{1/n}\cdot\left[\frac{nR^{1/n+3}+R^{1/n+3}}{2\cdot\left(3n+1\right)}\right]$$

$$\Rightarrow Q=\frac{2\pi n}{n+1}\cdot\left(\frac{\Delta p}{2CL}\right)^{1/n}\cdot\left[\frac{\left(n+1\right)R^{1/n+3}}{2\cdot\left(3n+1\right)}\right]$$

$$\Rightarrow Q=\pi n\cdot\left(\frac{\Delta p}{2CL}\right)^{1/n}\cdot\left[\frac{R^{1/n+3}}{\left(3n+1\right)}\right]=\frac{\pi nR^3}{3n+1}\cdot\left(\frac{\Delta pR}{2CL}\right)^{1/n}$$

$$\Rightarrow \underline{\underline{Q=\frac{\pi R^3}{3+1/n}\cdot\left(\frac{\Delta pR}{2CL}\right)^{1/n}}}$$

Herschel-Bulkley

1) Forcebalance along the pipe: $\tau_w=\frac{\Delta pR}{2L}$

2) As shown in the derivation of Power law flow: $\tau=\frac{r}{r_w}=\tau_w$

3) Expression for Herschel-Bulkley: $\tau=\tau_0+C\left(\frac{dv}{dr}\right)^n$

For the liquid to flow $\tau\left(r\right)\geq\tau_0$

$$\tau\left(r\right)=\frac{\Delta p}{2L}r=\frac{r}{r_w}\tau_w\geq\tau_0$$

4) τ_0 is reached at radius $r_0\Rightarrow r_0=\frac{2L}{\Delta p}\tau_0$

Fluid will flow as a plug within r_0 and as a Power law fluid outside with shear rate relation as in 3):

Combining 1), 2), 3) and 4):

$$\tau\left(r\right)=\frac{\Delta p}{2L}r=\tau_0+C\left(\frac{dv}{dr}\right)^n=\frac{\Delta p}{2L}r_0+C\left(\frac{dv}{dr}\right)^n$$

For $r > r_0$:

$$\frac{\Delta p}{2L} r = \frac{\Delta p}{2L} r_0 + C\left(\frac{dv}{dr}\right)^n \Rightarrow C\left(\frac{dv}{dr}\right)^n = \frac{\Delta p}{2L}\left(r - r_0\right)$$

$$\Rightarrow \left(\frac{dv}{dr}\right)^n = \frac{\Delta p}{2LC}\left(r - r_0\right) \Rightarrow \frac{dv}{dr} = \left(\frac{\Delta p}{2LC}\right)^{1/n} \cdot \left(r - r_0\right)^{1/n}$$

Defining $r - r_0 = \hat{r} \Rightarrow \frac{dv}{d\hat{r}} = \left(\frac{\Delta p}{2LC}\right)^{1/n} \cdot \hat{r}^{1/n}$

$$\Rightarrow v\left(\hat{r}\right) = \int \left(\frac{\Delta p}{2LC}\right)^{1/n} \cdot \hat{r}^{1/n} d\hat{r} = \left(\frac{\Delta p}{2LC}\right)^{1/n} \cdot \left[\frac{n}{n+1} \hat{r}^{(n+1)/n}\right]$$

$$\Rightarrow Q = 2\pi \cdot \int_0^{\hat{r}_w} v\left(\hat{r}\right) \cdot \left(\hat{r} - r_0\right) d\hat{r} = 2\pi v_0 \cdot \int_0^{\hat{r}_w} \left(1 - \left(\frac{\hat{r}}{\hat{r}_w}\right)^{(n+1)/n}\right) \cdot \left(\hat{r} - r_0\right) d\hat{r}$$

$$= 2\pi v_0 \cdot \int_0^{\hat{r}_w} \left(\hat{r} + r_0 - \hat{r}^{\frac{1}{n}+2} \cdot \hat{r}_w^{\,-(n+1)/n} - r_0 \cdot \hat{r}^{(n+1)/n} \cdot \hat{r}_w^{\,-(n+1)/n}\right) d\hat{r}$$

$$= 2\pi v_0 \cdot \left[\frac{1}{2}\hat{r}\left(r_0\left(2 - \frac{2n\hat{r}_w^{\,-(n+1)/n} \cdot \hat{r}_w^{\,(n+1)/n}}{2n+1}\right) - \frac{2n\hat{r}_w^{\,-(n+1)/n} \cdot \hat{r}_w^{\,\frac{1}{n}+2}}{3n+1} + \hat{r}\right)\right]_0^{\hat{r}_w}$$

$$= 2\pi v_0 \cdot \left[\frac{1}{2}\hat{r} \cdot r_0 \cdot 2 - \frac{1}{2}\hat{r} \cdot r_0 \cdot \frac{2n\hat{r}_w^{\,-(n+1)/n} \cdot \hat{r}_w^{\,(n+1)/n}}{2n+1} - \frac{\frac{1}{2}\hat{r} \cdot 2n\hat{r}_w^{\,-(n+1)/n} \cdot \hat{r}_w^{\,\frac{1}{n}+2}}{3n+1} + \frac{1}{2}\hat{r} \cdot \hat{r}\right]_0^{\hat{r}_w}$$

$$\Rightarrow Q = 2\pi v_0 \left[\hat{r} r_0 - \frac{1}{2}\hat{r} r_0 \frac{2n\overbrace{\hat{r}_w^{\,-(n+1)/n} \cdot \hat{r}_w^{\,(n+1)/n}}^{\frac{-n+1}{n}+\frac{n+1}{n}=0}}{2n+1} - \frac{1}{2}\hat{r} \frac{2n\overbrace{\hat{r}_w^{\,-(n+1)/n} \cdot \hat{r}_w^{\,\frac{1}{n}+2}}^{\frac{-n+1}{n}+\frac{1}{n}+2=1}}{3n+1} + \frac{1}{2}\hat{r}^2\right]_0^{\hat{r}_w}$$

$$Q = 2\pi v_0 \left[\hat{r}_w r_0 + \frac{1}{2}\hat{r}_w^{\,2} - \frac{1}{2}\hat{r}_w r_0 \cdot \left(\frac{2n}{2n+1}\right) \cdot \hat{r}_w^{\,0} - \frac{1}{2}\hat{r}_w \left(\frac{2n}{3n+1}\right) \cdot \hat{r}_w^{\,1}\right]$$

$$\Rightarrow Q = 2\pi v_0 \left[\hat{r}_w r_0 + \frac{1}{2}\hat{r}_w^{\,2} - \frac{n}{2n+1}\hat{r}_w r_0 - \frac{n}{3n+1}\hat{r}_w^{\,2}\right]$$

$$Q = 2\pi v_0 \left[\hat{r}_w r_0 \left(1 - \frac{n}{2n+1} \right) + \hat{r}_w^{\,2} \left(\frac{1}{2} - \frac{n}{3n+1} \right) \right]$$

$$\Rightarrow Q = 2\pi v_0 \left[\hat{r}_w r_0 \left(\frac{2n+1-n}{2n+1} \right) + \hat{r}_w^{\,2} \left(\frac{3n+1-2n}{2(3n+1)} \right) \right]$$

$$Q = 2\pi v_0 \left[\hat{r}_w r_0 \left(\frac{n+1}{2n+1} \right) - \hat{r}_w^{\,2} \left(\frac{n+1}{2(3n+1)} \right) \right]$$

$$Q = \pi v_0 \left[\hat{r}_w r_0 \left(\frac{2n+2}{2n+1} \right) - \hat{r}_w^{\,2} \left(\frac{n+1}{3n+1} \right) \right]$$

Use that $\hat{r}_w = r_w - r_0$:

$$\Rightarrow \underline{Q_{Herschel-Bulkley} = \pi v_0 \left[(r_w - r_0) r_0 \left(\frac{2n+2}{2n+1} \right) - (r_w - r_0)^2 \left(\frac{n+1}{3n+1} \right) \right]}$$

Now we add * and ** together to find Q_{tot} :

$$Q_{tot} = \pi v_0 r_0^{\,2} + \pi v_0 \cdot \left[(r_w - r_0) r_0 \left(\frac{2n+2}{2n+1} \right) - (r_w - r_0)^2 \left(\frac{n+1}{3n+1} \right) \right]$$

$$\Rightarrow \underline{Q_{tot} = \pi v_0 \cdot \left[r_0^{\,2} + \left(\frac{2n+2}{2n+1} \right) \cdot (r_w - r_0) r_0 - \left(\frac{n+1}{3n+1} \right) \cdot (r_w - r_0)^2 \right]}$$

where $r_0 = \tau_0 \dfrac{2L}{\Delta p}$ and $v_0 = -\left(\dfrac{\Delta p}{2\mu_0 L} \right)^{1/n} \cdot \dfrac{n}{n+1} \cdot (r_w - r_0)^{(n+1)/n}$

Appendix C MATLAB Scripts

Script for Finding the Power Law Parameters: ”Parameters_PL”

```
clear all
close all
clc

%% Taking values from Anton-Paar
load flow_fresh6040.txt
data = flow_fresh6040;
ant=size(data);
n=ant;              %Number of measuringpoints

rate=data(1:n,1);   %1st column
stress=data(1:n,2); %2nd column


%% Plotting and fitting line to get C and n
plot(rate,stress)
hold on
f = fit(rate, stress, 'power1')
plot(f,rate,stress)
title('Plot')
xlabel('Shear rate')
ylabel('Shear stress')
```

Pipe Flow for Power Law Fluid Script: ”Flowrate_PL”

```
clc
clear all
close all
%% Input from Anton-Paar:
C = 2.802;                                  % (a) Consistency parameter
[Pa*s^n]
n = 0.6573;                                 % (b) Flow behavior index n
[dim.less]

%% Input based on seperate measurements
rho = 950;                                  %Density [kg/m^3]

%% Loading data
load flow_fresh_S6040.txt
data = flow_fresh_S6040;
ant=size(data);
no=ant;                                  %Number of measuringpoints
mu =data(1:no,3);                        %Viscosity [Pa*s]

%% Designing Pipe by guessing R and L:
R = 0.0125;                              %Inner radius R [m]
D = 2*R;                                 %Diameter D [m]
L = 1.8;                                 %Length of pipe [m]
h = 1.8636;                              %Total fluid height [m]
%% Flow Equation for Power Law:
g = 9.81;                                           %Gravity [m/s^2]
```

```
Hp = rho*g*h;                                          %Hydraulic potential
[Pa]

Q = ((pi*R^3)/(3+1/n))*((Hp*R)/(2*C*L))^(1/n);         %Flow rate [m^3/s]
Q_l = Q/0.001                                          %Flow rate [l/s]

A = pi*R^2;                                            %Area [m^2]
v = Q/A                                                %Veloity [m/s]
v_cm = v*10^2;                                         %Veloity [cm/s]

%% Checking the Flow Regime and Entry Length

for i = 1:length(mu)
    Re(i) = (rho*v*D)/mu(i);                           %Reynolds number
    f(i) = 64/Re(i);                                   %Friction factor in a
circularpipe
end

Re(1)
Re(length(Re))

if Re <= 2300
    disp('Laminar flow')
    L_entry_lam = 0.05*Re*D;                              %Entry length
laminar flow

    L_entry_lam(1)
    L_entry_lam(length(L_entry_lam))
elseif Re >= 4000
    disp('Turbulent flow')
    L_entry_turb = 1.359*Re^(1/4)*D;                      %Entry length
turbulent flow
else
    disp('Transitional flow')

end
```

Script for Finding the Herschel-Bulkley Parameters: ”Parameters_HB”

```
clear all
close all
clc

%% Taking values from Anton-Paar
load flow_fresh_S6040.txt
data = flow_fresh_S6040;
ant=size(data);
n=ant;              %Number of measuringpoints

rate=data(1:n,1);   %1st column
stress=data(1:n,2); %2nd column

%% Plotting and fitting line to get C and n
plot(rate,stress)
hold on
f = fit(rate, stress, 'power2')
```

```
plot(f,rate,stress)
title('Plot')
xlabel('Shear rate')
ylabel('Shear stress')
```

Pipe Flow for Herschel-Bulkley fluid Script: ”Flowrate_HB”

```
clc
clear all
close all

%% Input from Anton-Paar:
C   = 1.078;                                % (a) Consistency parameter
[Pa*s^n]
n   = 0.791;                                % (b) Flow behavior index n
[dim.less]
t_0 = 18.64 ;                               % (c) Yield point

%% Input based on seperate measurements
rho = 950;                                  %Density [kg/m^3]

%% Loading data
load flow_fresh_S6040.txt
data = flow_fresh_S6040;
ant=size(data);
no=ant;                                 %Number of measuringpoints
mu =data(1:no,3);                       %Viscosity [Pa*s]

%% Flow capacity setup parameters
R = 0.0125;                             %Inner radius R [m]
D = 2*R;                                %Diameter D [m]
L = 1.8;                                %Length of pipe [m]
h = 1.8636;                             %Total fluid height [m]

%% Flow Equation for Herschel-Bulkley:
g = 9.81;                                           %Gravity [m/s^2]
Hp = rho*g*h;                                       %Hydraulic potential
[Pa]
r_0 = (t_0*2*L)/Hp;
v_0 = ((Hp/(2*C*L))^(1/n))*(n/(n+1))*(R-r_0)^((n+1)/n);

Q = v_0*pi*(r_0^2+((2*n+2)/(2*n+1))*r_0*(R-r_0)+((n+1)/(3*n+1))*(R-r_0)^2);
%Flow rate [m^3/s] (minus only indicates direction)

Q_l = Q/0.001                                       %Flow rate [l/s]

A = pi*R^2;                                         %Area [m^2]
v = Q/A                                             %Veloity [m/s]
v_cm = v*10^2;                                      %Veloity [cm/s]

%% Checking the Flow Regime and Entry Length

for i = 1:length(mu)
    Re(i) = (rho*v*D)/mu(i);                        %Reynolds number
    f(i) = 64/Re(i);                                %Friction factor in a
circularpipe
end
    Re(1)
```

```
    Re(length(Re))

if Re <= 2300
    disp('Laminar flow')
    L_entry_lam = 0.05*Re*D;                              %Entry length
laminar flow
    L_entry_lam(1)
    L_entry_lam(length(L_entry_lam))
elseif Re >= 4000
    disp('Turbulent flow')
    L_entry_turb = 1.359*Re^(1/4)*D;                      %Entry length
turbulent flow
else
    disp('Transitional flow')
end
```

Volume Distribution Script by H. A. Asheim: ”volumedistribution”

```
%% LogNormal dropletdistribution
clear all
clf
clc
load forfann703015all.txt
data=forfann703015all;
ant=size(data);
n=ant(1);               % number of measuringpoints, 1st column Excel
file

   A=data(1:n,2);       % areal calculated by ImageJ, 2nd column
Excel file
   dmax=data(1:n,3);    % Feret diameter, 3rd column Excel file
    dmin=data(1:n,4);   %Minimum Feret diameter, 4th column Excel
file

%% Volume, assumed rotational ellipsoids
pf=1.6075;
for i=1:n
V(i)=4/3*pi*(dmin(i)/2)*(dmax(i)/2)^2;                              %
volume, rotational ellipsoid
Sf(i)=pi*( (dmax(i)^(2*pf) + 2*dmax(i)^pf*dmin(i)^pf)/3)^(1/pf);  %
surface, rotation ellipsoide
end
%% Empirical distribution
   Vs=sort(V);        % sort dropletvolume in ascending order

   Vsum(1)=Vs(1);
   for i=2:n
   Vsum(i)=Vsum(i-1)+Vs(i);
   end
   Vtot=Vsum(n);
   Fe=Vsum/Vtot;      % Fe(Vs) = empirical cummulative distribution
%% Surface area
    for i=1:n
   S(i)=(6*pi^(1/2)*Vs(i))^(2/3);    % surfaces, sorted
   end
   osp=40e-3; %surface tension
```

```
   Stot=sum(S);
   Srel=Stot/Vtot;
   Sfrel=sum(Sf)/Vtot;
%% Block diagram showing empirical probability density
nf=10;  % Number of discretization points
Vint=linspace(0,Vs(length(Vs))*1.001,nf); % dividing into intervals
for j=1:nf-1
   % finding volume increase in each interval
   Vf(j)=0;
   for i=1:length(Vs)
       if Vs(i)>Vint(j)& Vs(i)<Vint(j+1)
   Vf(j)=Vf(j)+Vs(i);
       end
   end
   Vip(j)=(Vint(j)+Vint(j+1))/2;             % interval midpoint
   fV(j)=(Vf(j)/(Vint(j+1)-Vint(j)))/Vtot;  %  empirical probability
density
end

 %% Mean value and variance of measured data
 Em=0;
for i=2:n
Em=Em+Vs(i)^2/Vtot;
end
var=0;
 for i=2:n
     var=var+Vs(i)^3/Vtot;
 end
 sm=var^0.5;

%% Expected estimates of location parameter: my and scale parameter:
s2
 my=log(Em)-0.5*log(1+var/Em^2);
 s2=log(1+var/Em^2);

 %% Deviation
 f=0;
 for i=1:n
Fi=0.5*erfc(-(log(Vs(i))-my)/(2*s2)^0.5);
f=f+(Fi-Fe(i))^2;
 end
 f=f/n; %average deviation
 errm=100*f^0.5;

%% Calculation of LogN-distribution before optimization
x=linspace(0.001,Vs(n));
for i=1:length(x)
fv(i)=(1/(2*s2*pi)^0.5)/x(i)*exp(-(log(x(i))-my)^2/(2*s2));
Fv(i)=0.5*erfc(-(log(x(i))-my)/(2*s2)^0.5);
end

 %-----------------  optimize ---------------------------------
global Feg xg
Feg=Fe;           % empirical cummulative distribution
```

```
xg=Vs;              % x-axis
pa0= [my s2 ];    % initial parameter estimate
[pa,fval]=fminunc(@optfun,pa0);

 % optimized estimate of location paramete: my and scale parameter:
s2
 myopt=pa(1);
 s2opt=pa(2);
 % writing out
 disp([ '....LogNormal distribution, adjusted to measured droplet
volumes.'])
 disp(['.................  From starting data --------- '])
disp(['Standard deviation of measured data :
',num2str(sm,'%5.3e\n')])
disp(['Total droplet volume           : ',num2str(Vtot,'%5.3e\n'),'
mm^3'])
disp(['Surface area/droplet volume    : ',num2str(Srel,'%5.3e\n')])
disp(['Surface area/droplet volume rotational ellipsoid    :
',num2str(Sfrel,'%5.3e\n')])
 % surface
 C=(6*sqrt(pi))^(2/3);
  Sf(1)=0;
 for i=2:length(x)
 Sf(i)=Sf(i-1)+ C*fv(i)/x(i)^(1/3)*(x(i)-x(i-1));
 end

Sfmax=Sf(length(x));
Sf2=C*exp((1/18*(-6*my+s2)));          % analytical

disp(['.................  Direct fitting --------- '])
disp(['Mean value                  : ',num2str(Em,'%5.3e\n')])
disp(['Standard deviation                : ',num2str(sm,'%5.3e\n')])
disp(['Surface area/droplet volume    :',num2str(Sf2,'%5.3e\n'),'
(1/mm )'])
disp(['Error while fitting             : ',num2str(errm,'%5.3e\n'),'
%'])


%%  LogN-distribution based on optimized parameters
 z=linspace(0.0001,2*Vs(n), 300);
for i=1:length(z)
fao(i)=(1/(2*s2opt*pi)^0.5)/z(i)*exp(-(log(z(i))-
myopt)^2/(2*s2opt));
Fao(i)=0.5*erfc(-(log(z(i))-myopt)/(2*s2opt)^0.5);
end
   m=exp(myopt+s2opt/2);                        % mean value, 1.
moment of distribution
 sd=((exp(s2opt)-1)*exp(2*myopt+s2opt))^0.5;   % standard deviation
 sdi2=0;
 for i=2:length(z)
     sdi2=sdi2+(z(i)-m)^2*fao(i)*(z(i)-z(i-1));
 end

 sdi=sdi2^0.5;  % standard deviation with numerical integration
```

```
 err=100*fval^0.5;
 dfsd=(1+(sd/m^2)^0.5);
disp(['.................  Optimized fitting --------- '])
disp(['Mean value                    ',num2str(m,'%5.3e\n')])
disp(['Standard deviation                  ',num2str(sd,'%5.3e\n')])
disp(['Error while fitting                ',num2str(err,'%5.3e\n'),'
%'])


  xmax=1.1*Vs(n);
   subplot(2,1,1)
 hold on
 plot(Vs,Fe,'.')
 plot(x,Fv,'k')
  plot(z,Fao,'r--')
  plot([Em Em],[0 1],'r')
   % plot([Em+sm Em+sm],[0 1],'m-')
 hold off
 xlabel('\bf Droplet volume: V_d (\mum^3)')
 ylabel('\bfCummulative: F  (-)')
 grid
 %legend('Measured ','_Distribution: F_N(m,s)','Optimzed
distribution','Mean value: m','m + Measured standard deviation')
 legend('Measured data','Logarithmic distribution:
F_N(m,s)','Optimized distribution','Mean value: m')
 legend('Location','SouthEast')
axis([0 xmax 0 1 ])

 %% density
 maxf=1.2*max([max(fv),max(fao)]);
subplot(2,1,2)
hold on
%bar(Vip,fV)
 plot(x,fv,'k')
plot(z,fao,'r--')
 %plot([Em Em],[0 1],'r-.')
    %plot([Em+sm Em+sm],[0 1],'m-')
% plot([E E],[0, max(f)],'b-.')
hold off
xlabel('\bf Droplet volume: V_d  (\mum^3)')
 ylabel('\bf Distribution density: f_v')
 %legend('Distribution density: f_v(m,s)','Optimized distribution
density','  MÂlt middelverdi','m + MÂlt standardavvik')
 legend('Direct estimate','Optimized estimate')
grid
 axis([0 xmax 0 maxf ])
% legend(' Grouped measurements','Adjusted to logN')
```

”optfun” Function Used in ”volumedistribution” Script:

```
  function f = optfun(pa)
  %Minimizing least squares between cumulative F(my,s2) and
empirical F
  global Feg xg
  % parameters to be optimized
 my=abs(pa(1));
 s2=abs(pa(2));
 %estimating objectfunction: sum of least squares
 f=0;
 for i=1:length(xg)
Fi=0.5*erfc(-(log(xg(i))-my)/(2*s2)^0.5);
f=f+(Fi-Feg(i))^2;    %
 end
 f=f/length(xg); %mean deviation
 disp([' my= ',num2str(my),'    s= ',num2str(s2^0.5),'   f=
',num2str(f)])
```

Appendix D Constant Determination for Flow Models

Power Law as Appropriate Model

E30-70

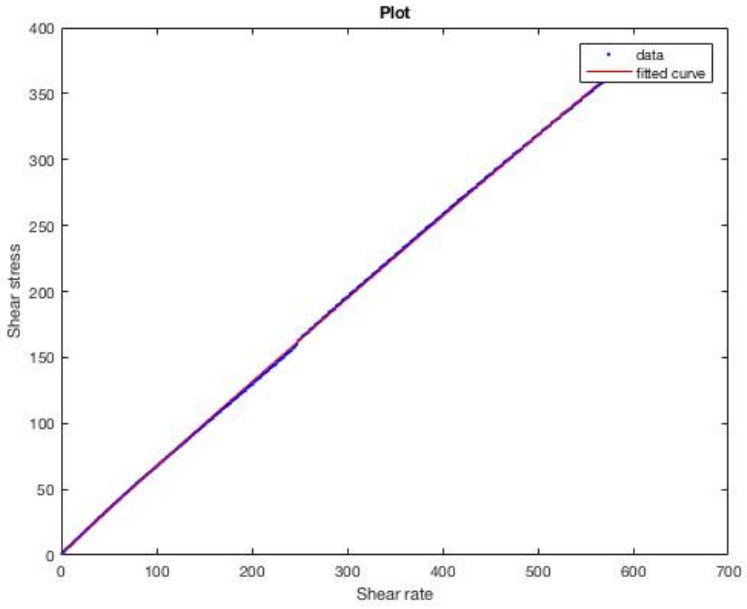

Figure D.1: Curvefit from MATLAB, E30-70 emulsion

E40-60

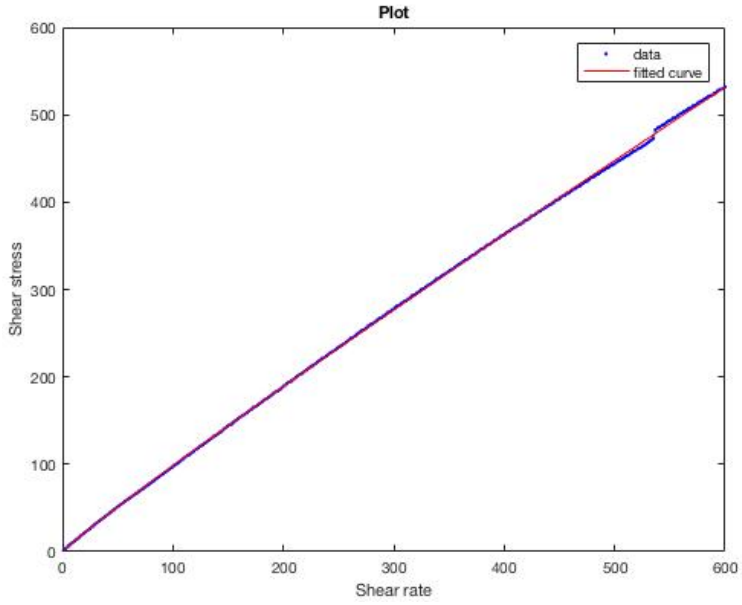

Figure D.2:Curvefit from MATLAB, E40-60 emulsion

E50-50

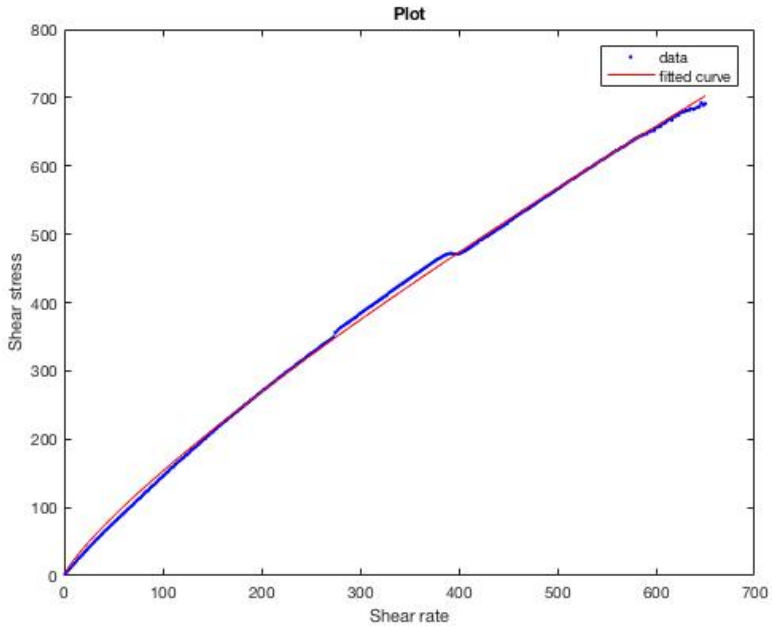

Figure D.3: Curvefit from MATLAB, E50-50 emulsion

E60-40

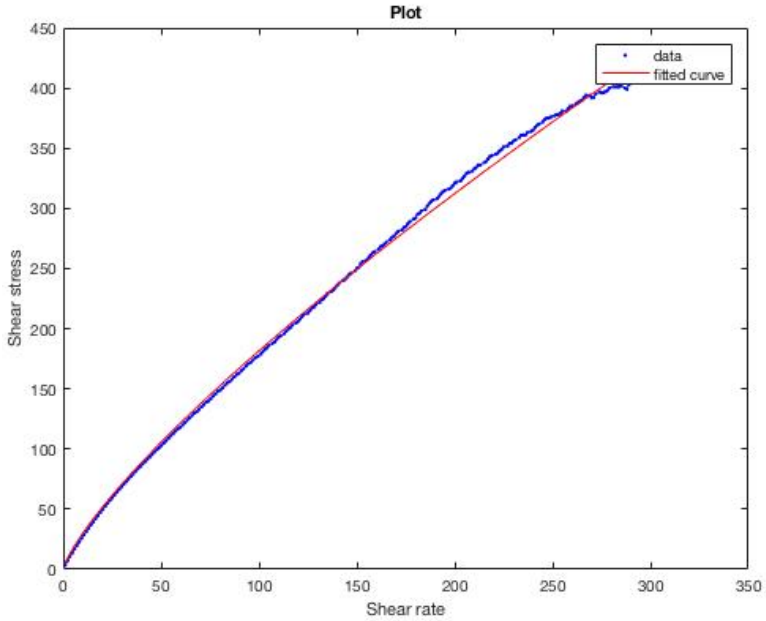

Figure D.4: Curvefit from MATLAB, E60-40 emulsion

All these plots and corresponding constants are found by running the ”constants_powerlaw” script in MATLAB.

Table D.1: Overview of the Power law constants found in MATLAB, including 95% confidence bounds

Emulsion	C	95% confidece bounds	n	95% confidence bounds
E30-70	0.7976	(0.7893, 0.8059)	0.9638	(0.9621, 0.9655)
E40-60	1.288	(1.2740, 1.3030)	0.9414	(0.9396, 0.9432)
E50-50	3.608	(3.5200, 3.6960)	0.8139	(0.8099, 0.8179)
E60-40	4.961	(4.7760, 5.1470)	0.7818	(0.7748, 0.7888)

Herschel-Bulkley as Appropriate Model

S60-40

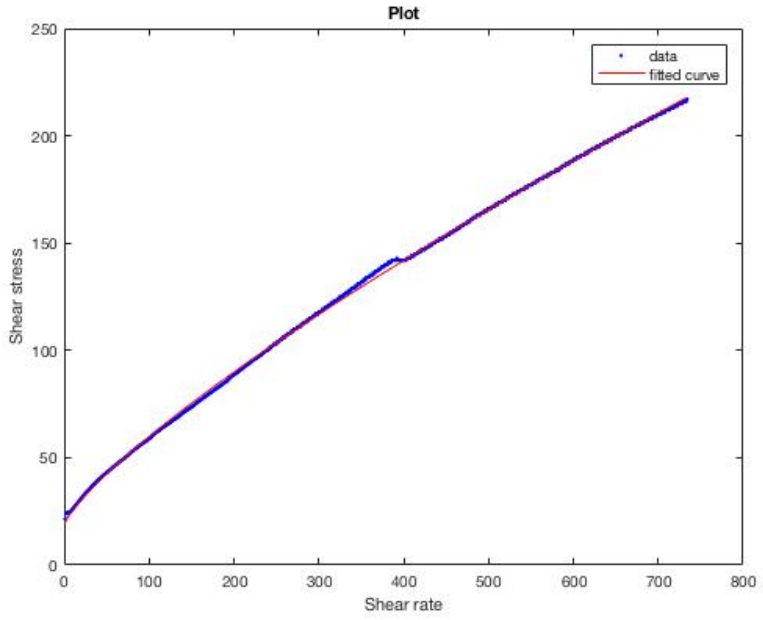

Figure D.5:Curvefit from MATLAB, S60-40 emulsion

Table D.2:Overview of the Herschel-Bulkley constants found in MATLAB including 95% confidence bounds

S60-40	Constant	95% confidece bounds
C	1.078	(1.0490, 1.1070)
n	0.791	(0.7872, 0.7948)
τ_0	18.64	(18.220, 19.060)

This plot and constants are found by running the ”constants_herschelbulkley” script in MATLAB.

Power Law as Inappropriate Model

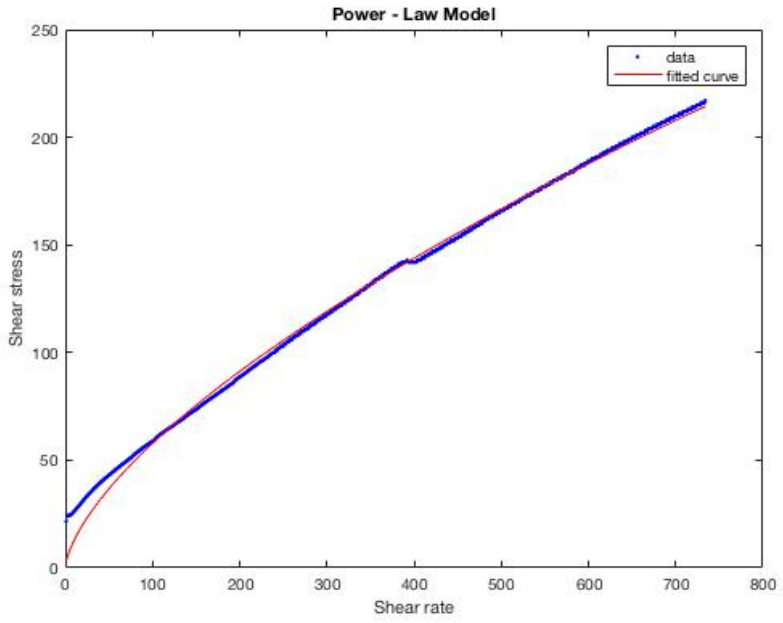

Figure D.6: Curvefit from MATLAB using the inappropriate model, S60-40 emulsion

Table D.3: Overview of the Power law constants found in MATLAB by using the inappropriate model, including 95% confidence bounds

Emulsion	C	95% confidece bounds	n	95% confidence bounds
S60-40	2.802	(2.731, 2.873)	0.6573	(0.6532, 0.6614)

Herschel-Bulkley as Inappropriate Model

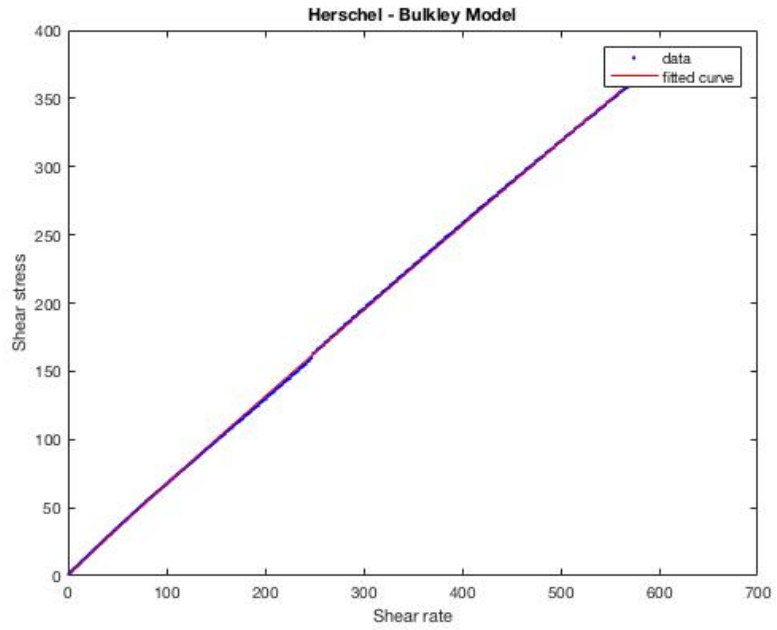

Figure D.7: Curvefit from MATLAB using the inappropriate model, E30-70 emulsion

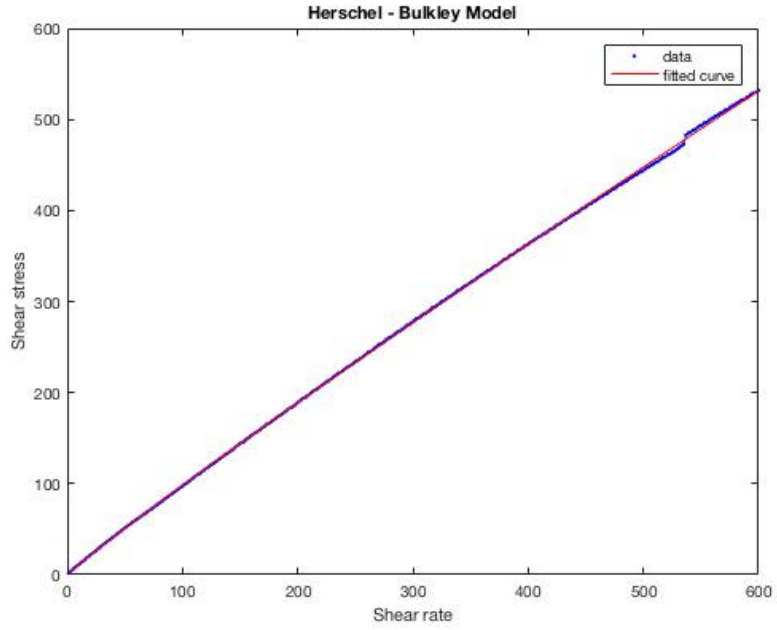

Figure D.8: Curvefit from MATLAB using the inappropriate model, E40-60 emulsion

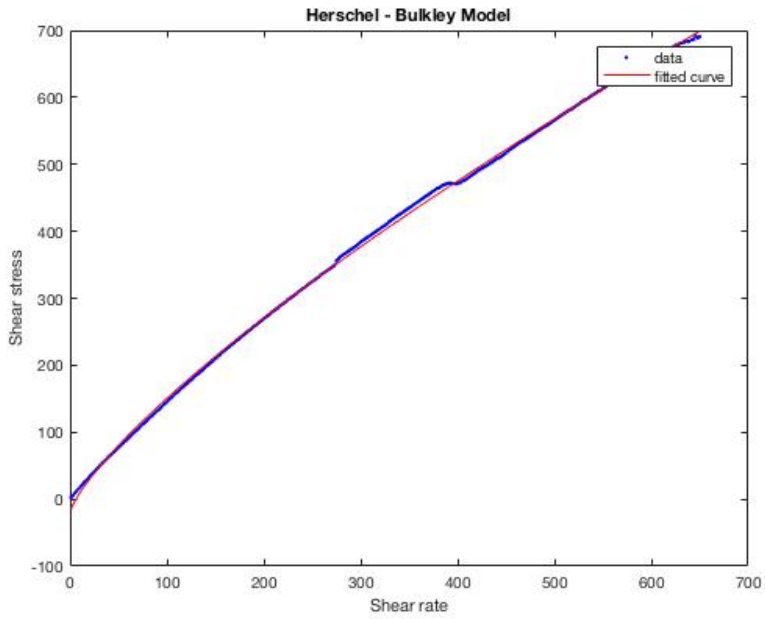

Figure D.9: Curvefit from MATLAB using the inappropriate model, E50-50 emulsion

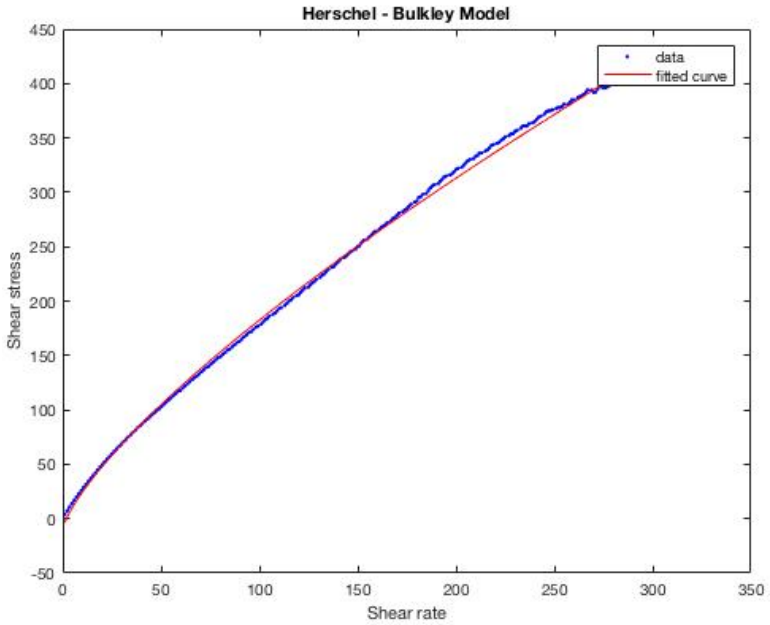

Figure D.10: Curvefit from MATLAB using the inappropriate model, E60-40 emulsion

Table D.4: Overview of the Herschel-Bulkley constants found in MATLAB by using the inappropriate model, including 95% confidence bounds

E30-70	**Constant**	**95% confidece bounds**
C	0.8061	(0.7876, 0.8247)
n	0.9622	(0.9587, 0.9657)
τ_0	-0.2819	(-0.8231, 0.2593)
E40-60	**Constant**	**95% confidece bounds**
C	1.305	(1.273, 1.337)
n	0.791	(0.7872, 0.7948)
τ_0	-0.483	(-1.319, 0.3529)
E50-50	**Constant**	**95% confidece bounds**
C	4.956	(4.736, 5.176)
n	0.7684	(0.7619, 0.7749)
τ_0	-19.95	(-22.61, -17.29)
E60-40	**Constant**	**95% confidece bounds**
C	6.206	(5.645, 6.767)
n	0.746	(0.7312, 0.7608)
τ_0	-10.12	(-14.02, -6.22)

Appendix E Rheological Measurements

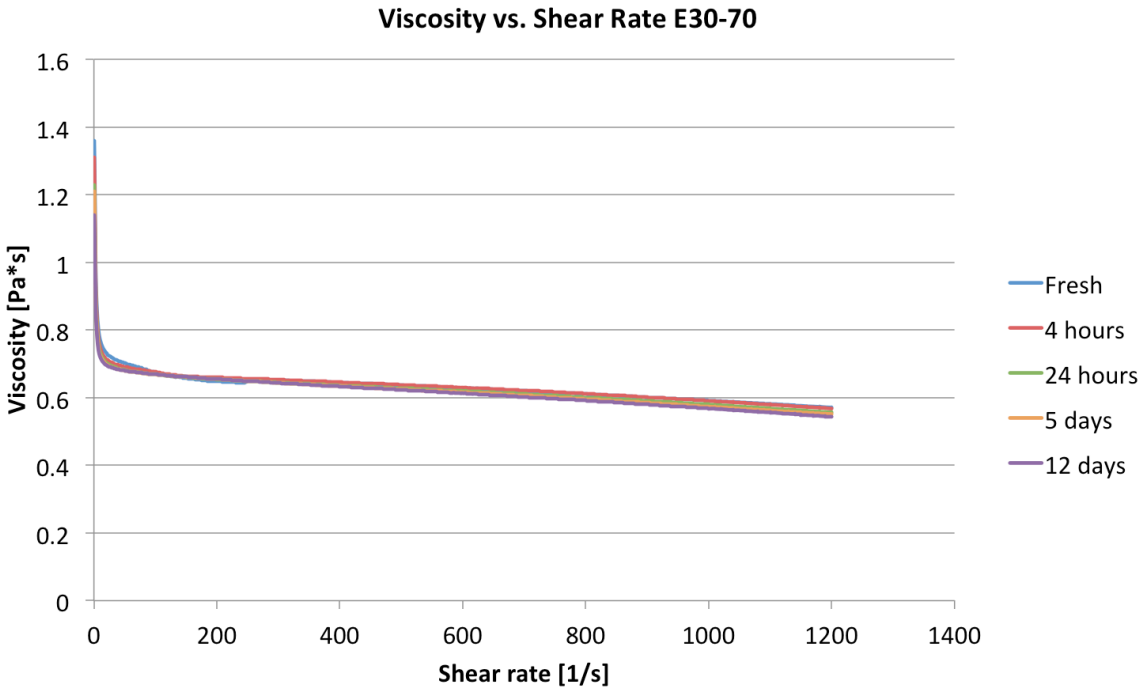

Figure E.1: Viscosity vs. shear rate with aging for E30-70

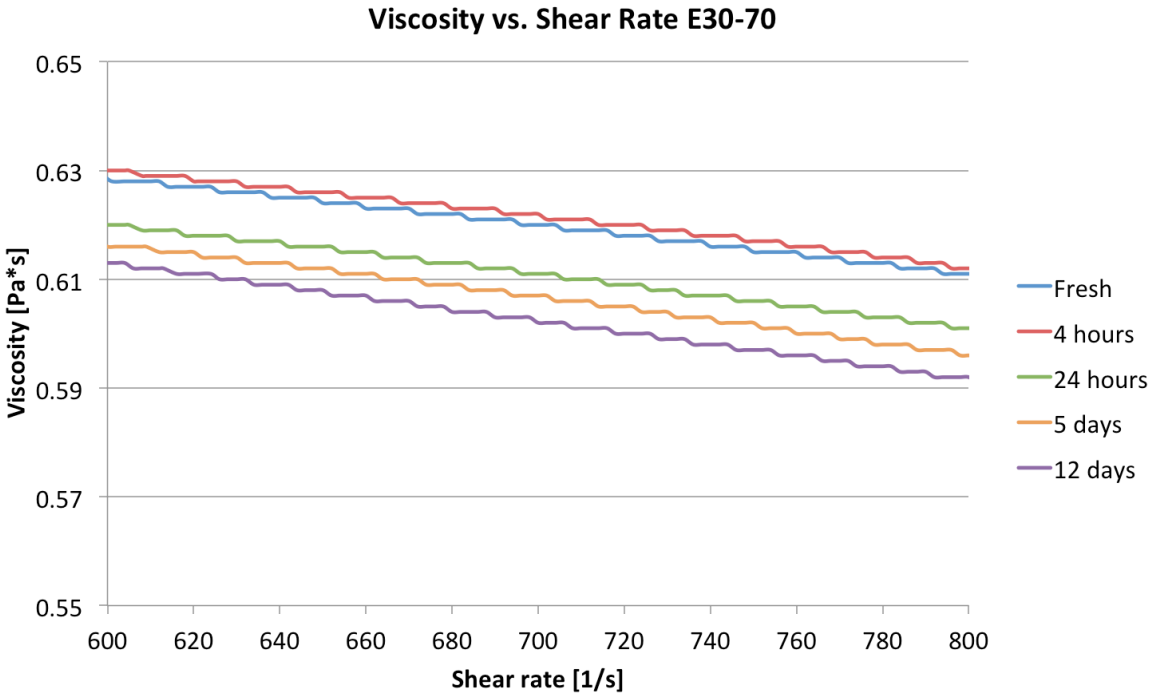

Figure E.2: Zoomed section of Figure E.1

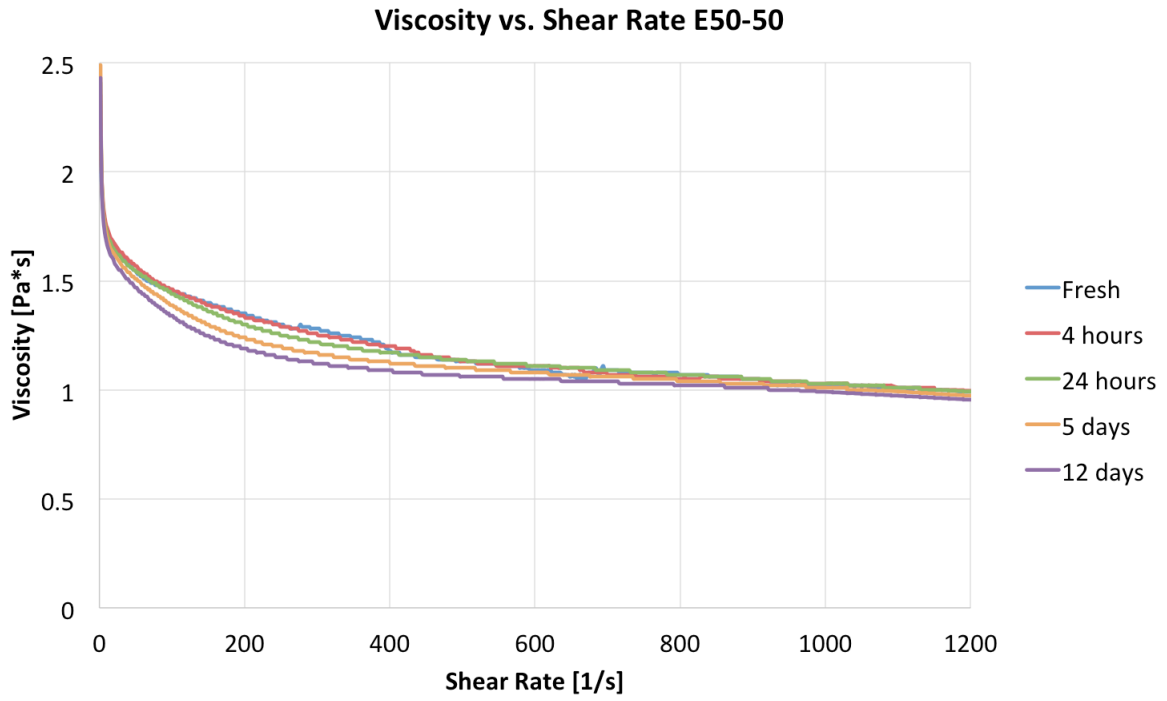

Figure E.3: Viscosity vs. shear rate with aging for E50-50

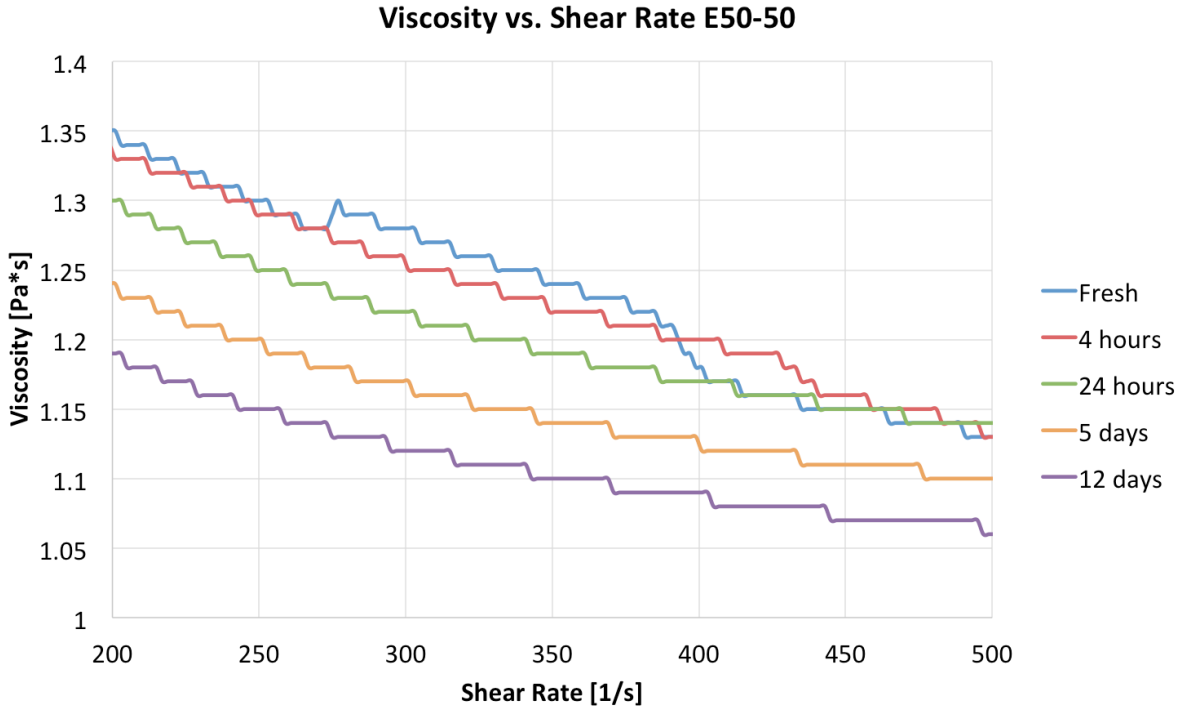

Figure E.4: Zoomed section of Figure E.3

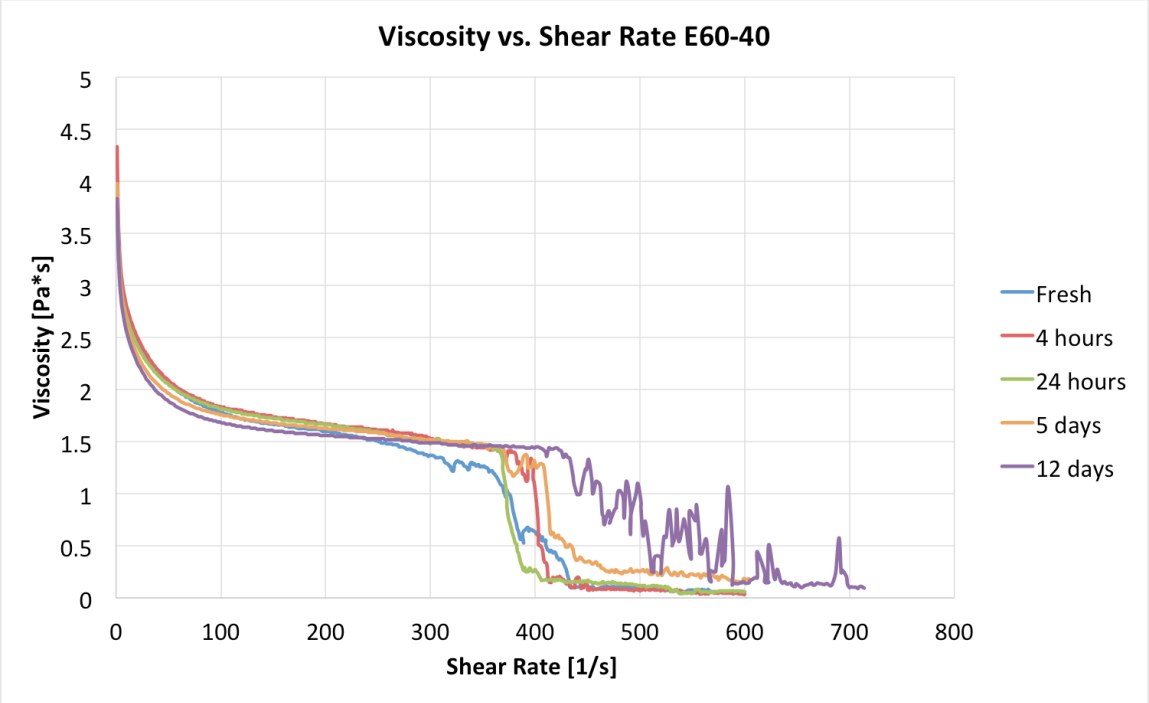

Figure E.5: Viscosity vs. shear rate with aging for E60-40

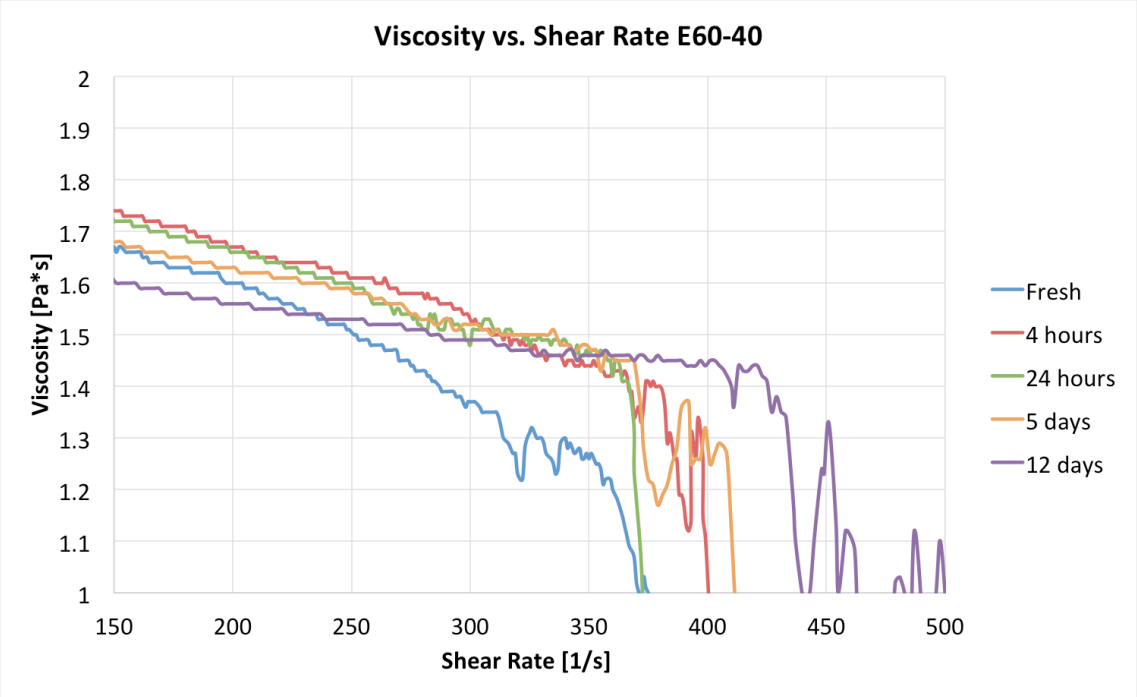

Figure E.6: Zoomed section of Figure E.5

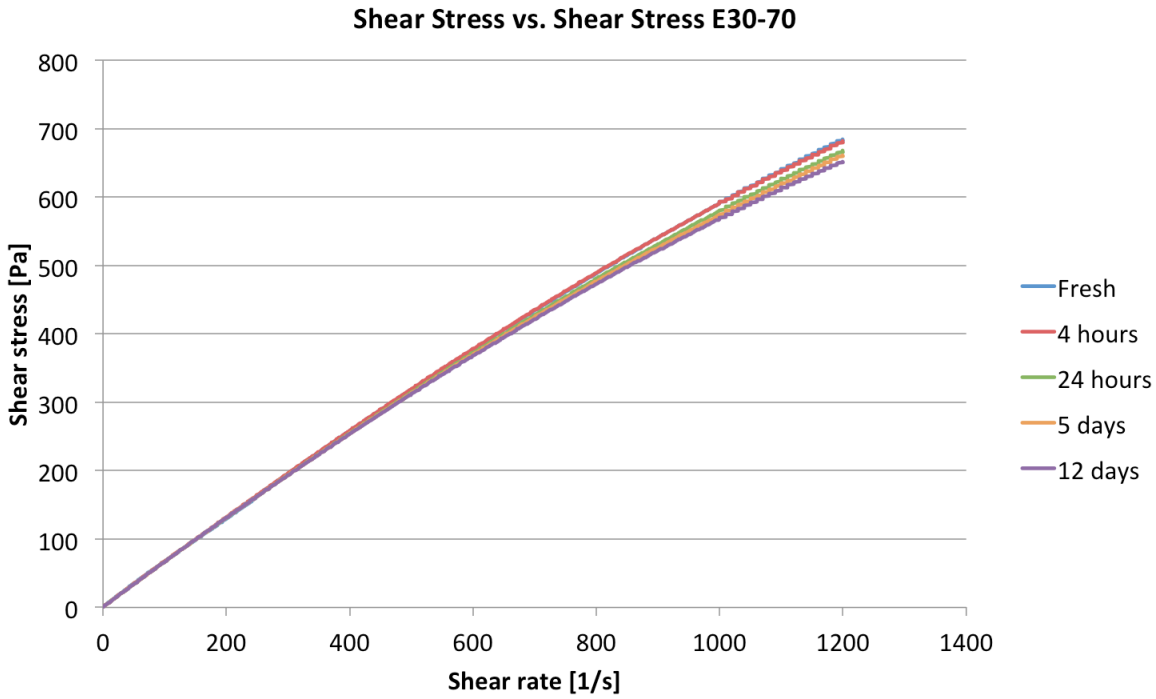

Figure E.7 Shear stress vs. shear rate with aging for E30-70

Figure E.8: Zoomed section of Figure E.7

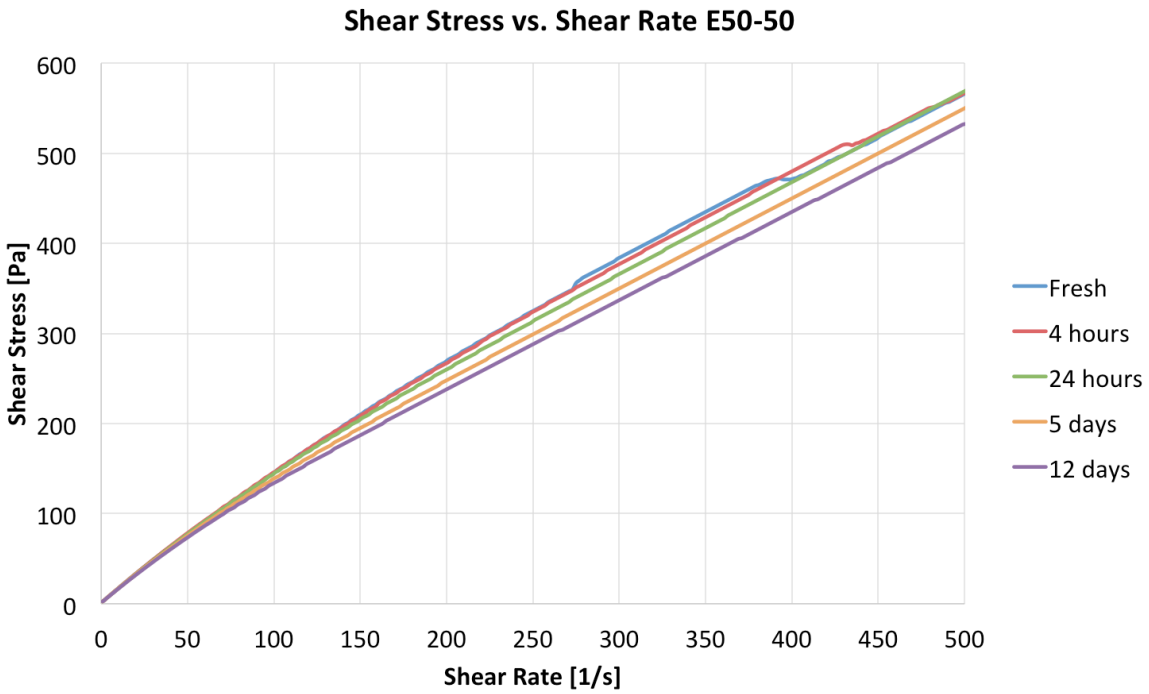

Figure E.9: Shear stress vs. shear rate with aging for E50-50

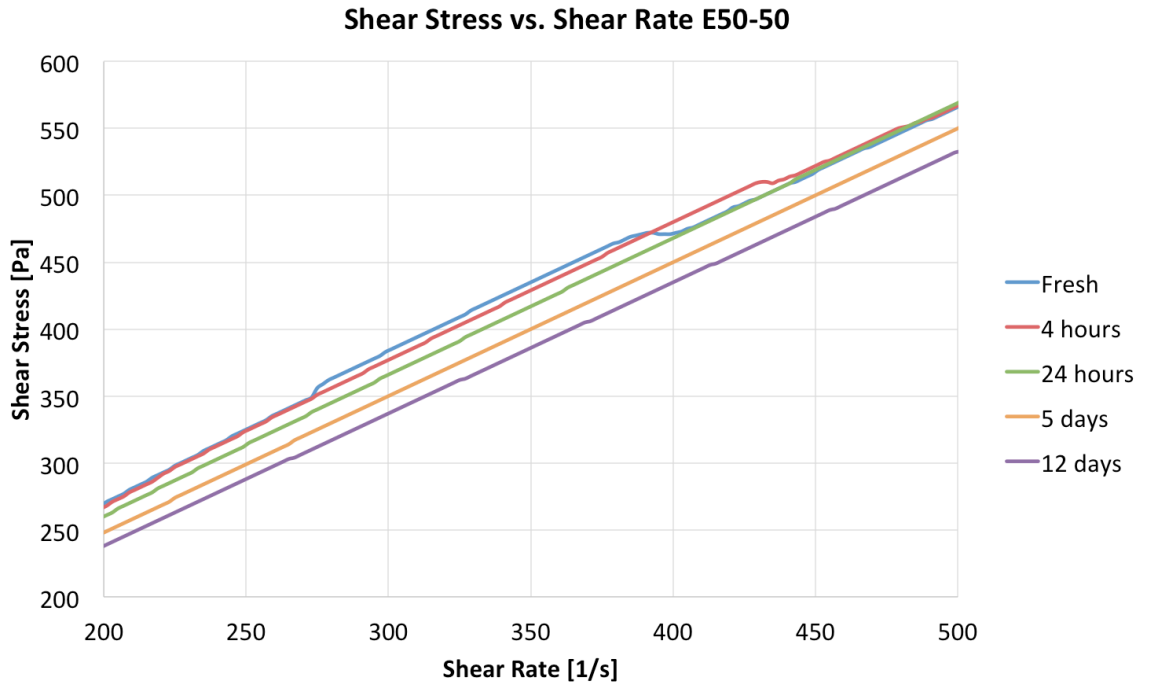

Figure E.10: Zoomed section of Figure E.9

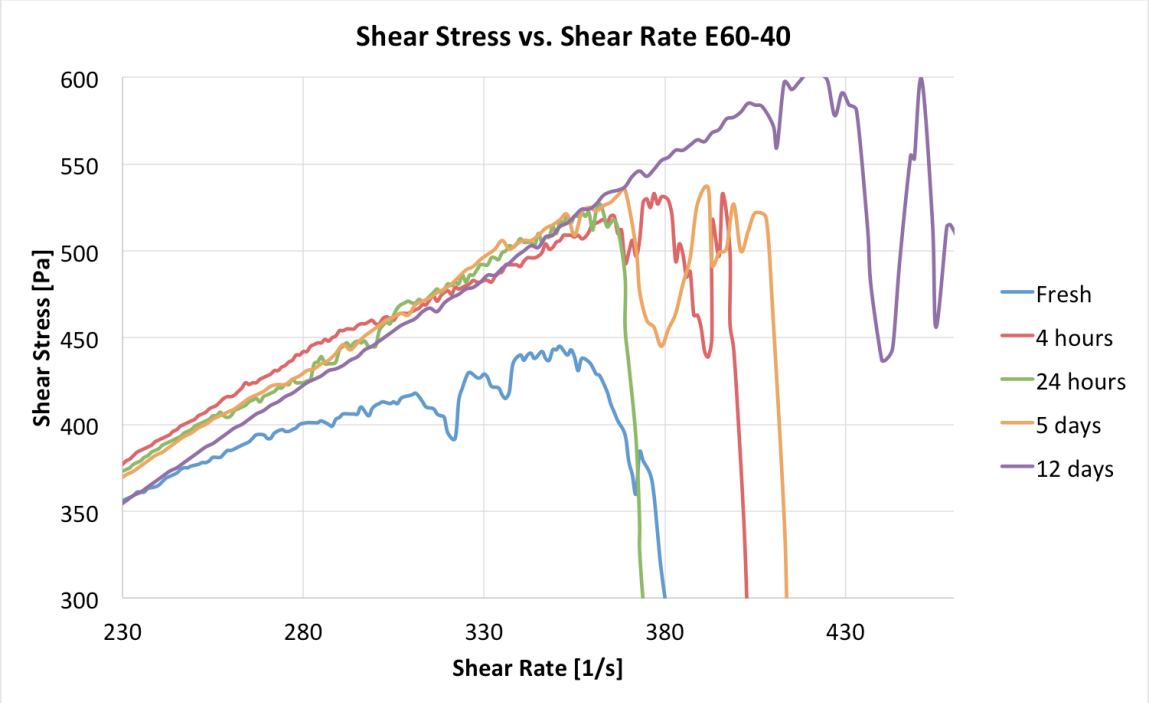

Figure E.11: Zoomed section of Figure 5.8

Appendix F Aging: Measured Droplet Volumes and Logarithmic Distributions

Measured Droplet Volumes

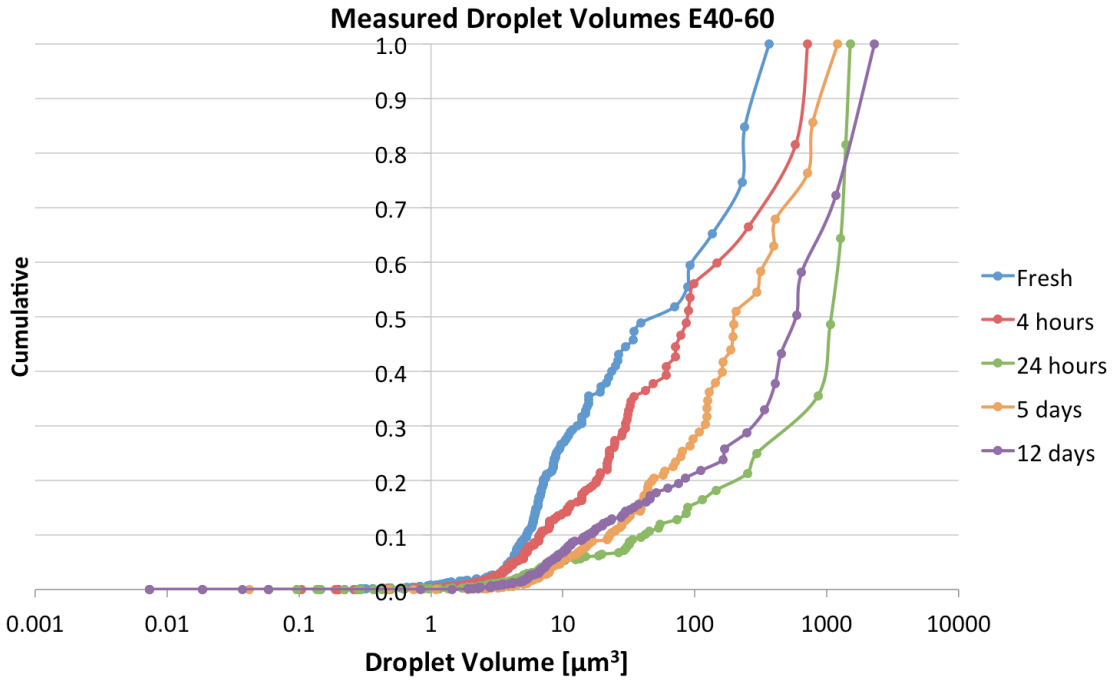

Figure F.1: Droplet volumes found for the E40-60 emulsion, with logarithmic x-axis

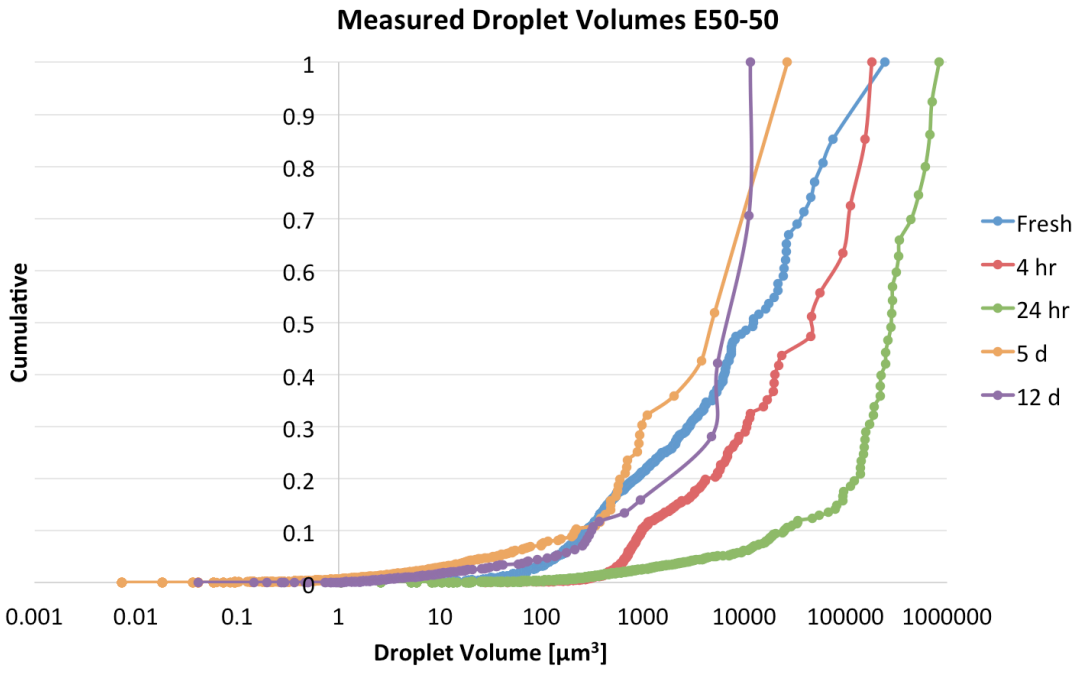

Figure F.2: Droplet volumes found for the E50-50 emulsion, with logarithmic x-axis

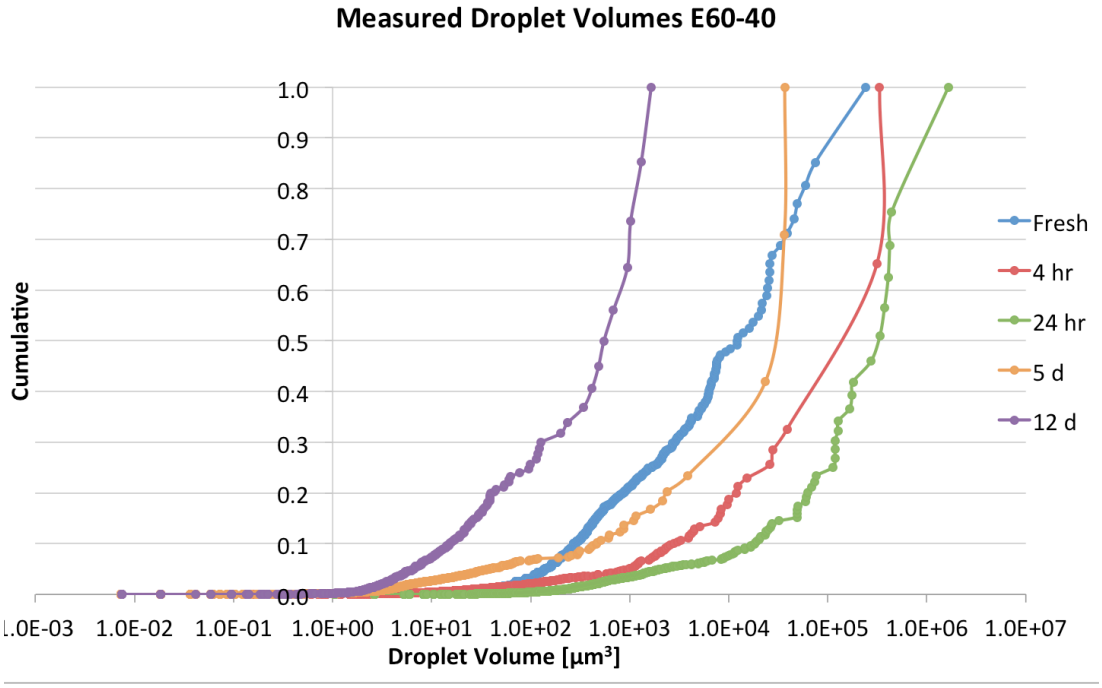

Figure F.3: Droplet volumes found for the E60-40 emulsion, with logarithmic x-axis

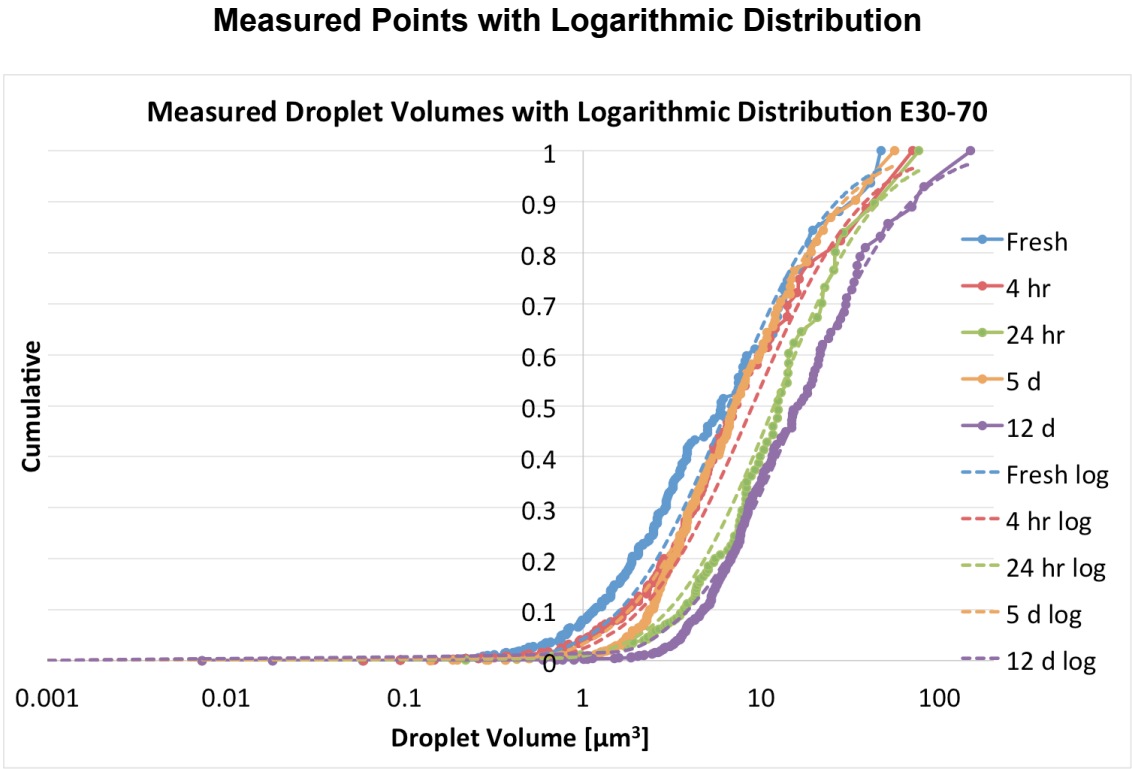

Figure F.4: E30-70 emulsion with logarithmic volume distribution estimated from the measured points found by microscopic image analysis, logarithmic x-axis

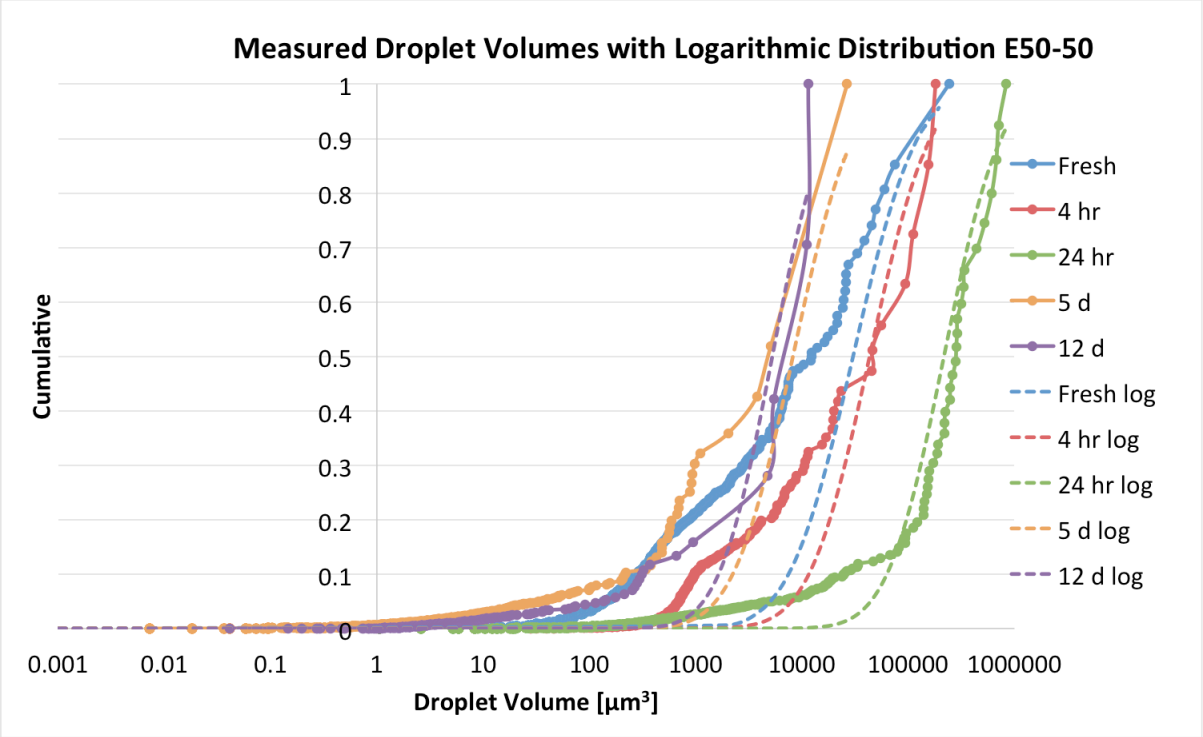

Figure F.5: E50-50 emulsion with logarithmic volume distribution estimated from the measured points found by microscopic image analysis, logarithmic x-axis

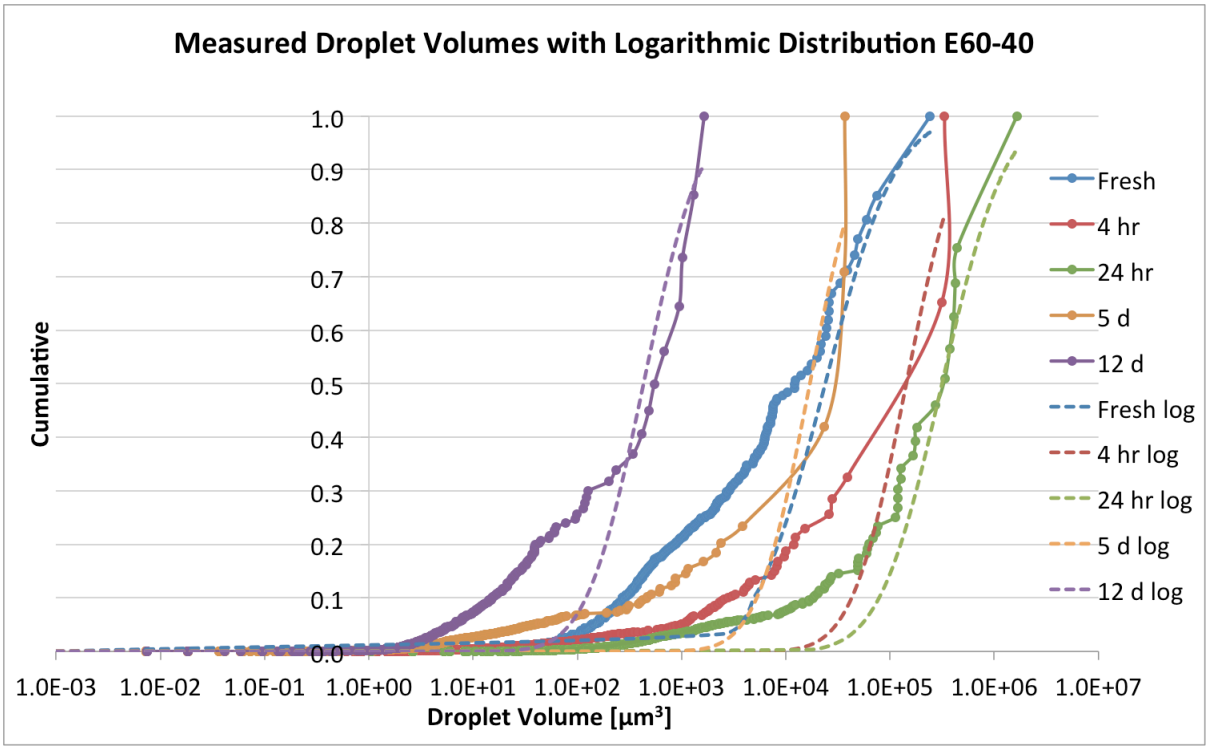

Figure F.6: E60-40 emulsion with logarithmic volume distribution estimated from the measured points found by microscopic image analysis, logarithmic x-axis

Appendix G Aging: Average/Maximum Droplet Size Compared

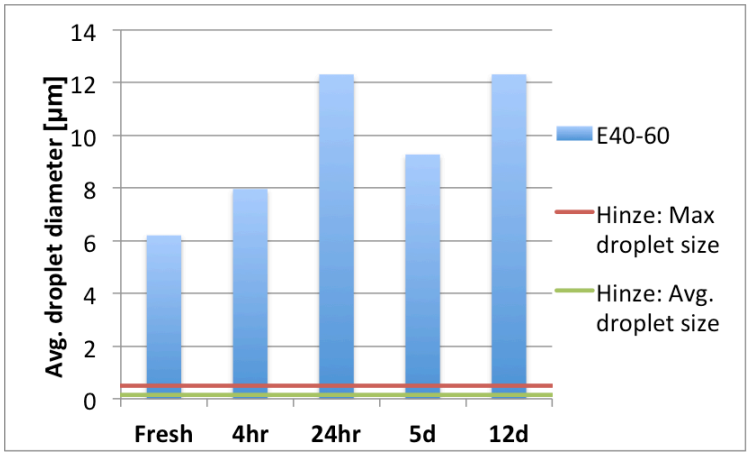

Figure G.1: Average droplet diameter with aging, E40-60

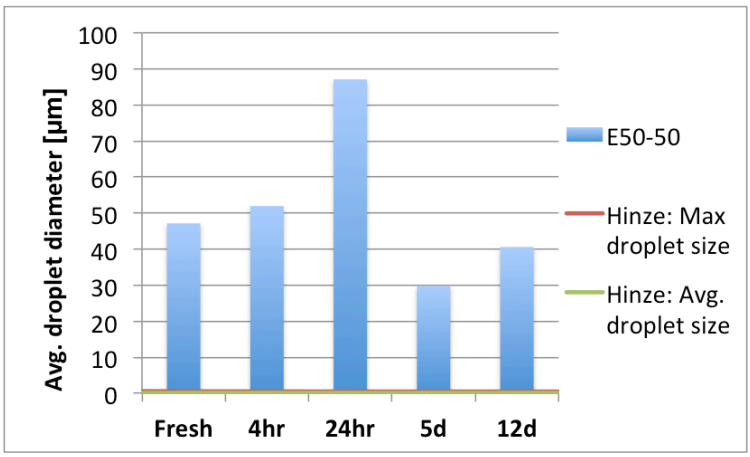

Figure G.2: Average droplet diameter with aging, E50-50

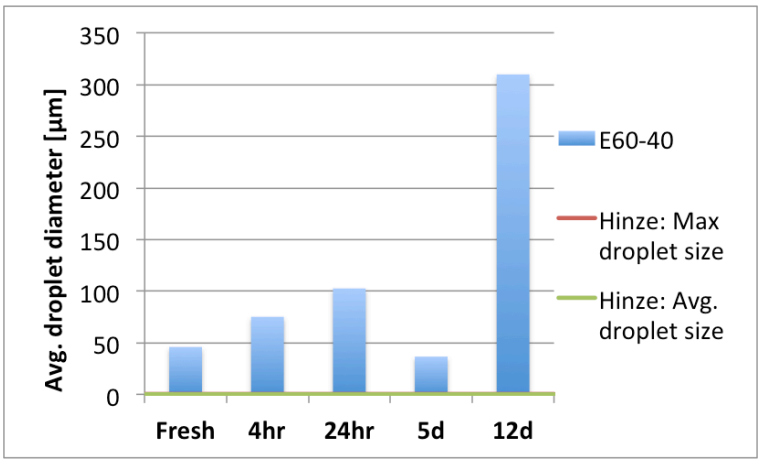

Figure G.3: Average droplet diameter with aging, E60-40

Appendix H Visual Separation

Figure H.1: Visual separation of a E30-70 emulsion in temperature 20 °C, time from left to right is 3, 4, 10 and 12 days

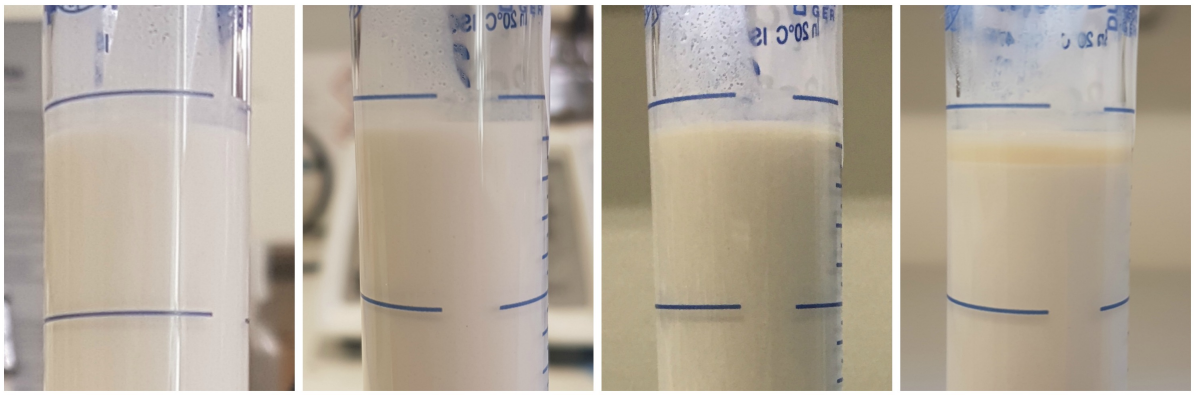

Figure H.2: Visual separation of a E60-40 emulsion in temperature 20 °C, time from left to right is 1, 4, 10 and 22 days